Sigrid Berg

Capacitive micromachined ultrasonic transducers

Acoustic challenges and proposed solutions

Sigrid Berg

Doctoral Thesis

NTNU – Trondheim
Norwegian University of
Science and Technology

NTNU

NTNU – Trondheim
Norwegian University of
Science and Technology

Sigrid Berg

Capacitive micromachined ultrasonic transducers

Acoustic challenges and proposed solutions

Thesis for the degree of Philosophiae Doctor

Trondheim, October 2012

Norwegian University of Science and Technology
Faculty of Information Technology,
Mathematics and Electrical Engineering
Department of Electronics and
Telecommunications

NTNU – Trondheim
Norwegian University of
Science and Technology

Abstract

Capacitive Micromachined Ultrasonic Transducer (CMUT) have been subject to research by several research groups during the last two decades. Despite many potential advantages over traditional piezoelectric ultrasound transducers, the CMUT technology has not yet made a proper commercial breakthrough. One issue which we believe need more investigation is the control of the acoustic crosstalk, both through the silicon substrate and through the adjacent fluid medium.

The work presented in this thesis concerns the modeling of immersed CMUT arrays and the investigation of two different acoustic crosstalk effects which may harm the transducer response. The CMUT array is modeled with an analytical model describing the motion of the single acoustically isolated CMUT cell as a combination of free acoustic vibration modes. Several CMUT cells may be connected to form larger elements, and the vibration modes of adjacent CMUTs are coupled through the fluid outside, by an acoustic impedance matrix. In addition, the model may also include the motion of the silicon substrate and the influence from the source impedance of the electronics.

The first crosstalk effect which we focus on in this work, is the generation of surface acoustic waves (SAWs) along the surface of the silicon substrate supporting the CMUT array. If the SAWs are not damped in any way, they may couple to waves in the fluid at certain steering angles, and cause a drop in transmission efficiency at these angles. In the presented simulation we show that the silicon substrate must be limited in thickness in order for the backing material to be able to damp the SAWs. If the CMUT array is mounted on top of a stack of silicon substrates containing transmit and receive circuitry, the thickness and composition of both the bonding materials and the silicon substrates must be taken into account. We have compared three different bonding techniques, surface liquid interdiffusion (SLID) bonding, anisotropic conductive adhesive (ACA) and direct fusion bonding, and we show that fusion bonding is the technique which is best

suited for high frequency CMUT arrays with several IC chips underneath. The penetration depth of the SAWs is frequency dependent, and we show that a high frequency CMUT array with center frequency around 30 MHz, stacked on top of three circuit layers, should have a total silicon thickness below 100 μm. If the acoustic backing material instead is placed between the CMUT array and the first circuit chip, other bonding techniques than fusion bonding may also be used, and the thicknesses of the IC chips are no longer of importance. However, the transmission of the electric signal through or around the backing layer might be a challenge.

The other crosstalk effect which has been investigated in this thesis, is the inter-element coupling at the CMUT-fluid interface. We refer to this effect as dispersive guided modes, and show that the excitation of local resonances in the interface region may affect the overall transmission from the array at frequencies well within the 100 % bandwidth of the transducer. These waves are not damped by the acoustic backing material. Many CMUT designers choose to have larger distances between CMUT cells in neighbor elements than between CMUTs within an element. We denote this as double periodicity. We have compared the effect of the dispersive guided modes in arrays with the same distance between all the CMUT cells, regardless if they are in the same or in adjacent elements (denoted as single periodicity), and arrays with double periodicity. Simulations show that the response from arrays with double periodicity is affected by the crosstalk even at broadside radiation, whereas the effect becomes apparent at off-axis beam steering for arrays with single periodicity.

Through simulations, we have shown that it is possible to mechanically damp the dispersive guided modes substantially by introducing a lossy coating material of a few micrometer thickness. The PDMS material RTV516 from GE Silicones seems to have material properties which are well suited for such damping. We have also shown that introducing a low electric source impedance in the transmit electronics may reduce the effect of the local CMUT-fluid resonances on the detected signal.

Preface

This thesis is submitted in partial fulfillment of the requirements for the degree of Philosophiae Doctor (PhD) at the Norwegian University of Science and Technology (NTNU). The work was carried out at Department of Electronics and Telecommunications with professor emeritus Arne Rønnekleiv as thesis advisor.

My journey toward the PhD degree started in August 2004, and eight years later, I am finally at the end. I would first like to thank my thesis advisor prof. emeritus Arne Rønnekleiv, for introducing me to the exciting field of micromachined ultrasonic transducers. Throughout the years, he has patiently answered all my questions (sometimes many times over), and always had new and interesting ideas and suggestion. I would also like to express my gratitude to prof. emeritus Kjell Arne Ingebrigtsen for helping proofreading parts of my thesis, and for many interesting conversations and good ideas for further investigations.

I wish to thank prof. Jostein Grepstad, head for the Norwegian PhD Network on Nanotechnology for Microsystems, for hiring me as the coordinator of the network, and thus providing financially for me and my family for the last two years of my PhD-work. It has been a pleasure working with you! I would also like to thank prof. Trond Yttedal, head of the SMiDA project and deputy head of the PhD Network, with whom I have collaborated both in administrative and scientific matters throughout the eight years I have spent at the department.

The measurements performed in this thesis would not have been possible without effort of PhD-candidate Kjersti Midtbø and the staff at SINTEF Microsystems and nanotechnology in Oslo, who manufactured the first CMUTs ever in Norway. Thank you! In addition, I would like to thank the department engineers; Tore Barlindhaug, who helped with the design and soldering of the circuit boards, Gaurav Sharma, who wire bonded numerous CMUT array elements to the circuit boards, and Terje Mathiesen, who pro-

List of papers

IEEE Transactions on Ultrasonics, Ferroelectrics and Frequency Control, vol. 59, no 7, pp. 1537-1549, July 2012

VII **Neighbor Coupling Resonances in CMUT Arrays Immersed in Fluids**

Sigrid Berg and Arne Rønnekleiv

Submitted to IEEE Transactions on Ultrasonics, Ferroelectrics and Frequency Control, 21. March 2012.

Publication not included in the thesis

Challenges with Acoustic Backing of CMUT Arrays on Silicon With Integrated Electronics
Sigrid Berg and Arne Rønnekleiv
Proc. IEEE Ultrasonics Symposium, 980-983,(2009)
This paper is not included in the thesis because its content is fully covered by Paper VI.

Author's contribution

All the papers included in this thesis were written by the author, except for the part concerning receive amplifiers in Paper IV, which was written by prof. Trond Ytterdal, Dept. of Electronics and Telecommunications, NTNU. The simulations and measurements presented in this thesis were performed by the author. The only exceptions are the circuit simulations done in Eldo (Mentor Graphics) in Paper IV, which were performed by prof. Trond Ytterdal. However, it should be noted that the author had access to computational programs describing the CMUT model developed by prof. Arne Rønnekleiv, and published in 2005 [1]. The author has further developed the CMUT model and written computational programs describing this.

The CMUTs which were subject for measurements in the presented work were manufactured at SINTEF MiNaLab, Oslo, Norway in collaboration with PhD candidate Kjersti Midtbø from Dept. of Electronics and Telecommunications, NTNU. Department engineers Terje Mathiesen, Tore Barlindhaug, and Gaurav Sharma at Dept. of Electronics and Telecommunications, NTNU, helped the author prepare the measurements, by producing

printed circuit boards, soldering electronic components and wire bonding the CMUT array elements to the circuit board.

Contents

Chapter 1

Motivation

1.1 SMiDA project

This PhD thesis is a part of the project Smart Microsystems for Diagnostic Imaging (SMiDA), which was initiated in 2004 as an interdisciplinary research project at the Department of Electronics and Telecommunications at NTNU. The main goal has been to develop technology for a high frequency, miniaturized ultrasound transducer, capable of high resolution imaging of atherosclerotic plaques. Expertise from analog circuit design, electrooptics, micromachining, and ultrasonics have been involved in developing the technical solutions to the challenges stated in the project description [2]. These include RF MEMS switching [3], development of custom made integrated circuits for analog signal amplification [4], optical detection and characterization methods [5], and development of a micromachined ultrasonic transducer array for high frequency imaging. The last topic listed will be the main focus of this work, namely capacitive micromachined ultrasonic transducers (CMUTs).

The application of the proposed imaging modality is using a 30-MHz CMUT array for intravascular imaging of atherosclerotic plaques. However, there are a number of other possible applications, some of which are presented here.

1.2 High frequency ultrasound imaging

Magnetic resonance imaging (MRI), computed tomography (CT), single photon emission CT (SPECT), positron emission tomography (PET), and optical coherent tomography (OCT) have all been used for high resolution imaging of human organs and of small animals. However, the cost is high

and the capability for real time imaging with high frame rates is limited. High frequency ultrasound may on the other hand provide both high resolution and high frame rates in real time, at the expense of penetration depth.

Commercial high frequency ultrasonic systems, referred to as ultrasonic biomicroscopes or UBMs [6], often consist of single-element transducers combined with mechanical scanning. A spatial resolution better than 15 μm has been reported in such systems [7]. However, because of the mechanical scanning, it is hard to achieve high frame rates with a wide field of view. Another drawback is that single-element transducers have a fixed geometric focus, which limits the image quality away from the focus [8]. High frequency ultrasound transducers combined with electronic steering and custom-made electronic circuits for transmission and reception will be of great benefit to many imaging applications.

A possible drawback for ultrasound is that the maximum imaging range is determined by the operating frequency. As a general rule of thumb, it is possible to obtain a good signal-to-noise ratio (SNR) down to a few hundred times the wavelength in the imaging medium. In tissue this results in a maximum imaging depth of 1 - 2 cm at 30 MHz. Imaging of areas which lie deeper than a few centimeters calls for invasive procedures, where the transducer enters the body, either through a body orifice (oral, vaginal or anal), or through the skin and into the blood stream (intravascular).

Capacitive micromachined ultrasonic transducers have been subject to research since the mid 1990s [9, 10], but have not yet had a substantial commercial impact. A lot of the research on CMUTs have focused on transducers in the frequency range between 3 - 10 MHz. This is the most common frequency range for ultrasonic imaging, and it covers many important applications such as cardiac- and fetal-imaging. However, it is believed that the most important advantages of CMUTs for medical imaging will be apparent at higher frequencies. This will be further discussed in the following chapters. Some possible applications for high frequency ultrasound is presented here.

1.3 High frequency medical imaging applications

1.3.1 Vascular imaging

Many aspects of medical diagnostics involve blood flow. To obtain satisfactory vessel wall resolution and detect blood flow in small vessels, high frequency ultrasound is an advantage. Vessels of importance are for instance

the coronary arteries, which supply the heart muscle with blood, and microvessels growth (angiogenesis) caused by cancer. The characterization of the microvascularization in tissue can help distinguish between benign and malignant tumors.

Intravascular ultrasound (IVUS) of coronary arteries

Coronary artery disease is caused by the formation of atherosclerotic plaques in the coronary arteries. Atherosclerotic plaques are divided in two subgroups, stable- and unstable plaques. Unstable plaque, often referred to as vulnerable plaque, is defined as a plaque at increased risk of rupture and causing thrombosis and lesion progression [11]. The rupture triggers the emergence of blood clots that block the blood flow (stenosis). Most heart-attacks and many strokes are caused by ruptured plaques that have not initially been blocking the blood stream [12].

The most common imaging technique in clinical use to diagnose coronary heart disease, is angiography. This is an x-ray based imaging modality where contrast agents are inserted into the coronary arteries using a catheter while x-ray images are acquired. The images differentiates between soft tissue and blood flow, and hence, provide useful information of areas where the blood flow is partially- or fully obstructed. The major drawback of this technique is that it does not provide any information about what might be hidden behind the artery walls, hence, areas with vulnerable plaques that do not cause stenosis will not be discovered [13].

To obtain sufficiently high image resolution to detect atherosclerotic plaques with ultrasound, high acoustic frequencies are needed. Since the attenuation per cm is very high at high frequencies ($\sim$15 dB/cm at 30 MHz), the transducer needs to be very close to the plaque. The only way to obtain this is for the transducer to enter the body, and preferably through the vascular system. This is called intravascular imaging, and is performed using catheters that are inserted into an artery or vein and guided towards the area of interest. The diameter of catheters for intravascular imaging of the coronary arteries are 1 mm.

There are some commercially available IVUS imaging systems [14–17]. Electronically steered ring arrays and rotational single-element transducers are available, all of which are based on piezoelectric materials. One of the main drawbacks of such probes is the price, since probes usually are disposed after the examiation. If a CMUT array for IVUS is successfully developed and put into large scale production, the price for single-use equipment will not necessarily be too high.

Ultrasound imaging of microvascularization

Angiogenesis is the formation and growth of new blood vessels. Physiological angiogenesis occurs in normal tissue and organ development, such as tissue reproduction and wound healing. On the other hand, pathological angiogenesis occurs in tumor formation and other angiogenesis-dependent diseases [18]. From preclinical studies it can be concluded that the growth and metastases of tumors depend on angiogenesis [19]. The vascularization level of a tumor is believed to be a good indication of the tumor's metastatic potential. The ability to image such vascularization would improve the accuracy of diagnosis of cancerous tissue, and can also be used to investigate whether the tumor responds to treatment [20].

During blood flow imaging, the ultrasound wave undergoes a frequency shift when encountering a moving target. This is the Doppler-effect. The frequency shift is used to determine the speed of the blood flow. In major arteries the flow is fast and the diameter of the vessels is large. However, the diameter of the vessels providing a cancerous tumor with blood might be down to 100-200 μm, and the speed of the blood flow slows down to 2 mm/s. To image such small vessels with slow blood flow, high frequencies are required. An interesting modality can be the combination of high frequency Doppler-imaging with 3D volumetric images. This will also be able of visualizing the heterogeneity of the tumor. [21, 22]

Another modality which is used in blood flow imaging, especially for small vessels, is the injection of contrast agents, consisting of microbubbles. The image contrast is much higher from areas with gas filled bubbles than from the normal tissue, hence, improving the detection of flow.

1.3.2   Imaging of the eye

Clinically important tissues in the anterior of the eye lie within a few milimeters of the lens surface. Optical microscopes provide valuable information about the surface of the eye, but not about the underlying structures. To resolve the anatomy of interest neither MRI nor computed tomography (CT) can provide the sufficient image quality. High frequency ultrasound may be a suitable technique for such imaging [23, 24]. Commercial systems are available, imaging at 10-50 MHz. The 50 MHz probe can provide an axial resolution of 35 μm and lateral resolution of 60 μm [25].

There are three main applications of interest for ultrasound imaging of the eye; investigation of glaucoma, visualization of anterior segment lesions (including tumors and cysts), and measurement of corneal thickness and topology [24]. Glaucoma is an eye disorder, where the optic nerve is

damaged, often caused by elevated pressure in the eye. Increased pressure causes changes in the angle between the cornea and the iris, and this can be visualized by ultrasound imaging. Such images may also be valuable in the differentiation between the various types of glaucoma. Characterization of tumors, cysts and other lesions in the eye is another application where high frequency ultrasound might be useful. It can both be used preoperatively, to give the surgeons as accurate information as possible of the diseased anatomy before the surgery, and also to assess the result of the operation. Most changes in the cornea can be observed directly, but when there are damages to the surface, it might be hard to evaluate the internal changes, corneal dimensions or other underlying changes in the anterior chamber of the eye. [24, 26, 27]

1.3.3 Imaging of the skin

In skin imaging, optical methods are useful in examining the surface, but the ability to penetrate into the deeper layers of the skin is not good enough for some applications. High frequency ultrasound in the 40-50 MHz range may provide images that can resolve the various layers of the skin, and be especially useful in the evaluation of cutaneous melanomas (skin cancer). Measuring the tumor thickness and depth might give valuable information about the prognosis of the melanoma. Since ultrasound imaging in this case is a non-invasive technique, it can easily be used for dynamic studies of the response to tumor therapy. In inflammatory skin diseases, such as psoriasis, ultrasound imaging can be used to assess the psoriasis activity and efficacy of treatment. Basic studies of skin aging and wound healing might also benefit from the high resolution provided by high frequency ultrasound imaging. [24]

1.3.4 Imaging of cartilage

Osteoarthritis (OA) is one of the most frequent causes of pain, loss of function and disabilities in adults [28]. Early stage diagnosis of OA may help patients to slow down or even stop the development of the disease through lifestyle changes or by medical treatment. Conventional ultrasound examination of the articular cartilage performed externally on the body surface around the joint has limited accuracy because of the inadequacy in frequency and, hence, resolutions used. In contrast to this, minimally invasive arthroscopy-based ultrasound with adequately high frequency may be a better alternative to assess the cartilage.

In vivo [29] and in vitro [30] studies of minimally invasive assessment of cartilage using IVUS transducers showed that high frequency ultrasound may provide valuable information about the cartilage surface and thickness.

1.3.5   Small animal imaging

There is a growing interest towards the imaging of small animals in basic research. Animals like mice and zebrafish can be used as animal models for assessing drug and gene therapy and evaluate the growth and metastases of cancer. The early development of the mammalian heart is another example of studies which interest the research community [23]. The study of animal models can help researches pinpoint when important morphological changes occur in the embryonic development. Solid state transducers operating at up to 70 MHz with a resolution of 30 μm are commercially available for small animal imaging [31].

Chapter 2

Medical Ultrasound Imaging

2.1 History

The first patent on using sound waves for range measurements was filed just a few months after Titanic crashed into an iceberg and sank in 1912. During World War I, the need of locating submarines and mines resulted in the development of the first sonars, where the distance to objects were measured using transmission and reception of sound waves [32]. Towards the beginning of World War II the first radar was developed by the U.S. Navy, using electromagnetic waves in a pulse-echo fashion to detect hostile aircrafts [33].

After World War II the knowledge of the pulse-echo technique from sonars and radars was used to develop various systems of probing the human body for medical reasons. By the early 1970s the first commercial B-mode static scanners became available [33]. The invention and exponential increase in the use of transistors during the following decades was an important factor for the further development of the ultrasound scanners. It has become a popular diagnostic tool in many areas of medicine. Most well known are probably abdominal and obstetric imaging and echocardiography (imaging of the heart).

Ultrasound is in most cases a non-invasive imaging technique. As long as guidelines are followed, it has no known harmful effects, which is an advantage compared to x-ray, computed tomography (CT) imaging and Positron Emission Tomography (PET). Another important advantage of ultrasound is the low cost and that it is more portable than magnetic resonance imaging (MRI), PET and CT scanners. The portability of ultrasound scanners have improved dramatically during the last few years, when handheld and laptop size scanners have become available [34].

2.2   Principle of ultrasound imaging

Ultrasound is defined as acoustic waves above 15 kHz, which is the upper limit of the audible range for humans. In solids, sound waves can be both longitudinal and transversal. In longitudinal waves, the particle motion is in the same direction as the wave, whereas in transverse waves, the particles move perpendicular to the propagation direction of the wave. For a transverse wave to travel, the medium must be rigid. As one particle begins to move it must be able to pull on its nearest neighbor. If the medium is not rigid as is the case with fluids, the particles will slide past each other. This sliding action prevents one particle from displacing its neighbor in a direction perpendicular to the energy transport, hence, waves traveling through a bulk of fluid (liquid or gas) are always longitudinal. Due to its high water content, human tissue is often modeled as a fluid. Hence, transverse waves are usually disregarded in medical ultrasound modeling. However, the transverse waves must be taken into account in transducer design, since the materials in the ultrasonic transducers are solids.
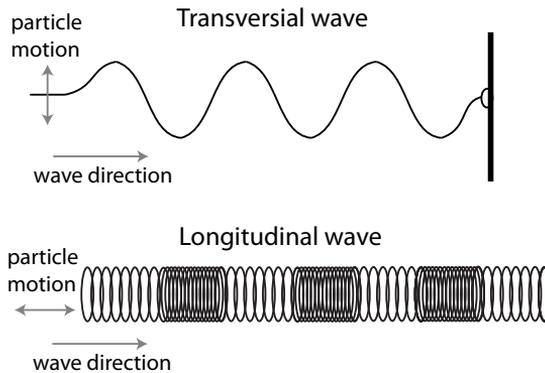
Figure 2.1: Illustration of transversal and longitudinal waves.

The variation in acoustic impedance for different kinds of human tissue (e.g. fat, muscle, bone, connective tissue, blood) is the basis of ultrasonic imaging. To collect data for the image, an ultrasonic pulse is transmitted into the body by a transducer, and as the wave hits the various layers of tissue, the wave will be partially transmitted and partially reflected, as illustrated in Fig. 2.2. The transducer then records and samples the reflected signal, and based on the time-of-flight, the system calculates the depth of the reflector. The amplitude of a signal from a certain depth determines how bright the pixel(s) representing that exact depth will be. To image a 2D-plane, ultrasound pulses must be transmitted and received
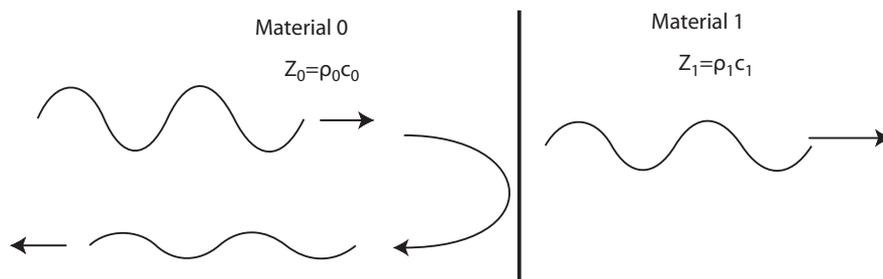
Figure 2.2: Illustration of transmission and reflection at the interface between materials with different acoustic impedance.

from many directions. This is called beam steering, and is further elaborated in Sec. 2.3 and illustrated in Fig. 2.5.

The result is displayed on the screen as a gray-scale image. An example is shown in Fig. 2.3, where the four chambers of the heart clearly can be identified.
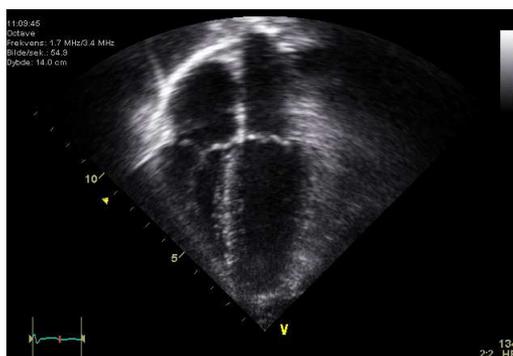
Figure 2.3: Example of ultrasound image of the heart (Wikimedia Commons).

2.3 Ultrasound imaging system

The ultrasound imaging system consists of a number of essential components which are schematically described in Fig. 2.4. Between the transducer, in one end of the system, and the display unit in the other, are multiplexers, switches, amplifiers, analog-to-digital converters and beamformers. In addition, there is an image processing unit, and many systems also contain Doppler-processing units, which enable the imaging of blood flow.
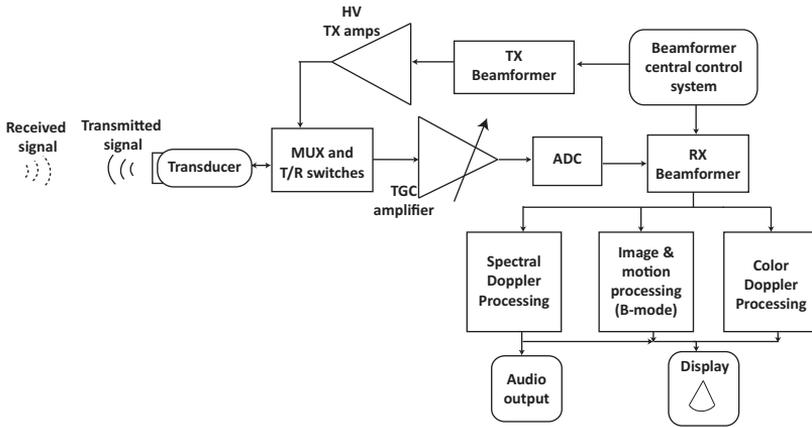
Figure 2.4: Block diagram showing the most important parts of an ultrasound system [35].

The beams can be steered in different directions either by mechanical- or electronic scanning, as shown in Fig. 2.5. In mechanical scanning, a motor either moves the whole transducer or only the active elements in order to aim the beam in different directions. Electronic scanning, on the other hand, involves time delays which are introduced between array elements to steer the beam.
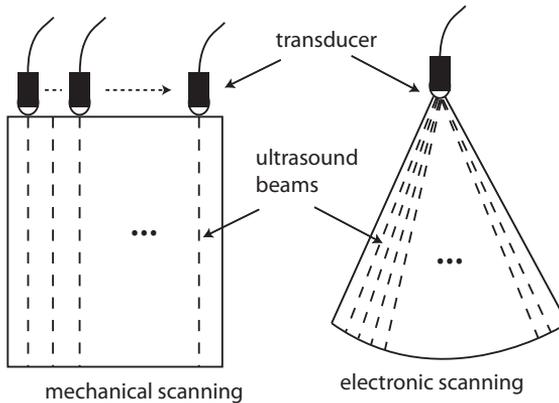
Figure 2.5: Illustration of ultrasound image formation.

To make an image of good quality, electronic focusing is needed. In transmission, time delays are added to the elements of the transducer, so that the energy of each element reaches the same focus spot at the same time. Similarly, time delays are added to the received signal before it is

summed up to form the image. A transmitted pulse can only be focused to one specific depth. However, during the receive mode, the focus can be swept through a range of depths to pick up multiple echoes produced by one transmitted pulse. This is called dynamic focusing on reception. Electronic focusing using time delays is illustrated in Fig. 2.6. Electronic beam steering is also achieved using added time-delays. This allows imaging of areas which are much larger than the transducer aperture. This is especially useful when imaging the heart, due to the limited space between the ribs, and in fetal imaging, where the area of interest is a lot larger than the width of the transducer.
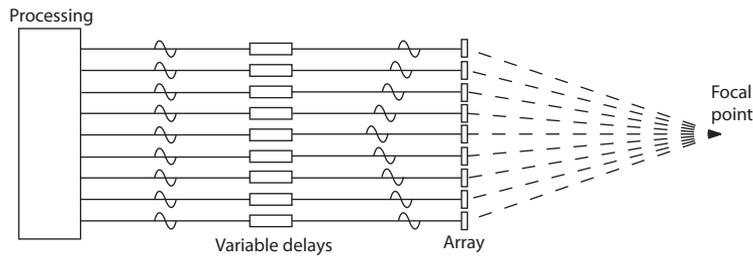
Figure 2.6: Focusing by introducing varying delays [35].

Traditionally, most of the signal processing, both hardware and software, have been placed in a large portable rack, and with the display screen on top. Transducers have been connected to the rack with a cable containing one wire for each array element. During the last years more compact ultrasound systems have been developed. Laptop size systems with less hardware, and more software processing, and even pocket-size hand held systems are available. This enables general practitioners and even ambulances to use ultrasound when diagnosing patients [36].

Image quality

The quality of ultrasound images depend on many different factors. The spatial image resolution is one important quality parameter, which indicates the minimum distance between two targets that are possible to separate in the image. The resolution in depth, Δz, also known as range resolution, is depending on the length of the transmitted pulse, T_p, which is inversely proportional to the transducer bandwidth, B_w [37]:

$$\Delta z \propto \frac{cT_p}{2} \propto \frac{c}{2B_w},$$
(2.1)

where c is the velocity of sound in the imaging medium (typically 1540 m/s in human soft tissue). The absolute length of the pulse is dependant on the bandwidth of the transducer and the frequency of the transmitted pulse. Increased frequency improves the range resolution, and transducers with large bandwidths are preferred.

The lateral resolution (across the beam) is proportional to the $F_\#$ of the transducer and the wavelength:

$$\Delta r \propto F_\# \lambda \tag{2.2}$$

The $F_\# = r/a$, where r is the focal depth and a is the active aperture of the transducer, and the wavelength $\lambda = c/f$, where f is the transmit frequency. An increased transmit frequency yields smaller wavelengths, which in turn leads to better resolution. If the lateral resolution is to be kept constant along a beam, the active aperture, a, needs to increase as the focal depth, r, increases.

High frequency is beneficial for the image resolution, but the drawback is that the attenuation increases with increasing frequency. A rule of thumb is that the attenuation in human soft tissue is 0.5 dB/cm/MHz [37]. Thus, high frequency transducers are best suited for superficial imaging applications.

2.4   Transducers

A general definition of a transducer, is that it is a device that can transform energy from one domain to another. In ultrasonics, it transforms electric signals into mechanical waves, and vice versa.

Piezoelectric ultrasound transducers

In traditional ultrasonic transducers for medical imaging, the active part of the transducer is a piezoelectric ceramic, often lead-zirconate-titanate (PZT). The piezoelectric ceramic contracts and expands depending on the polarity of the voltage applied across the material, and applying an oscillating voltage causes a vibration in the transducer. If it is in contact with a fluid (or human tissue), the vibration will excite a pressure wave into the fluid. If an incoming wave hits the transducer, it will excite a vibration in the ceramic which generates a voltage between the electrodes.

The characteristic acoustic impedance of the transducer is an important property because it determines the effectiveness of coupling of acoustic energy from the transducer to the tissue. The acoustic impedance of PZT

is in the range of 30 MRayl, which is 20 times higher than the acoustic impedance of human tissue. Such a large difference in impedance will result in strong reflections of waves at the PZT-tissue interface, and very little energy will be transmitted into the body. To obtain a lower acoustic impedance, most commercially available transducers are made of a composite material consisting of a matrix which includes bars of piezoelectric ceramic and polymer (often epoxy) fillings in between. In addition, one or several $\lambda/4$-thick elastic matching layers are attached in front of the composite. This works as an impedance transformer that further improves the impedance match between the transducer and the tissue. As a result, the ultrasonic energy couples more efficiently into the imaging medium. Acoustic backing materials are needed to damp substrate ringing, and hence, improve the bandwidth. A sketch of a typical piezoelectric transducer with matching layers and backing is shown in Fig. 2.7. [37]
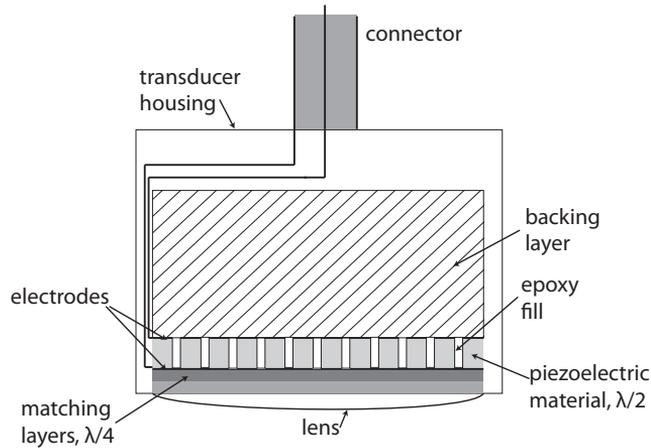
Figure 2.7: Sketch of a typical piezoelectric transducer. The PZT material is mounted between one (or several) matching layers and an acoustic backing layer. Some transducers also include a lens material at the front.

Piezoelectric materials are anisotropic, which means that their acoustic properties depend on the direction of the material. There is also coupling between the different material directions, which implies that an electric field in one direction can lead to strain in both the parallel and transverse directions. The use of composite materials have proven important not only to reduce the acoustic impedance, but also to control the excitation of unwanted vibration modes. In addition to the thickness mode, PZT composite transducers will have a low frequency radial mode, which depends on the shape of the transducer, and lateral modes which depend on the periodic-

ity of the lattice [38]. Lateral modes of 1-3 piezocomposite transducers are described theoretically and experimentally in [39], and it is shown that an almost uniform vibration pattern at the resonance frequency of the thickness mode can be achieved. However, at the resonance frequency of the first and second lateral mode, the vibration amplitude of the polymer areas of the transducer were higher than the ceramic, and the phase of the ceramic and polymer vibration were $180°$ out of phase. If this vibration pattern is excited within the frequency range of operation, it will reduce the efficacy of the transducer greatly.

To push the resonance frequency of the lateral mode high enough to not interfere with the frequency band used for imaging, a small distance (smaller than $\lambda/2$) between the ceramic bars and a high volume fraction of ceramic is needed [38, 40]. However, the acoustic impedance of the transducer increases with the volume fraction, resulting in a trade-off between the frequency of the first lateral mode and the acoustic impedance of the material [39, 41].

In many applications it is necessary to steer the ultrasonic beam electronically, to obtain a field of view which is wider than the width of the transducer. In order to steer $\pm 45°$ without generating grating lobes, the pitch between transducer elements can not be larger than half the wavelength of the propagating wave in tissue [37].

Limitations and challenges

For the imaging modalities mentioned in Chapter 1, high frequency ultrasound imaging is needed. Many high frequency ultrasound systems use mechanically-scanned, single-element transducers with a fixed focus, and have great limitations regarding frame rates and the uniformity of the image resolution [42]. Creating multi-element piezoelectric transducers for high frequencies is challenging due to the small size of ceramic bars needed. The ceramic slab needs to be sawed into $\lambda/2$-thick bars, a process which becomes very labor intensive when $\lambda/2$ is in the range of 10-50 μm. The typical saw blades thickness is about 30 μm, but distances down to 13 μm is possible when using diamond blades [43].

There are, however, some examples of high frequency multielement piezoelectric transducers. A 1-3 piezocomposite has been used in a 30 MHz array with 128 elements [44]. The array had an element pitch of approximately 2λ in water, or 100 μm. The dicing kerf was less than 12 μm, and a 6 dB bandwidth of 74 % was obtained. Cannata *et al.* demonstrated a 64-element 35 MHz composite transducer using 2-2 composite [43], and reported a 6 dB bandwidth of 55 % and a resolution of 50 μm to 100 μm. As an alternative to mechanical dicing of the PZT-slab, researchers have fabricated arrays

using thin sheets of piezo-polymer materials [45]. The low lateral coupling and low acoustic impedance of polyvinylidene-fluoride (PVDF) makes the material possible to use for high frequency array design. However, the low capacitance of the material and the high parasitic capacitance of typical preamplifiers have proven problematic for typical preamplifiers.

3D-imaging has become an important image modality during the last decade. Instead of visualizing one plane of an organ at a time, the physician would like an image of a whole volume. When a 2D-image is created, a 1D-transducer which steers the beam in the azimuth direction is used. This is illustrated in the left part of Fig. 2.8. To image a volume, we need to steer the beam in the elevation direction as well, and the transducer must be two-dimensional. The number of elements increases from N to N^2, and having separate connections to each element becomes impossible.
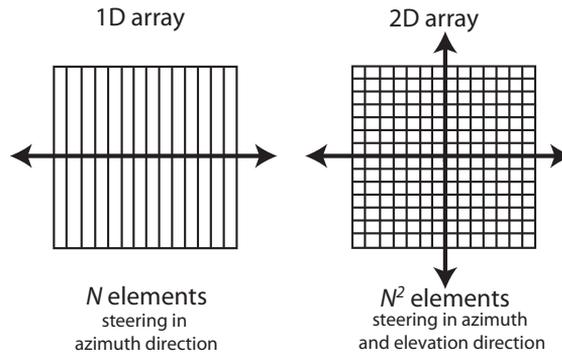
Figure 2.8: 1D-arrays have N elements whereas 2D-arrays have N^2 elements.

This challenge calls for smart solutions with more integrated electronics close to the transducer. Some of the signal processing, such as multiplexing, signal amplification and other parts of the beamforming electronics must be placed in the transducer unit. This will reduce the amount of data that must be transferred to the ultrasound system.

A solution to both the above mentioned challenges could be to use capacitive micromachined ultrasonic transducers instead of piezoelectric ceramic transducers. CMUTs are made with photolithographic techniques on silicon originally developed for integrated circuit (IC) processing, and the limitations regarding dimensions are not an issue. The integration of electronics can also be easier using CMUT arrays, since they are fabricated in the same kind of processes and same or similar materials as integrated circuits (IC). Furhtermore, they can be connected to custom ICs through 3D-stacking.

This will be discussed further in Chapter 4.

Chapter 3

Capacitive Micromachined Ultrasonic Transducers

3.1 Brief history of capacitive transducers

Capacitive air transducers have existed for a long time. An instrument for absolute measurement of sound was reported in 1917 [46], where a diaphragm, made of a thin steel plate, was mounted in an air-filled gap, with a metal plate on one side. The diaphragm vibrated as a function of an incoming sound wave, and based on measurements of the change in capacitance between the diaphragm and the plate, the pressure in the incoming wave was calculated. A similar device for capacitive sensing in liquids was shown in 1979 [47].

Air transducers may also be used for measurements of distance, for instance in robotics, and in nondestructive evaluation (NDE) of a variety of materials. Piezoelectric transducers are not very efficient in air because of their high acoustic impedance. Extensive use of matching layers and air backing is needed, which deteriorates the bandwidth and sensitivity [48]. Capacitive transducers with membranes vibrating over air filled cavities may, however, provide a much better acoustic match, because of its low impedance. For high frequency operation, the uniformity in size and depth of the cavities and the thickness and smoothness of the membranes are essential, hence, a fabrication technique with a high degree of accuracy and reproducibility is needed [49–51].

The photolithographic techniques used in integrated circuit fabrication have been developed during the last decades, and these techniques have also proven important in the development of capacitive transducers. The first silicon-based capacitive ultrasonic transducers using such micromachining

techniques was reported by Suzuki *et al.* in 1989 [52]. The purpose of the
device was to function as a proximity sensor operating in air in the frequency
range between 100 kHz and 400 kHz. Similar transducers have also been
reported by Schindel *et al.* [48, 53] and Ladabaum *et al.* [10] in 1995. The
latter introduced the term Micromachined Ultrasonic Transducers (MUT),
while Capacitive Micromachined Ultrasonics Transducer (CMUT) was es-
tablished as a term in 1998 [54–56].

   The first examples of CMUTs in immersion applications was demon-
strated in 1996 [57, 58], and the improved acoustic matching compared to
piezoelectric transducers is also valid for operation in fluids. Imaging results
from CMUT arrays was first shown in 1998 [59], and the first commercial
medical transducer using CMUT-technology was released by Hitachi in 2009
[60, 61].

3.2   Principle of operation

The active acoustic part and top electrode of the CMUT is a membrane
which is partially or fully covered with a conductive material. The mem-
brane is suspended over a vacuum gap in a heavily doped silicon substrate,
which constitutes the bottom electrode.
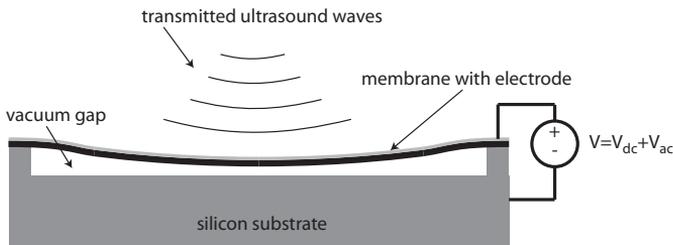
Figure 3.1: Sketch of a single CMUT. The CMUT is biased with a DC-
voltage, deflecting the membrane towards the substrate, whereas the AC-
voltage causes it to vibrate and transmit ultrasonic waves into the medium.

   A DC-bias voltage applied between the top and bottom electrode pulls
the membrane towards the substrate due to electrostatic attraction. If an
AC-voltage is applied to the biased membrane, harmonic membrane motion
is obtained. In this mode of operation it acts as a transmitter. If a bi-
ased CMUT membrane is subject to an impinging ultrasonic pressure field,
the membrane motion leads to harmonic changes in the capacitance of the
device, generating an AC-detection current. In this mode, it works as a

receiver. Fig. 3.1 shows a sketch of a single CMUT in a biased state.

If the DC-bias increases, the membrane will be pulled closer to the bottom substrate. When the electrostatic forces because of DC-bias exceeds the mechanical restoring forces in the membrane, the membrane will be pulled into collapse. In this state, the center part of the membrane is in contact with the substrate. It has been shown that it is possible to operate CMUTs in collapsed mode [62, 63]. The operation frequency in collapsed mode is higher than in conventional mode due to the reduced vibrating area of the membrane. A more thorough description of the collapsed mode operation is given in Sec. 3.3.

The membrane thickness, cavity depth, and shape of the CMUT cell can be adjusted to obtain the required resonance frequency, sensitivity and output pressure. The resonance frequency of the CMUT is mainly determined by stiffness and size of the membranes, where small and/or stiff membranes are needed to obtain high resonance frequencies. The maximum output pressure is determined by the maximum membrane deflection, hence, given by the cavity depth. However, high DC-bias voltages must be applied to obtain large deflections. It is therefor important that the electronics connected to the array can handle such voltages, and that the transducer is properly shielded from the human tissue. A measure for sensitivity is the electromechanical coupling coefficient. The coupling is highest when the CMUTs are operated close to collapse.

Transducer elements are formed by electrically connecting many CMUT cells. As illustrated in Fig. 3.2, we use the notion CMUT about a single CMUT cell, element or array element about a group of CMUTs which is electrically connected. A fully populated array is denoted as a CMUT array or transducer array.

Ring-arrays [64, 65], 1D-linear arrays [42, 66] and fully populated 2D-arrays [67–69] have been demonstrated. The fill-factor of the array is defined as the ratio of the active membrane area to the total area of the transducer. Increasing the fill-factor, by for instance introducing rectangular CMUTs instead of square or circular ones, will increase the average displacement and, hence, a higher output pressure and receive sensitivity may be obtained [70]. However, if the distance between CMUT cells is too small, the support structures may bend as the membranes deflect, and this can lead to nonlinearities in the transducer response [71].

Nonlinearities in the CMUT

The electrostatic force between the electrodes depends on the square of the applied voltage (see Ch. 6.2), hence, the second harmonic of the applied
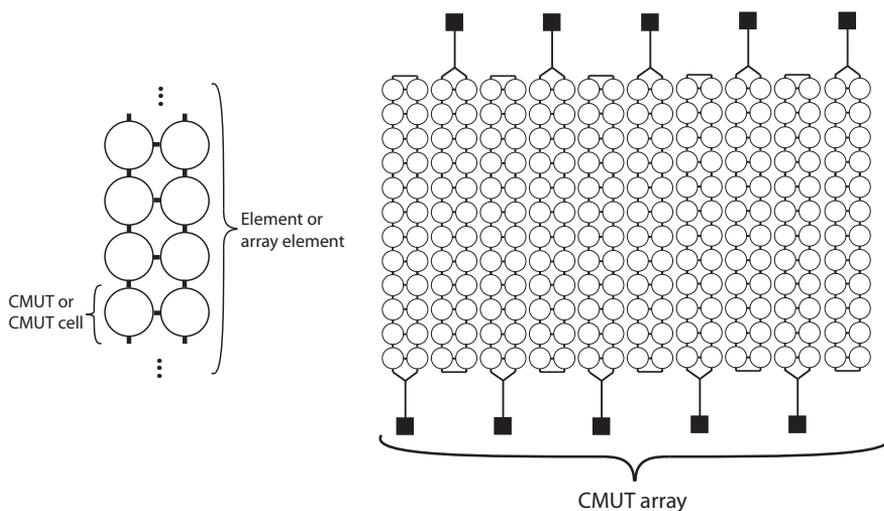
Figure 3.2: In this work the following notation of the building blocks of a CMUT array is used: A single capacitor is denoted simple as CMUT or CMUT cell. Several CMUT cells which are electrically connected is denoted element or array element, whereas a complete transducer array simply is denoted as CMUT array or just array. The sketch shows a 1D-linear array.

voltage will be generated. To operate the capacitor at the first harmonic, a DC-bias voltage is needed in addition to the RF signal, such that the total applied voltages is the time varying signal: $V(t) = V_{DC} + V_{AC}\cos(\omega t + \phi)$. As long as the bias voltage is much larger than the time varying signal, the dominant time varying voltage which influences the electromechanical force is the harmonic signal: $V(t)^2 = V_{DC}V_{AC}\cos(\omega t + \phi)$.

The membrane deflection towards the bottom electrode, give a slight elongation of the membrane material. This change of the shape and size of the membrane may change the stretching force in the membrane. As long as the lateral dimensions of the membrane is much larger than the cavity depth, the elongation will be minimal, and this effect may therefore be neglected in CMUT modeling.

The deflection may also cause bending of the areas supporting the membrane. This may lead to nonuniformities in the collapse voltage [71] and cause a stronger acoustic coupling between neighbor cells. Hence, there must be a minimum distance between CMUT cells to avoid nonlinear effects caused by perturbation of the support structure.

3.3 CMUT operation regimes

The CMUTs may operate in three different ways. The first and most commonly described regime of operation is the conventional mode, where the sum of the DC- and AC-voltage is kept lower than the collapse voltage at all times, and the membrane never is in contact with the substrate. The maximum AC-displacement will be at the center of the membrane. In Fig. 3.3, the conventional mode operation is marked as number 1.

Operation of the CMUT in the collapsed regime was first reported by Bayram *et al.* [62] and further discussed by Huang *et al.* [63] and Oralkan *et al.* [72]. The applied bias voltage is increased above the collapse voltage in order to pull the membrane into collapse. The sum of DC- and AC-voltage is kept above the snapback voltage, so that the center of the membrane always is in contact with the substrate. In a circular membrane, the maximum AC-displacement will be along a ring formed between the center of the CMUT and the edge. The collapsed regime is marked as number 2 in Fig. 3.3. Finite element analysis (FEA) has revealed that a CMUT operating in the collapsed regime has a coupling coefficient higher than a CMUT operating in the conventional mode [62]. This has been verified by experiments [63, 72] showing higher output pressures and improved coupling coefficient because of stronger actuation forces and higher capacitance as the electrode spacing was reduced in the collapsed regime. The ability to change the

center frequency in the collapsed regime by varying the DC-bias, resulting in change of the area of contact between the membrane and the substrate, was also shown. However, the frequent substrate-membrane contact may prevent a reliable and stable operation in this mode [73]. Some hysteretic behavior has been observed [63], and this is not fully investigated. It is believed to be caused by changes in the adhesion between the membrane and the substrate over time in addition to effects caused by the surface contact during collapse. Another reliability issue is the possible charging of the membrane and stiction problems during collapse.
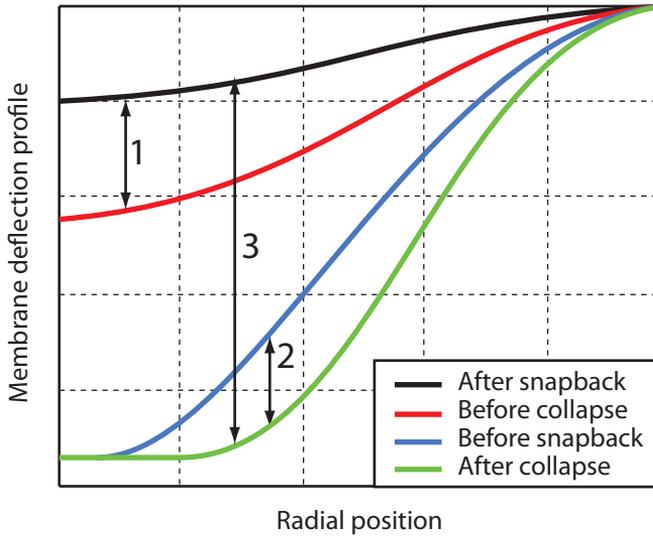
Figure 3.3: Illustration of the three operation regimes of CMUTs. The conventional regime is number 1, the collapsed regime is number 2, whereas the collapse-snapback regime is number 3. The sketch is based on FEM simulations made by Bayram *et al.* [62, 74].

For high power transmission it has been suggested to operate the CMUTs in the collapse-snapback regime [74]. The DC-bias is initially below the collapse voltage. A short high voltage pulse is applied in order to make the membrane collapse and snap back during the cycle of the pulse. This leads to a large membrane displacement amplitude which results in high output pressures. In [74] a pulse of 1 μs was used, and the output pressure of the collapse-snapback operation was more than doubled compared to the conventional mode. The collapse-snapback regime is marked as number 3 in Fig. 3.3. Device reliability might also be an issue in the collapse-snapback

regime. The large displacements of the membrane may be damaging for the membrane and electrode materials.

Even though collapse regime operation seems to have a number of advantages, it does not seem to have convinced the research community. The charging of the membrane when it is in contact with the substrate is probably the biggest concern.

In this thesis we have mainly focused on the conventional regime of operation, however, in Paper I and II we have included simulations of CMUTs operating the the collapsed regime.

3.4   Advantages and challenges of CMUTs

There are many possible advantages for CMUT arrays compared to traditional piezoelectric transducers. Some are already mentioned, such as the improved impedance match in both fluid and air [56, 75]. With a good impedance match, it is possible to achieve wide bandwidths. Piezoelectric transducers are usually limited to 60 - 80 % bandwidth, whereas bandwidths above 100 % easily can be achieved for CMUT arrays. As discussed in Ch. 2.3, the bandwidth is an important parameter in determining the image resolution, and wider bandwidths provide better image resolution. Comparison of image quality in in-vitro images between CMUT arrays and piezocomposite transducers show that the radial resolution is improved [76, 77], the contrast is significantly enhanced, and field of view is superior in images from CMUT arrays [78].

One great advantage with CMUTs it the manufacturing process. The photolithographic techniques enable very small dimensions both in depth and laterally. It also gives freedom to the designer to vary the size and shape of CMUT cells and array elements as he likes. The CMUT fabrication process meets the need for small elements and minimal kerf between adjacent elements, which is important in high frequency ultrasound imaging.

Micromachining fabrication involves parallel processing of several wafers, hence, the production cost can be low when a process is optimized. Since CMUTs and integrated circuits (ICs) are made in the same materials, and using the same kind of fabrication processes, the integration of custom made transmit and receive circuitry can be realized using through wafer vias and 3D-stacking of the transducer chip and several IC chips. [67, 77]

Possible challenges for CMUTs in medical imaging is low sensitivity leading to limited penetration depth [76, 77]. Many different membrane sizes, shapes, and configurations have been tested in order to improve the efficiency of the transducer. An improved transmission and reception efficiency

using rectangular and tent configurations compared to square membranes has been shown [70]. Improved electromechanical coupling coefficient and uniformity of the membrane deflection was shown through finite element analysis (FEA) simulations by introducing trenches in the edge areas of the membrane, and by altering the shape of the supporting structure [79]. Dual electrode CMUTs have also been suggested to improve the sensitivity in reception [73, 80].

CMUTs have a lower dielectric constant than PZT, thus the capacitance of a CMUT element i significantly smaller and the electrical impedance much larger than a PZT element. This may reduce the signal-to-noise ratio and should be corrected to obtain the depth of penetration currently obtained by PZT arrays. Tuning the CMUT impedance, using passive components such as inductors, capacitors, and resistors have been suggested [77]. These can be placed in the probe handle, probe connector, and/or the ultrasound system, depending on the topology of the particular tuning circuit that is selected. Pre-amplifiers can also be used to alleviate the SNR problem, but these must be placed in the probe handle to minimize parasitic capacitances between the CMUT and the pre-amp [77].

Charging effects is a well known reliability problem in CMUTs and other MEMS devices [60, 81, 82]. Charges can be trapped in the dielectric layer within the cavity. This may happen during the fabrication process or due to the strong electrical fields within the transducer cavities during operation [83]. The trapped charges may shield the electrode surface, thus causing unpredictable changes that depend on both frequency and amplitude of the applied electric signal. In collapsed mode operation the trapped charges may create electrostatic forces that prevent the membrane from snapping back after collapse [84]. Introduction of isolation posts in the cavities, allows for collapse mode operation without trapped charges and hysteresis effects [83, 85, 86]. Hence, the reported improved transduction efficiency in collapsed mode operation compared to conventional mode may be maintained [63].

Another effect which should be properly understood and controlled is the acoustic crosstalk both in the fluid-CMUT interface and in the supporting structure. This will be thoroughly described and discussed in Chapter 5.

Chapter 4

Fabrication

Fabrication of CMUTs can either be performed by surface micromachining or wafer bonding. Both techniques are briefly explained below.

4.1 Surface micromachining

In surface micromachining, as the name indicates, the processing is done on the surface of a silicon wafer by means of thin film deposition, thin film etching and photolithography. The process usually starts with a low resistivity silicon wafer, which is heavily doped to achieve high conductivity at the surface. This will become the bottom electrode of the CMUT. A silicon nitride (Si_3N_4) layer is deposited on the wafer, followed by a sacrificial layer which is deposited and patterned to form the cavity. The membrane layer is deposited on top of the sacrificial layer. Silicon nitride is most commonly used as a membrane material, and both Low pressure chemical vapor deposition (LPCVD) [59] and Plasma enhanced chemical vapor deposition (PECVD) nitride [87] has been shown. Polysilicon membranes have also been demonstrated [88]. To form the cavities, the sacrificial layer is selectively etched through small etch holes in the membrane. Afterwards, the etch holes are sealed and the membrane is etched to its final thickness. A metal layer is finally sputtered on top of the membrane and then patterned to form the top electrodes and connection pads [89]. The process steps are illustrated in Fig. 4.1.

There are however some limitations in the surface micromachining technique [90]. For high frequency devices the fill-factor is limited because of the small size of the active area. For low frequency operation one wants large and thick membranes, and high output pressures require large cavity depths. However high stresses and stiction problems involved in thin film
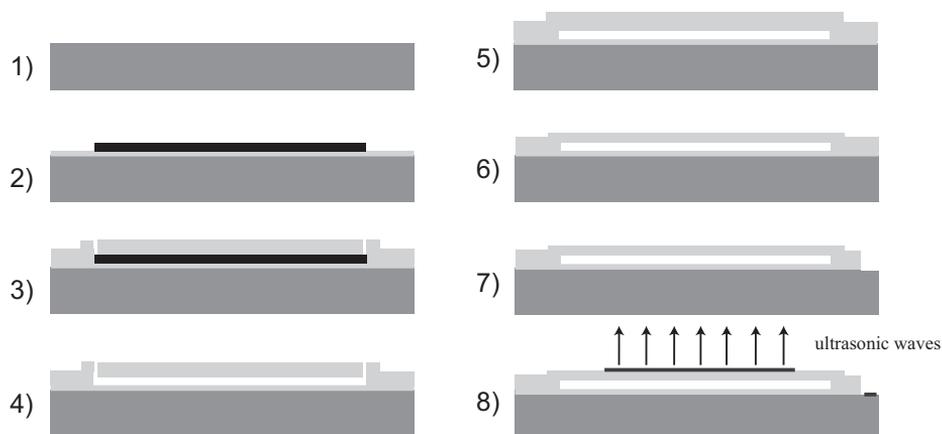
Figure 4.1: Illustration of a CMUT made through surface micromachining. 1) Initial silicon wafer. 2) A layer of silicon nitride is deposited on the bottom wafer, and a sacrificial layer deposited and patterned to define the cavity. 3) Silicon nitride is deposited to define membrane. Small etch holes are patterned in the Si_3N_4. 4) Sacrificial layer is removed to release the membrane. 5) Etch holes are sealed with an additional layer of Si_3N_4. 6) The membrane is etched to its final thickness. 7) Opening in the silicon nitride is etched to provide electrical contact to the bottom wafer. 8) The top electrode and contact to the bottom electrode is made by metal deposition and patterning.

depositions makes it difficult and unpractical to deposit thick sacrificial layers and to release large membranes.

The presence of etch holes in the membranes affects the uniformity of the membranes and it reduces the fill-factor of the array. Caliano *et al.* [91] have suggested a reverse fabrication method, where the etch holes are placed at the bottom of the cavity instead of the membrane side. Other advantages of this technique compared to some forms of surface micromachining, is that the acoustically active membrane is LPCVD silicon nitride instead of PECVD silicon nitride, since LPCVD is known to have less defects than PECVD [92]. The electric interconnects are placed on the back side of the device, and instead of having bulk silicon as the support structure for the CMUTs, this technique suggests to replace it with an acoustic backing layer, which will prevent substrate ringing [93]. The process steps are described in Fig. 4.2 [91, 94].

4.2   Wafer bonding

An alternative way of fabricating CMUTs is through wafer bonding, also referred to as bulk micromachining. One avoids the wet sacrificial layer etch and its associated problems, and this makes it possible to fabricate larger membranes. The membranes and cavities are defined on separate wafers which are bonded under vacuum conditions. The cavities are etched into the bottom silicon wafer, which also works as the bottom electrode of the device. The membrane (e.g. Si_3N_4) is deposited on another silicon wafer, which in turn is bonded to the bottom wafer. Afterwards, the silicon of the top wafer is removed, and metal for the top electrode is sputtered and patterned. This is illustrated in Fig. 4.3.

CMUTs realized through wafer bonding was first reported in 2003 by Huang et. al [90]. Compared to surface micromachining techniques, wafer bonding shows a higher degree of predictability and involves fewer process steps. This reduces the process turnaround time and potentially increases the yield. It sets less process limitation on the size and shape of the membrane and the cavity. A variety of materials may be used for the membrane, e.g. high resistivity silicon [90, 95, 96] and LPCVD silicon nitride [97–99] have been demonstrated.

4.3   CMUT-electronics integration

One of the claimed benefits of using CMUT arrays as ultrasonic transducers is the relative ease to integrate the electronic circuits that are needed for
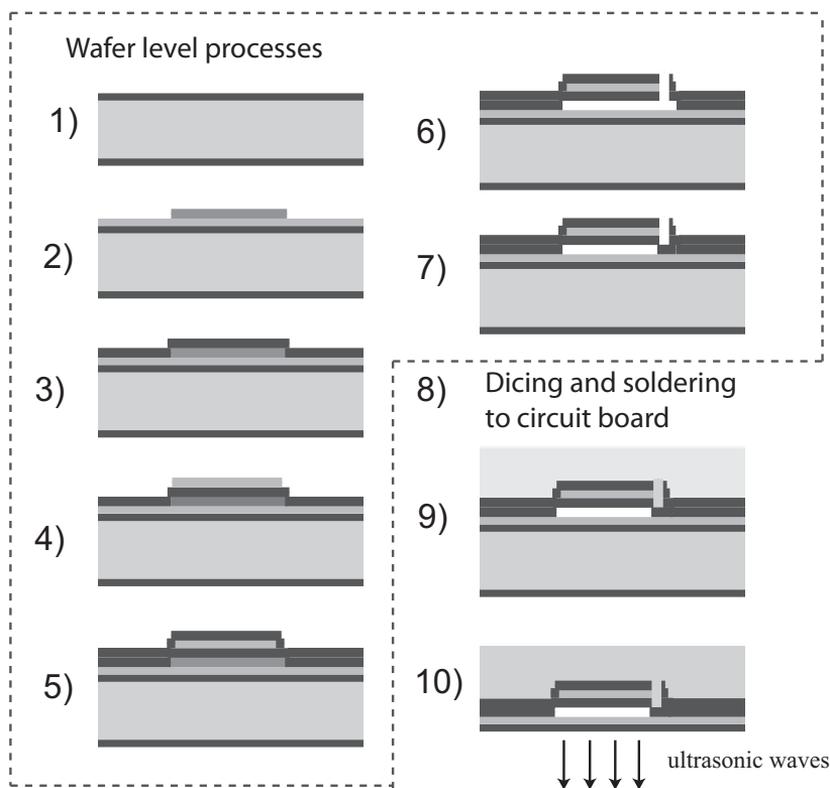
Figure 4.2: Illustration of CMUT made through the reverse fabrication process. 1) Initial silicon wafer coated with a layer of silicon nitride. 2) Evaporation of ground electrode (aluminium), followed by a deposition and patterning of a sacrificial layer of chromium, which defines the cavities. 3) A layer of PECVD silicon nitride is deposited to form the back plate of the CMUT cell. 4) Aluminium is sputtered and patterned to form the bottom electrode. 5) A layer of PECVD silicon nitride is deposited to protect the electrode surface. 5) Etching holes are opened to access the sacrificial layer, and the cavity is evacuated. 7) The cavity is sealed using PECVD silicon nitride. 8) The wafer is diced and soldered either to a flexible circuit board or a rigid PCB. 9) Acoustic backing is cast on the device side of the chip. 10) The LPCVD silicon nitride layer on the back side of the wafer and the silicon bulk are removed to release the membrane.
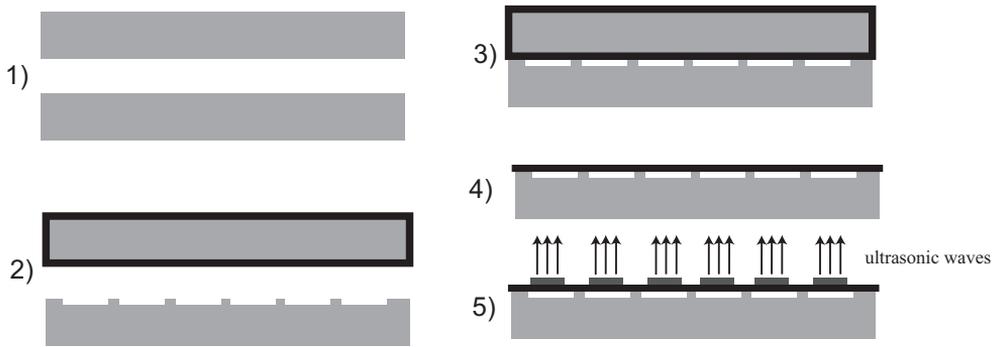
Figure 4.3: Illustration of CMUT fabrication by wafer bonding. 1) Top and bottom silicon wafer. 2) Cavities etched in bottom wafer and membrane deposited on top wafer. 3) Top and bottom wafer bonded together. 4) Removed the handling wafer on the top. 5) Top electrode deposited and patterned.

both transmission and reception. One approach that has been investigated is to integrate the CMUT cells in a standard BiCMOS process [100], and the integration of CMUT and signal conditioning electronics on the same silicon substrate has been reported [101, 102]. With these techniques, the CMUT and electronics compete for the same die area, something that might limit both the sophistication of the electronics and the signal-to-noise ratio. Another CMUT-on-CMOS technique is the monolithic integration [103–106], where the CMUT is manufactured on top of an already made CMOS circuit with analog switching electronics.

A different approach is to make electronic circuits and CMUT arrays on separate wafers and bond these to form a stack, connecting to each array element with through wafer vias [107]. Flip-chip bonding between a 2D CMUT array and a custom designed integrated circuit for volumetric ultrasound imaging, using anisotropic conducting film (ACF) or using Sn/Pb solder balls has been demonstrated [108]. With flip-chip bonding techniques several silicon wafers with electronic circuits can be bonded in layers underneath the CMUT substrate, forming a 3D-stack. 3D-integration of electronics is advancing fast, and new bonding techniques are being developed in order to bond very thin layers together. This might prove beneficial in the development of future CMUT arrays with integrated electronics.

As an alterative to through wafer vias, trench isolation of the substrate has been suggested [95, 109]. The electrical signal is brought to the back of

the device through a highly conductive silicon substrate, and neighboring array elements are separated electrically by trenches on both the device layer and the bulk silicon.

In high frequency transducers for intravascular imaging or other invasive applications, it might be necessary to include a lot of the transmitter and receiver electronics in the front-end of the transducer. In Paper VI we present simulation results showing the radiation response from infinite CMUT arrays with three silicon layers underneath. We examine three different bonding techniques, namely Solid Liquid Interdiffusion (SLID) bonding, direct fusion bonding, and anisotropic adhesive, and show the importance of considering the composition of the stack to prevent surface acoustic waves from damaging the response. This is further commented in Section 5.1.4.

4.4 CMUTs made in the SMiDA-project

An important part of the SMiDA-project has been fabrication of CMUT arrays. The processing has been performed at SINTEF MiNaLab in Oslo, and PhD-candidate Kjersti Midtbø from the SMiDA-project at the Department of Electronics and Telecommunications at NTNU has been actively involved. Two generations of CMUTs have been processed, and both are based on the wafer bonding process described above. The main difference between them is that the first generation (CMUT 1) had electric contacting on the top, whereas the second generation (CMUT 2) had through silicon vias (TSV) from the bottom electrode, enabling electric contacting from the back side of the array and ground potential on the front. The geometric properties of the CMUTs are given in Table 4.1, and a brief description of the CMUT arrays that are used in measurements presented in this thesis is given below. In addition to the described arrays, other geometries were included in the processing of CMUT 1 and other membrane stacks were fabricated on bottom wafers equal to those described as CMUT 2. For further details, we refer to [97, 110–112].

4.4.1 CMUT 1: with top electrode contacting

The first generation of CMUTs were fabricated with top electrode contacting, as shown in Fig. 4.4(a). The fabrication process is described by Midtbø *et al.* [97]. This was a linear 1D-array where two rows of CMUTs were connected to form elements. The CMUTs were originally designed for collapsed mode operation at 30 MHz center frequency in fluid with a 3 dB bandwidth of 100 %. Measurements in conventional mode operation showed resonance

Table 4.1: Geometric properties of CMUT 1 and 2.

	CMUT 1	CMUT 2
Membrane radius [μm]	5.7	5.7
Cavity gap [nm]	120	60
Cell pitch [μm]	12.5	12.5
Element width [μm]	25	25
Electrode radius [μm]	3.5 (top electrode)	4 (bottom electrode)
Electrode line width [μm]	2	NA
Membrane thickness, LPCVD [nm]	100	100
Membrane thickness, SiO$_2$ [nm]	NA	50
Top electrode thickness [nm]	500 (aluminium)	150 (titanium)
Membrane thickness, PECVD [nm]	NA	150
Number of CMUTs per element	2 $\times$ 104	2 $\times$ 104
Number of elements per array	36	36
Array area [mm^2]	0.9 $\times$ 1.3	0.9 $\times$ 1.3

frequencies around 10 MHz at low DC-bias voltages.

On the top wafer, a 100 nm silicon oxide layer was grown before the a 100 nm layer of LPCVD silicon nitride was deposited. In the bottom wafer, 120 nm deep cavities were etched by Reactive Ion Etching (RIE). The wafers were pre-bonded in room temperature, and further annealing was done by heat treatment. The top wafer was etched by Tetramethylammonium Hydroxide (TMAH) to expose the membranes. Finally, the aluminium was deposited and patterned to form the top electrodes. The CMUT 1 is shown in Fig. 4.4(a). Fig. 4.4(b) shows a chip with 36 elements, each connected to a bond pad at the edge of the chip. The active part of the chip is 0.9 $\times$ 1.3 mm^2, and total size of the chip is 4 $\times$ 4 mm^2.

4.4.2   CMUT 2: with through silicon vias and bottom electrode contacting

The second generation of CMUTs differs from the first in many aspects, however, the radius, CMUT cell pitch, and element size are the same as in CMUT 1. The main difference is that the electrical connections to the array elements are achieved by via-holes through a thinned silicon wafer, and connected to lines of aluminium on the back side of the array. The front side is uniform and electrically grounded. The fabrication process is described by Due-Hansen *et al.* [110, 111], however the membranes in the CMUTs described in this thesis differ from those described in the beforementioned

(a)   (b)
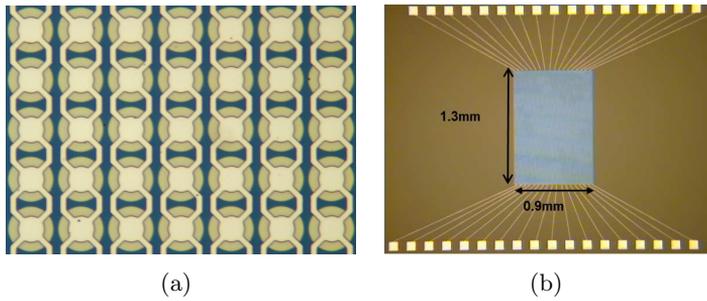
Figure 4.4: (a) Optical microscope image of CMUT 1 with symmetric elec-
trodes. The top electrodes are the bright yellow pattern, while the mem-
branes are circles with a darker tone of yellow (b) A chip showing an array
with 36 line elements. Each bond pad is connected to a line of 2×104
CMUTs. (Courtesy Kjersti Midtbø)

papers.

The CMUT cells are organized in groups of two by two cells, and a
via hole is placed at the center of the cavity of one of the four cells. The
preparation of the bottom wafer was performed as follows. First, the TSVs
and the areas for the CMUT cavities were etched by RIE in the bottom
wafer. Then, thermal SiO_2 was grown for electrical isolation, and the TSVs
and etched cavities were filled with polysilicon which was doped to enable
good conductivity. Following the polysilicon deposition, the wafer surface
was polished by Chemical-mechanical planarization (CMP) to obtain a flat
surface suitable for CMUT cavity etching, and to expose monocrystalline
silicon for wafer bonding. The CMP was performed at Fraunhofer ISiT.
The cavities of the CMUTs, with a nominal depth of 60 nm, were realized
by RIE of polysilicon and SiO_2. A 25 μm $\times$ 25 μm section of the bottom
wafer is illustrated in the upper part of Fig. 4.5. The CMUT cavities have
the same area and shape as the area covered with polysilicon and silicon
oxide in the illustration of the bottom electrode. The lower part of Fig. 4.5
illustrates side views of the diagonal and through the center of two adjacent
CMUTs. The view along the diagonal of the cluster shows two cavities,
each with a diameter of 11.4 μm, whereas the view across the center of two
CMUTs shows a cavity length of 23.9 μm.

The membranes of CMUT 2 consist of four different layers forming a
stack. The two bottom layers are the result of the wafer bonding process,
whereas the two topmost layers are deposited afterwards. To prepare the
handling wafer for the wafer bonding process, a 50 nm SiO_2 layer was grown
and a 100 nm thick silicon nitride membrane was deposited using LPCVD.
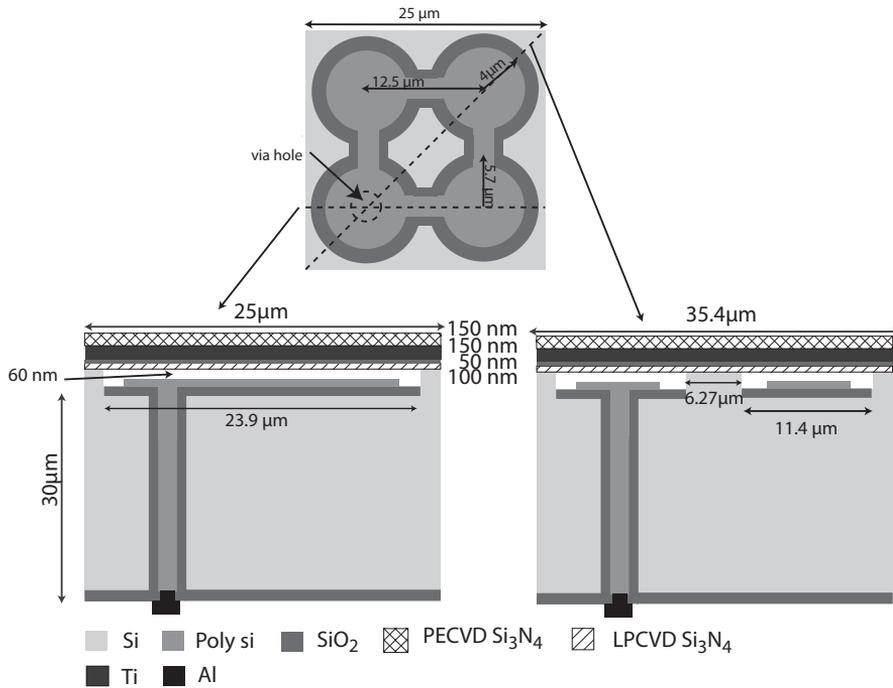
Figure 4.5: The top of the figure shows an illustration of the bottom electrode of a two by two cluster of CMUTs. The via hole is placed at the center of one of the CMUTs. A side view of the wafer is shown in the lower part of the figure. The bottom silicon wafer is thinned to about 30 μm and aluminum is patterned on the backside to connect to the poly silicon filling of the via hole. The membrane consists of four layers, 100 nm LPCVD silicon nitride at the bottom, 50 nm silicon oxide and 150 nm titanium in the middle and 150 nm PECVD silicon nitride at the top.

The handling wafer was then fusion bonded to the bottom wafer. An opening was etched in the handling wafer to access the membranes before the bottom wafer was thinned to 30 μm thickness. A titanium layer of 150 nm, working as the top electrode, was deposited on top of the exposed oxide layer covering the silicon nitride membrane. As a fourth layer, silicon nitride with a thickness of 150 nm was deposited by PECVD. All the layers add stiffness and weight to the CMUT membranes to match the design requirements. On the back side of the bottom wafer, the via holes from the clustered CMUTs are connected by aluminium lines forming elements with a total size of 25 μm $\times$ 1300 μm.

(a)   (b)
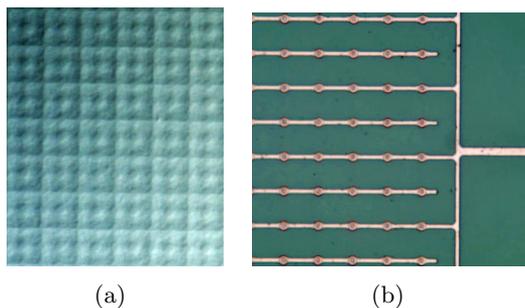
Figure 4.6: a) Optical microscope image of the membrane side of CMUT 2. The 2×2-CMUT clusters can clearly be seen. b)Optical image of the backside of CMUT 2. Each circle is connected to the via hole which connects two by two CMUTs. In this particular configuration there is one bond pad on each side of the array, and each pad connects to every second row of CMUTs.

In Fig. 4.6(a), a optical microscopy image, using a Nomarski-prism to enhance deflection of the surface. The image clearly shows the clusters of two by two CMUTs which are electrically connected through the bottom electrode and acoustically connected through the membrane. A section of the backside of the CMUT array is shown in Fig. 4.6(b), where each circle connects to one TSV, and each line connects 52 CMUT clusters, in total 2 × 104 CMUT cells. There are 36 lines of CMUTs on one array.

Chapter 5

CMUT Array Crosstalk

One of the challenges in the design of CMUT transducers meant for immersion applications, is to minimize the crosstalk between transducer elements caused by acoustic coupling through the fluid medium outside the array and through the silicon substrate supporting the CMUT membranes. In addition, there is electric coupling between the CMUT cells because of the fact that several cells are connected to form larger transducer elements.

In this work we focus on two main contributions to the acoustic crosstalk generated in CMUT arrays; surface acoustic waves which travel in the silicon substrate and dispersive guided modes which are generated in the CMUT-fluid interface [113, 114]. In the work presented in Paper I and VI we include substrate motion in the model, whereas in Paper II, III, IV, V, and VII we assume that the CMUT cells are mounted on a perfectly rigid substrate, and instead focus on the fluid coupled interaction between the CMUT membranes.

5.1   Waves in the silicon substrate

When CMUT arrays are excited by an AC-voltage, the membranes of the array will start to vibrate, and in order for the membranes to transmit acoustic energy into the medium of interest (e.g. the human body in medical imaging), a rigid supporting structure is needed. Without any support, the net forces transmitted into the fluid will be small. When a silicon substrate is present to support the CMUTs, excitation of the membrane will also lead to forces working on the bottom electrode and the membrane support, which both are part of the silicon substrate. This effect cannot be ignored [93, 115].

Longitudinal waves propagating into the substrate may be reflected from

the bottom and picked up by the CMUT. However, at most frequencies these waves are out of phase with the excitation signal. The exception is at frequencies where the substrate becomes resonant. This happens when the thickness of the substrate is an integer multiple of half of the wavelength [116]:

$$f_R = \frac{nv}{2t} \quad , \tag{5.1}$$

where f_R is the substrate resonance frequency, n is an integer, v is the longitudinal velocity of sound in the substrate and t is the substrate thickness. The resonance frequencies depends on the material properties and geometry of the substrate. For instance a substrate of 300 μm thickness and a longitudinal velocity of 8500 m/s will resonate close to 14 MHz and 28 MHz, and a 600 μm thick substrate will experience resonances around 7 MHz, 14 MHz, 21 MHz and 28 MHz. At these frequencies the substrate will resonate, and affect the device operation in a negative way. Thinning the substrate to increase the substrate resonance frequency to levels above the frequency range of interest might be a solution. However, in thin silicon substrates, plate modes, such as Lamb waves may be excited. In thicker silicon substrates, or when the CMUT array is backed with a damping material, plate modes will no longer be excited due to the losses and the thickness of the structure. However, surface acoustic waves (SAW) might still be excited. Such waves may become leaky, and affect the overall radiation from the array.

5.1.1   Surface acoustic waves

Surface acoustic waves (SAW), often referred to as Rayleigh waves, were first described by Lord Rayleigh in 1885 [117]. Surface waves travel along the surface of solids, and include both longitudinal and transverse motion, resulting in an elliptical particle motion [118]. The amplitude of the wave decreases with the distance from the surface, and motion is limited to a surface layer of thickness corresponding to about 1 - 2 wavelengths. This is illustrated in Fig. 5.1. The speed of the surface wave is slightly lower than the shear wave velocity of the material . Rayleigh waves may become leaky, and couple to a fluid medium adjacent to the solid.

   In CMUT arrays we seek to minimize the effect of the surface acoustic waves. There are, however, other areas where the generation of SAW may be useful. Most commonly, SAW is used in electronics devices, such as SAW filters, oscillators and transformers. These devices involve transduction of energy from the electric to the acoustic domain by the use of piezoelectric materials. In a SAW filter the electric signal is transformed to a surface
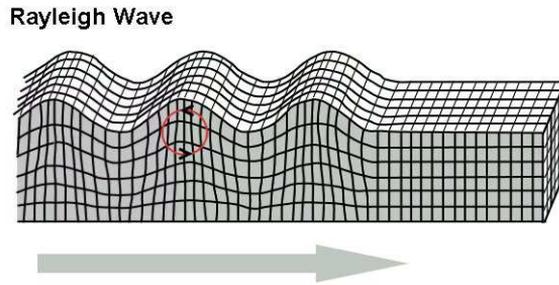
Rayleigh Wave

Figure 5.1: Illustration of a Rayleigh wave, also known as a surface acoustic wave, propagating in the direction indicated by the arrow. Courtesy Wikimedia Commons.

acoustic wave in one end of the device, and hence delayed as it propagates along the surface of the device. At the other end of the device the wave is transformed back to an outgoing electric signal. SAW filters were previously used as bandpass filters in TVs and they are still used in mobile telephones and satellite communications [119, 120].

5.1.2 Lamb waves

Lamb waves where first described in 1917 by H. Lamb [121]. Lamb waves are plate modes which are similar to surface waves except they can only be generated in plates which are a few wavelengths thick. These waves are complex vibrational waves that propagate parallel to the surface throughout the thickness of the material. With Lamb waves, a number of modes of particle vibration are possible, but the two most common are the zero-order symmetrical and asymmetrical modes, as illustrated in Fig. 5.2. The complex motion of the particles is similar to the elliptical orbits for surface waves. Symmetrical Lamb waves move in a symmetrical fashion about the median plane of the plate [118]. The asymmetrical Lamb wave mode is often called the "flexural mode" because a large portion of the motion moves in a normal direction to the plate, and little motion occurs in the direction parallel to the plate. In this mode, the body of the plate bends as the two surfaces move in the same direction.
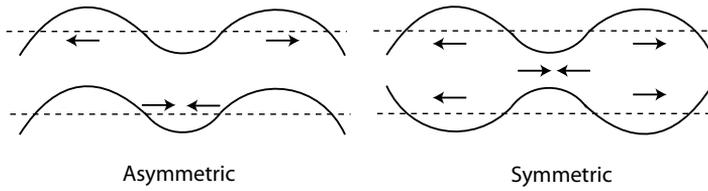
Figure 5.2: Illustration of a symmetric and asymmetric Lamb waves.

5.1.3   SAW and Lamb waves in CMUT arrays

When the CMUTs are excited, the forces on the top electrode serve to launch acoustic waves into the medium of interest, and simultaneously equal forces are placed on the substrate electrode and the structure supporting the edge of the membrane. These forces may excite surface acoustic waves traveling along the substrate surface, contributing to the total movement of the membranes. Because of the existence of the soft, cushion-like membranes, the waves are not easily damped by the fluid medium. However, the surface wave is not entirely protected by the membranes, resulting in partial damping of the waves in the areas without CMUT cavities and also somewhat by the cushioning effect of the membranes. This induces leakage of acoustic energy into the fluid, which may affect the radiation pattern [114].

The excitation of surface waves is strong when the phase velocity of the surface wave matches the phase velocity along the array of the wave excited in the fluid outside the array. At a certain steering angle, the surface displacement from the SAW will be almost in phase with the membrane vibrations, and the excited wave is enhanced. At a slightly different steering angle, the two displacements are out of phase, and the excitation goes through a minimum. Examples of this is shown in Paper I and VI. As shown in Fig. 5.1, the SAW is exponentially damped as it penetrates into the substrate. For an acoustically absorbing backing material to damp the surface wave, the substrate can not be thicker than a certain limit. If the substrate is thicker than this limit, the impedance of the surface may become close to or lower than the impedance of the fluid (1.5 MRayl for pure water) for certain steering angles. When this happens, the resonance and antiresonance will severely affect the transmit efficiency.

Unwanted acoustic effects because of waves in the substrate has been investigated by several research groups. Trailing echoes due to substrate ringing is clearly observed in immersion transducers with 650 μm substrate thickness at 7 MHz [93]. The radiation patterns from unbacked CMUT

transducers with 180 μm and 480 μm thick substrates are compared at 4 MHz, and it is shown that Lamb waves are generated in the silicon wafer, which gives a significant dip at 22° and 32° steering angle respectively [59, 122]. It is also shown that the angle at which the dip in the radiation pattern occurs is dependent on the transmit frequency [59]. Those measurement results are reproduced using the model presented in Ch. 6.3, and presented in Fig. 3 and 4 of Paper VI. Both surface acoustic waves in semi-infinite substrates and Lamb waves in thin substrates were investigated through finite element analysis and boundary element method (FEA/BEM) by Wilm *et al.* [114]. The simulations show that both these wave modes may affect the radiation pattern of the array.

5.1.4 Minimizing the effect of substrate ringing

To minimize unwanted acoustic waves in the substrate, a damping material should be attached to the back side of the transducer. To avoid reflection of waves at the interface between the backing material and the substrate, the backing material should have an acoustic impedance which matches the silicon substrate. The material should also be lossy, so that the energy entering the backing is efficiently dissipated. High thermal conductivity may also be beneficial to enable the transfer of heat from the transducer device [123]. Backing materials are usually composites consisting of heavy metal particles, often tungsten, and a softer filling material, such as epoxy. It is possible to tune the acoustic impedance of such composites by adjusting the volume fraction of metal particles [124, 125]. To achieve sufficiently damping and proper acoustic match it may be necessary to include rather thick layers of backing materials. If the available space for acoustic backing is limited, it has been proposed that using a structured bottom surface of the backing material might be beneficial [116, 126]. This might for instance be the case in intravascular devices. Thinning the substrate in order to avoid resonant modes occurring in the frequency spectrum of interest has also been proposed [115]. However, one must take care not to thin the substrate to the extent where it is not rigid enough to withstand the motion of the membrane, and hence not able to transfer the energy from the membrane vibration into waves in the fluid.

Jin *et al.* [122] suggest the introduction of deep trench isolation between neighboring elements to reduce Lamb wave cross coupling. In addition, they show that the reduction of the substrate thickness moved the radiation angle of the A0-mode of the lamb wave from 22° to 35°, and hence, into a less important area of the array response.

In the work presented in this thesis, we use an expanded version of the

CMUT array model presented in Ch. 6.3, where the motion of the silicon substrate is included. How the substrate motion is included in the model, is described in detail in Paper VI, and the same method is also used to achieve the results presented in Paper I. We show that the surface acoustic wave generated in the substrate by the excitation of the CMUT membranes, may under certain conditions affect the overall response of the array. It is the thickness of the substrate (or the thickness and composition of a 3D-stack containing a CMUT array on top and multiple integrated circuits underneath), which determine if the SAW damages the array response or not. If the substrate (or stack) is thin enough, the acoustic backing material manages to damp the SAW, and the overall response remains unaffected. We assume that the array has proper acoustic backing which prevents longitudinal waves from reflecting from the substrate bottom. However, we include simulation results showing how the ringing in the pulse response increases if reflections from the bottom of the backing material are allowed.

5.2 Dispersive guided modes

The most important contribution to crosstalk is often referred to as dispersive guided modes [113, 127] which are because of the geometric nature of the transducer and its interaction with the fluid [114]. This has been widely discussed during the last few years, [128–131]. The finite element method has been a useful tool to analyze crosstalk [130, 132], but analytical approaches have also been suggested [128]. The effect of such modes has been verified by experimental work by several groups [113, 129]. In our work we use the Fourier transform method described in Ch. 6.3 to model the resonant system and show how crosstalk affects especially the off-axis radiation pattern.

The total membrane motion is a combination of many vibration modes with different resonance frequencies, and the excitation frequency determines which mode is dominating. Beam steering to an off-axis direction involves phase shifts in the excitation of adjacent elements, where each element usually consist of more than one CMUT. Both asymmetric modes within each CMUT and interactions between membrane vibrations within an element, or in adjacent elements, can cause local resonances in the CMUT-fluid interface. The fluid acts as a coupling medium between the membranes, and the result may be a distortion of the overall array response. This is described through modeling and experiments in [129]. A schematic illustration of how fluid may be pushed from one membrane to the next when there are phase shifts between them is given in Fig. 5.3. In the figure the phase shift

between the CMUTs is 180°. Phase shifts used in an ultrasound imaging situation is usually much lower.
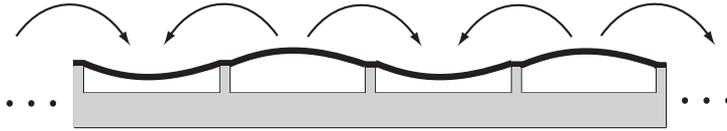
Figure 5.3: Illustration of fluid being pushed from one CMUT to another when there are phase differences between neighbor CMUTs.

If each transducer element only consist of one CMUT (or one line of CMUTs, if steering is perpendicular to the direction of the line), there will be phase shifts between every CMUT (or line) when the ultrasound beam is steered to an off-axis direction. Local resonances in the CMUT-fluid interface will in such an array be limited to excited asymmetric vibration modes in the CMUT cells. Examples of such modes is shown in Fig. 6.10 in Ch. 6. However, when several CMUTs are combined into larger elements, the applied voltage on all CMUTs within the element will be the same. In such a configuration the phase shifts needed for beam steering will be between elements, and not between single CMUTs. The surroundings experienced by the CMUTs within the elements will vary across the element when they are transmitting or receiving ultrasonic waves from skew angles. Hence, resonances between CMUTs within the element or CMUTs in adjacent elements might occur. An example of the transmitted power into plane waves in water is shown in Fig. 6.15, and it is also described in Paper II, III, IV, and VII.

The number of CMUTs per element affects how many possible resonances there are that might be excited. In Fig. 5.4 it is shown that the response from an array with 2 lines of CMUTs per element has one severe dip, while the array with 3 lines has 2 dips, and 4 lines per element results in 3 dips in the response.

The Q-factor of these notches are heavily influenced by the viscosity of the adjacent fluid. In Paper VII we show that the resonances have lower Q-factors when the CMUTs radiate into high viscosity fluids such as rapeseed oil, than in low viscosity fluids like water and kerosene. This shows that characterizing CMUT arrays only in vegetable oil, might be insufficient if one wants to have full insight into the acoustics at the CMUT-fluid interface.

Many CMUT designers choose to have a larger distance between CMUTs in adjacent elements than between CMUTs within the same element. We
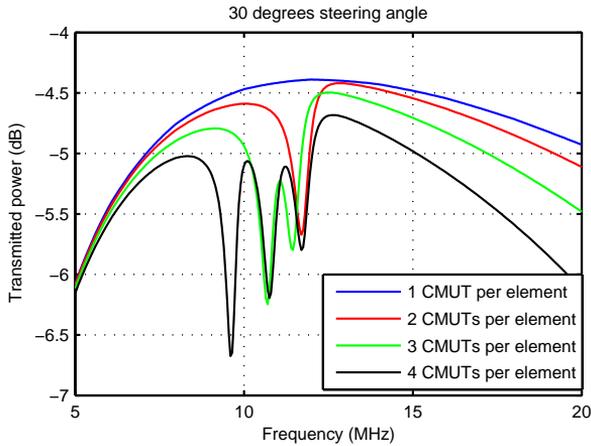
Figure 5.4: The number of CMUTs per element affects the number of reso-
nances that are generated when the ultrasonic beam is steered to an off-axis
direction. The simulation show CMUT arrays radiating 30 ° off-axis into
water.

choose to denote this as a double periodicity, and an illustration is given in
Fig. 5.5. In Paper VII we present simulations which show that resonances
may occur even at broadside radiation from arrays with double periodicity.
This is true if the elements connect three CMUTs or more in the width
direction. When there are only two CMUTs per element, both of them
are next to non-vibrating areas, and hence, experience similar physical con-
ditions. When there are more CMUTs in each element, the surroundings
will differ between the edge CMUTs and the center CMUTs of the element,
and hence, resonances may be excited even when there are no phase shifts
between elements.

5.2.1   Reduction of dispersive guided modes

Several proposals of crosstalk reduction have been presented over the last
years. An acoustic band gap consisting of an additional vacuum gap be-
tween the CMUT cells was introduced by Bayram *et al.* [133]. According to
finite element calculations the crosstalk was reduced by 10 dB in the conven-
tional operation mode without loss of acoustic pressure of the transmitter
element. Modified transmit waveforms have been proposed by Zhou *et al.*,
[134, 135], reducing crosstalk by 25 dB for small AC-excitation conditions.
This approach requires a programmable waveform transmitter as a part of
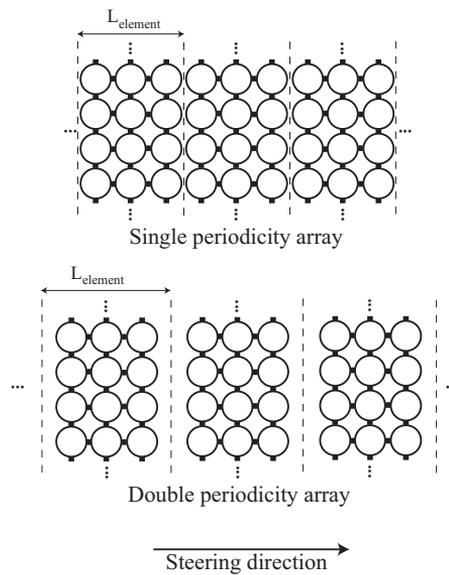
Figure 5.5: Arrays where the distance between the elements is the same as between CMUTs within the element, are denoted as single periodicity array, whereas when an additional element kerf is introduced, the arrays is denoted as double periodicity arrays.

the ultrasound scanner system.

Electrically damping of the resonances by introducing resistors between each CMUT cell was proposed by Rønnekleiv [1]. In simulations this was very efficient, but it might be a challenge to achieve in practice. The simulations also showed that increasing the viscosity of the fluid outside the array by a factor of 1000 compared to water at 3.5 MHz was effective as a mechanically damping of the unwanted resonances. This indicates that the viscosity of the interface material is of importance. In Paper II and VII, simulations show that a thin layer of a soft and lossy material covering the membrane reduce the acoustic crosstalk through the fluid medium. Adding a protective sealant layer on top of the CMUT membranes has been done by Campbell *et al.* [131] and Bayram *et al.* [113], however, their finite element simulations and experiments show that the crosstalk is present with both PDMS and Parylene coating.

Chapter 6

CMUT modeling

Mathematical modeling of capacitive micromachined ultrasonic transducers may be performed with both analytical [1, 57, 75] and numerical methods [62, 71, 136–138]. In reception, the CMUTs detect small ultrasonic signals that are reflected from the adjacent medium. Thus, a linearized small-signal analysis may be used when describing the CMUTs analytically. However, in transmission the magnitude of the vibration might be larger, and nonlinear analysis might be necessary. Numerical methods such as finite element analysis may be useful in such cases.

A simple approximation is to model the CMUT as a parallel plate capacitor. Taking electrostatic and mechanical forces into account, we may estimate the collapse voltage of the structure. To calculate the collapse voltage and resonance frequency more accurately, the shape of the membrane must be taken into account. For circular membranes, it is fairly easy to solve the differential equation describing the deflection of the membrane analytically, whereas for other geometries, numerical methods might be required.

In this chapter, we first give a brief description of finite element modeling of CMUTs, followed by a description of the CMUT as a capacitor. We show how the capacitor model makes it possible to model the CMUT-fluid interaction using equivalent circuits. The main part of the chapter is a thorough description of a CMUT model developed by professor A. Rønnekleiv. This model is based on an analytical capacitor model, where the coupling of several vibration modes of a single CMUT and the coupling between neighboring CMUTs are included. The model was first published in 2005 [1], and it is the basis of the simulations presented in the scientific papers in this thesis.

6.1   Finite element method

Finite element method (FEM) is a numerical method for solving differential-
or integral equations. The method essentially consists of assuming the piece-
wise continuous function for the solution and obtaining the parameters of
the functions in a manner that reduces the error in the solution. In ultra-
sound transducer design it is common to use FEM to analyze the physical
behavior of the transducer. Single elements, arrays of elements, and the
interaction with an adjacent fluid or backing material may be modeled by
FEM.

The defined geometric structure is divided into smaller elements by defin-
ing a mesh, and the differential equations describing the system are solved
for each node in the mesh. The accuracy of the solution depends on the size
of the mesh, and it is possible to vary the mesh size across the geometry.
The mesh grid size should typically be small in areas where there are large
or fast fluctuations in the solution, and large in areas where the variation is
small and predictable. The finite element method is especially useful when
complicated geometries are analyzed.

Many research groups have used finite element analysis to model CMUT
arrays or single CMUTs [71, 138]. Various geometries have been investi-
gated, such as circular, square, hexagonal, rectangular and tent structures.
Finite element analysis is not limited to axis-symmetric geometries, as most
analytical methods are. FEM may in principle analyze large geometries in
an accurate way, but it is possible to limit the number of elements by using
axis-symmetric properties of the geometry. However, since the computation
time depends on the number of elements, full 3D-models including a whole
array of CMUTs and adjacent fluid may become too time consuming to
solve.

In this work we have focused on an accurate analytical model which is
described in Sec. 6.3, hence, finite element models to analyze the CMUTs
was not used. However, the first generation of CMUTs made in the SMiDA
project (CMUT 1) have been analyzed by FEM using COMSOL Multi-
physics (COMSOL AB, Stockholm, Sweden) by Aksnes *et al.* [139]. Leirset
et al. [140] have compared measurements and FEM simulations of CMUT
element cross coupling in the second generation CMUTs (CMUT 2).

6.2   Capacitor model

As mentioned in 3.2, the CMUT is in principle a parallel plate capacitor with
one fixed-, and one free electrode. In a simple first-order model we neglect

all electrical fringing fields and membrane curvature, and we assume that all conductors and contacts are perfect. The CMUT is assumed to be operating in vacuum, and the restoring forces of the membrane increase linearly with the deflection.

A voltage, V, applied across the capacitor charges the two plates with $\pm Q$ respectively, according to the relation $q = \frac{c_m}{V}$. The electric energy per area is thus given by:

$$E = \frac{1}{2}c_m V^2 = \frac{q^2}{2c_m} \quad , \tag{6.1}$$

where c_m is the per area capacitance, V is the applied voltage, and q is the charge per area. If we consider a small change of deflection in an isolated small part of the membrane, the deflection becomes $w + dw$ and the change of electrical energy becomes:

$$E + dE = E + \frac{dE}{dw}dw \quad . \tag{6.2}$$

We can thus balance the per area work done by the electrical charge and the change in electrical energy:

$$\tilde{F}_q dw + \frac{dE}{dw}dw = 0 \quad . \tag{6.3}$$

We may solve eq. (6.3) for the electrostatic force $\tilde{F}_q$, and write:

$$\tilde{F}_q = -\frac{d}{dw}E = -\frac{d}{dw}\frac{q^2}{2c_m}\bigg|_{q=\text{const}} = \frac{q^2}{2c_m^2}\frac{dc_m}{dw} = \frac{1}{2}V^2\frac{dc_m}{dw} \quad , \tag{6.4}$$

where the per area capacitance, c_m, is found to be:

$$c_m = \frac{\varepsilon_0}{d_0 - w_0} \quad , \tag{6.5}$$

The deflection is denoted w_0, ε_0 is the permittivity of free space, and the distance, d_0, is a sum of the cavity depth and effective thicknesses of the material layers between the electrodes, given by:

$$d_0 = \sum \frac{h_i}{\varepsilon_{ri}} \quad , \tag{6.6}$$

where h_i is the thickness, and ε_{ri} is the permittivity of the material in layer i. The capacitance of the whole CMUT then becomes:

$$C_m = \frac{\varepsilon_0 A}{d_0 - w_0}dxdy \quad , \tag{6.7}$$

z-axis

initial position, unbiased membrane

top electrode

h_1

h_2 vacuum gap

h_3

bottom electrode

substrate

membrane deflected by w_0 due to bias voltage V_0

$\tilde{F}_{q0}$

w_0
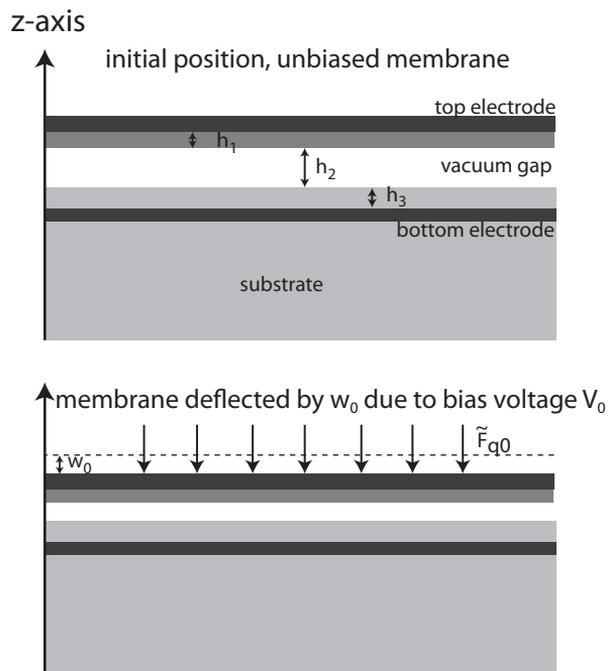
Figure 6.1: Simple sketch of the important geometric parameters of the parallel plate capacitor model.

where A is the area of the CMUT. Fig. 6.1 shows an example of a CMUT with a membrane thickness of h_1, a cavity depth of h_2 and an isolation layer between the bottom electrode and the cavity of thickness h_3.

There are three contributions to the total electrostatic force experienced by the membrane. Firstly, the force caused by DC-bias V_0, and deflection w_0; $\tilde{F}_{q0}$. Secondly, the force due to the small-signal AC-voltage v, $\tilde{F}_{qv}$ contributes, and the third force contribution is caused by the small-signal deflection w_1, denoted $\tilde{F}_{qw}$. The total applied voltage is thus a sum of a DC- and an AC-signal, given by $V = V_0 + v\sin(\omega t)$, and the square of the voltage is $V^2 = V_0^2 + 2V_0 v \sin(\omega t) + v^2 \sin^2(\omega t)$. The electrostatic force caused by the DC-voltage is found by substituting V_0 into eq. (6.4), and differentiating c_m with respect to the deflection w_0:

$$\tilde{F}_{q0} = \frac{V_0^2 \varepsilon_0}{2(d_0 - w_0)^2} \quad . \tag{6.8}$$

The force caused by the AC-voltage is similarly found using eq. (6.4), and substituting $2V_0 v$ for V:

$$\tilde{F}_{qv} = \frac{V_0 v \varepsilon_0}{(d_0 - w_0)^2} \quad . \tag{6.9}$$

The small-signal deflection w, brings the electrodes closer together, thus the electrostatic forces are further increased. This is often referred to as a spring softening effect, since it reduces the effective spring constant of the membrane. The increase in electrostatic force, F_{qw}, can be found by calculating $V_0^2 w \frac{d^2 c_\mathrm{m}}{dw_0^2}$, and results in the following expression:

$$\tilde{F}_{qw} = \frac{V_0^2 w \varepsilon_0}{(d_0 - w_0)^3} \quad . \tag{6.10}$$

To express the forces across the whole CMUT, we introduce an area, A. Since we describe the CMUT as a parallel plate capacitor, the area must be large for the model to be valid. The electrostatic forces from the small-signal voltage becomes:

$$F_v = \frac{\varepsilon V_0 A v}{(d_0 - w_0)^2} = K_v v \quad , \tag{6.11}$$

where

$$K_v = \frac{\varepsilon V_0 A}{(d_0 - w_0)^2} \quad . \tag{6.12}$$

The forces due to small-signal deflection is given by:

$$F_w = \frac{\varepsilon V_0^2 A w^2}{(d_0 - w_0)^3} = K_w w \quad , \tag{6.13}$$

where

$$K_w = \frac{\varepsilon V_0^2 A w}{(d_0 - w_0)^3} \quad . \tag{6.14}$$

K_w is the spring softening effect. This is because effective stiffness of the membrane is reduced by the added electrostatic forces induced by the small deflection. From eq. (6.14) it is apparent that an increased DC-voltage will lead to higher K_w, hence, a larger reduction of the spring constant. A softer membrane has a lower resonance frequency, and this is easily observed in measurements. In Fig. 6.2 we see the effect of K_w clearly as a reduction of resonance frequency with increasing DC-bias. In these measurements an array of 72×104 CMUT cells was excited in air, and the impedance was calculated based on measured reflection coefficient S11, using a network analyzer (HP8753E, Hewlett Packard).
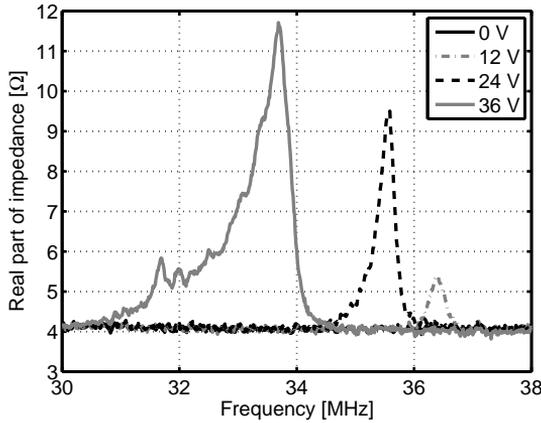
Figure 6.2: Example of spring softening effect in the CMUT membrane. A CMUT array with 72×104 CMUT cells is excited in air with different DC-bias voltage.

In addition to the electrostatic forces given in eqs. (6.11) and (6.13), there are mechanical forces acting on the CMUT. According to Newton's second law the forces needed to accelerate the membrane can be expressed as

$$F_{\mathrm{acc}} = -\omega^2 w M \quad , \tag{6.15}$$

where ω is the operating frequency, and M is the mass of the membrane.

The restoring forces in the membrane is given by

$$F_{\mathrm{f}} = -Sw \quad , \tag{6.16}$$

where S is the spring constant of the capacitor, expressing the stiffness of the membrane.

If the CMUT is immersed in a fluid, there are reaction forces from the fluid which affects the behavior of the CMUT. These forces are expressed as

$$F_{\mathrm{liq}} = -j\omega W Z_a \quad , \tag{6.17}$$

where Z_a is the acoustic radiation impedance of the membrane. The impedance can be expressed as a complex sum, $Z_a(\omega) = R_a + j\omega\chi_a$, where the real part represents the acoustic radiation and losses, and the imaginary part is frequency dependent and corresponds partly to the weight of the fluid which is excited by the membrane vibration, and partly to the non-radiation local deformation at the surface. The imaginary part will, however, only be present when there is a nonuniform vibration. As long as a uniform plate motion is assumed, the acoustic impedance will be real and not frequency dependent.

If we sum all the force contribution we get the following equation:

$$F_{\mathrm{acc}} - F_f - F_w - F_{\mathrm{liq}} - F_v = 0 \quad , \tag{6.18}$$

$$-\omega^2 w M + Sw - K_w w + j\omega w Z_a - K_v v = 0 \quad , \tag{6.19}$$

This equation determines the relation between the applied voltage, v, and the small-signal deflection, w. The voltage can easily be derived as:

$$v = \frac{w(-\omega^2 M + S - K_w + j\omega Z_a)}{K_v} \quad . \tag{6.20}$$

To complete the mathematical description of the CMUT we need to express the current, i, into the capacitance. The general equation for current into a capacitance as a function of voltage is $i = C\frac{dV}{dt}$. In this case the capacitance changes as a function of the deflection w, hence, we need to find the derivative of the capacitance with respect to w. From the derivation of the forces caused by the small-signal voltage, given in eqs. (6.11) and (6.12), we know that K_v is given by $V_0 \frac{\partial C_{\mathrm{m}}}{\partial w}$, hence, $\frac{\partial C_{\mathrm{m}}}{\partial w} = K_v/V_0$. The current is given by:

$$
\begin{aligned}
i &= \frac{\partial}{\partial t}(C_{\mathrm{m}} + \delta C_{\mathrm{m}})(V_0 + v) \quad , \\
&\approx j\omega C_{\mathrm{m}} v + V_0 \frac{\partial C_{\mathrm{m}}}{\partial w} j\omega w \quad , \\
&= j\omega C_{\mathrm{m}} v + j\omega w K_v \quad .
\end{aligned}
\tag{6.21}
$$

When the current and the voltage are found, the total admittance of the CMUT becomes:

$$Y(\omega) = \frac{i}{v} = j\omega C_{\mathrm{m}} + \frac{K_v^2}{Z_a + j\omega M + \frac{1}{j\omega}(\omega_{0f}M - K_w)} \qquad . \qquad (6.22)$$

This expression forms the basis of the equivalent circuit which we may use to describe the coupling between the electric and acoustic domain, as described in the following.

6.2.1 Equivalent circuit

The equations describing the interaction between the electric and acoustic domain, can also be represented by an equivalent circuit [141], as shown in Fig. 6.3. This is a classical two-port network with one electrical- and one mechanical port [142]. The electrical port is given by a small-signal voltage across a capacitor, C_m, given in eq. (6.7). The transformer ratio between the electric and acoustic domain is given by K_v, and described in eq. (6.12). The acoustic branch is described by a RLC-series. The transformer ratio
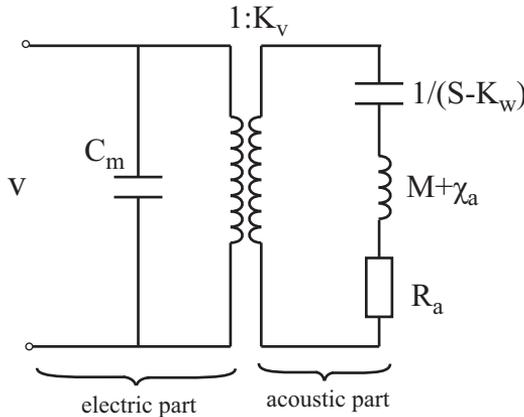
Figure 6.3: Basic equivalent circuit for a CMUT in fluid driven by a small-signal voltage v. The transformer ratio between the electric and acoustic domain is K_v.

between the electric and mechanical/acoustic domain can be included in the mechanical branch, as shown in Fig. 6.4, and the circuit becomes easier
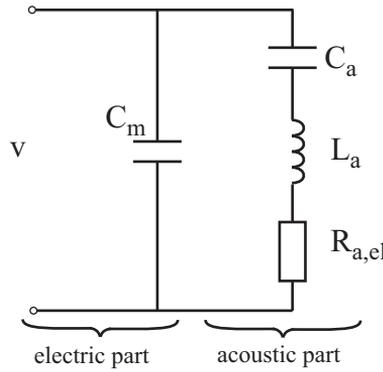
Figure 6.4: Basic equivalent circuit for a CMUT in fluid driven by a small-signal voltage v.

to handle mathematically. The admittance given in eq. (6.22) may be rewritten to fit with the elements of the circuit, and hence becomes:

$$Y = j\omega C_{\mathrm{m}} + \cfrac{1}{\frac{1}{j\omega C_a} + j\omega L_a + R_{a,el}} \quad . \tag{6.23}$$

The equivalent inductance, L_a, describes the mass of the membrane and the fluid which it excites. The equivalent capacitance C_a is given by the stiffness of the membrane, which is reduced by the spring softening effect described previously, and the equivalent resistance, $R_{a,el}$ expresses the loss in the acoustic branch of the circuit. Mathematically the circuit elements are given as:

$$C_a = \frac{K_v^2}{S - K_w} \quad , \tag{6.24}$$

$$L_a = \frac{M + \chi_a}{K_v^2} \quad , \tag{6.25}$$

$$R_{a,el} = \frac{R_a}{K_v^2} \quad . \tag{6.26}$$

The mechanical resonance frequency of the RLC-series occurs when the inductance, L_a, and the capacitance, C_a, cancel each other out ($\omega_{0m}L_a - 1/(\omega_{0m}C_a) = 0$). Hence, the total impedance of the acoustic branch at resonance is $Z_{\omega_{0m}} = R_{a,el}$. The resonance frequency, ω_{0m} is then found as:

$$\omega_{0m} = \frac{1}{\sqrt{L_a C_a}} = \sqrt{\frac{S - K_w}{M + \chi_a}} \quad . \tag{6.27}$$

There are two Q-values which we can define based on the equivalent circuit; the mechanical Q-value, Q_m, and the electrical Q-value, Q_{el}. The mechanical Q is defined as the ratio of the resonance frequency to the bandwidth of the RLC-branch. According to the theory of RLC-series circuits the Q_m-value is given by [143]:

$$Q_m = \frac{\omega_{0m}L_a}{R_{a,el}} = \frac{\omega_{0m}(M + \chi_a)}{R_a} \quad .$$
(6.28)

It can also be expressed in terms of C_a and $R_{a,el}$ as:

$$Q_m = \frac{1}{\omega_{0m}R_{a,el}C_a} = \frac{S - K_w}{\omega_{0m}R_a} \quad .$$
(6.29)

A soft and light-weight membrane is preferable in order to keep the mechanical Q low.

The electrical Q-value of the equivalent circuit is given by the ratio between the imaginary and real part of the admittance at resonance, and expresses the amount of electrical energy stored at resonance:

$$Q_{el} = \frac{Im(Y(\omega_{0m}))}{Re(Y(\omega_{0m})} = \omega_{0m}C_{\mathrm{m}}R_{a,el} = \frac{\omega_{0m}C_{\mathrm{m}}R_a}{K_v^2} \quad .$$
(6.30)

A low electrical Q-value implies a large real part of the admittance at resonance, $1/R_{a,el}$, compared to the imaginary part, $\omega_{0m}C_{\mathrm{m}}$. Low Q_{el} results in efficient transfer of energy from the source, v to the load, $R_{a,el}$.

6.2.2   Electromechanical coupling coefficient

The electromechanical coupling coefficient is an important parameter in transducer design. It gives an indication on how efficient the transducer transforms energy from one domain to the other. The coupling coefficient of the CMUT will increase with the bias voltage, and become close to 1 just before the CMUT collapses. However, if one wants to operate the CMUT in conventional mode, the bias voltage should be low enough to avoid an unexpected collapse.

Several authors have discussed the calculation of the coupling coefficient for CMUT arrays immersed in fluid [62, 137, 144]. We have chosen to follow the definition of the coupling coefficient in a lumped parameter model from Caronti *et al.* [144], which is based on the book by Kinsler *et al.* [142]. The coupling coefficient is expressed by the capacitances C_{m} and C_a as:

$$k^2 = \frac{1}{1 + C_{\mathrm{m}}/C_a} = \frac{C_a}{C_a + C_{\mathrm{m}}} \quad .$$
(6.31)

From this expression we see that it is also possible to express the electrome-chanical coupling coefficient in terms of the Q-values given above:

$$k^2 = \frac{1}{1 + Q_m Q_{el}} \quad .$$ (6.32)

The ideal transducer has an infinite bandwidth and zero insertion loss. Since such requirements are impossible to fulfill, we rather aim for a wide bandwidth and low insertion loss at the resonance frequency. Wide bandwidths and low insertion loss require low mechanical and electrical Q-values respectively. Thus, we would like the coupling coefficient to be as close to 1 as possible

It is important to be aware that the given definition of the electrome-chanical coupling coefficient is valid only when the circuit given in Fig. 6.4 is a precise description of the operation of the CMUT. This is the case at low frequencies, since the first order mode will dominate, and the equivalent circuit will be rather accurate. At higher frequencies several membrane modes will contribute to the total membrane motion, and hence, an accurate model requires several coupled equivalent circuits. The determination of Q-values and coupling coefficients becomes more complex. A CMUT model which includes the excitation of higher order modes will be further discussed in Sec. 6.3.

6.2.3 Collapse voltage

As stated in Ch. 3.2, the CMUT membrane will collapse onto the bottom electrode if the electrostatic forces induced by the applied DC-bias becomes larger than the restoring forces in the membrane. To find the collapse voltage, we may consider a CMUT which operates in vacuum, and hence, is mechanically unloaded, and disregard the time dependant variables of the equation. The basis is the force balance stated in eq. (6.19). However, since the CMUT is unloaded, F_{liq} is set to zero. Since the acceleration force, F_{acc}, is time dependant, it is also set to zero. Thus the force balance becomes:

$$-F_{\text{f}} - F_w - F_v = 0 \quad .$$ (6.33)

If we simplify the expression further, and disregard the spring softening contribution, F_w, the force balance becomes:

$$-F_{\text{f}} - F_v = 0 \quad ,$$ (6.34)

$$Sw_0 - \frac{V_0^2 \varepsilon_0 A}{2(d_0 - w_0)^2} = 0 \quad ,$$ (6.35)

where the expression for F_v is the force caused by DC-voltages and based on eq. (6.8). Since we are considering a static case, with no small-signal contributions, we use w_0 to denote the deflection. The required voltage, V_0, needed to obtain the deflection w_0 is hence:

$$V_0 = \sqrt{\frac{2Sw_0}{\varepsilon_0 A}}(d_0 - w_0) \quad . \tag{6.36}$$

The membrane displacement at the collapse voltage can be found through solving $dV_0/dw_0 = 0$, and becomes:

$$w_{\text{collapse}} = \frac{d_0}{3} \quad . \tag{6.37}$$

This results in a collapse voltage:

$$V_{\text{collapse}} = \sqrt{\frac{8Sd_0^3}{27\varepsilon_0 A}} \quad . \tag{6.38}$$

From this expression it is apparent that an increased gap d_0 results in larger collapse voltages. To prevent the CMUT from shorting when it collapses, an insulator layer is placed on one or both of the electrodes. This causes the membranes to stay in the collapsed position until the voltage is reduced enough to release the membrane. This voltage level is referred to as snap-back voltage. This is illustrated in the hysteresis curve in Fig. 6.5.
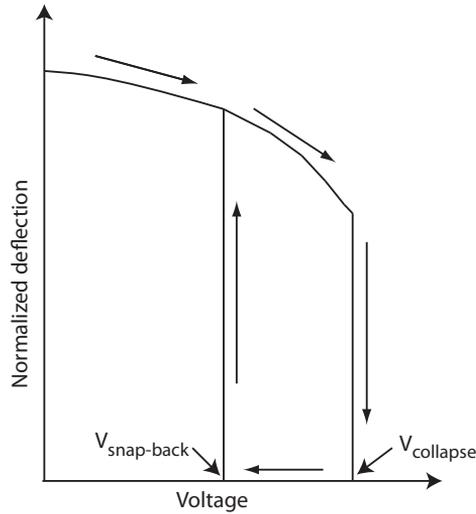
Figure 6.5: CMUT hysteresis.[75]

6.3   Complete analytical CMUT model

The CMUT model which is the basis for the simulations presented in this thesis, is described in the following section. The method, first developed by A. Rønnekleiv [1], has been used in all the published papers which are part of this thesis [145–150]. The model is an extension of the previously described capacitor model (Sec. 6.2).

The method allows us to analyze infinite CMUT arrays, where each element may consist of several CMUT cells. The acoustic coupling between vibration modes excited in a single CMUT and between neighbor CMUTs through the fluid medium, is taken into account. An important aspect of this model is that the various vibration modes of the single CMUT are orthogonal. Hence, forces caused by the excitation of one mode, will not do any work on any of the other modes. However, the coupling between the various vibration modes and between neighbor CMUTs is described through an acoustic impedance matrix.

In the implementation of the model, the DC-deflection and AC-vibration modes of circular single CMUT membranes are calculated independent of neighbor CMUTs, adjacent medium and backing materials. The general properties of a single CMUT are also independent of the excitation frequency, and must therefore only be calculated once. This approach saves computation time. However, the acoustic impedance matrix describing the

coupling between modes is dependant on the excitation frequency of the array and on the geometric layout of the array.

In the initial description given here, we assume that the CMUTs are laid out in an infinite periodic grid. However, it is possible to break the element period by introducing extra distance between elements, as shown in Fig. 5.5. In such cases the distance between CMUTs within the element is different from the distance between CMUTs in neighbor elements. This is treated in Paper III and VII, and an explanation of how these special layouts are modeled is given in the end of Sec. 6.3.2. In the initial model we assume that the supporting structure of the CMUT is fixed, hence, the bottom wafer may not vibrate because of excitation of the CMUTs. However, substrate ringing may also be included in the model, and a description of how this is done is given in Paper VI.

The description of the model is divided in two parts, first we describe the single CMUT model, and how the static DC-deflection and the various vibration modes are found. This is followed by a section on how the interaction between the CMUT array and the fluid is calculated, and how CMUTs are electrically combined into larger elements. The implementation of this model was done in Matlab (Mathworks Inc.).

6.3.1   Model of single isolated CMUT

The CMUT is modeled as a circular symmetric structure, which consist of a bottom silicon substrate, a cavity of defined and constant depth, a membrane, that may consist of several layers, and top- and bottom electrodes that may cover only parts of the total membrane area.

Deflection caused by DC-bias

To calculate the membrane's radial mode profile when it is biased, simple plate theory is used, including bending stiffness and stretching force. As an approximation, these are assumed to be uniform and isotropic in the xy-plane. The supporting structure at the outer radii of the cell is assumed to be fixed with zero tilt. The equations describe the relation between the mechanical forces in the membrane, and the applied pressure from the surroundings. The equations are based on those presented by Karasudhi [151], and the first is the field equation, which is a fourth order differential equation for a static deflection:

$$D\nabla^4 w_{\mathrm{DC}} - T\nabla^2 w_{\mathrm{DC}} = P \quad , \tag{6.39}$$

where T is the tensile force in the membrane, P is the sum of the force contributions from the pressure from the surroundings and the electrostatic force induced by the DC-voltage. We assume that P is circular symmetric. D is the bending stiffness of the membrane.

The homogenous 4th order differential equation, ($P=0$), has four linearly independent solutions. For circular symmetric membranes the solutions can be expressed as modified Bessel-functions of first and second kind, $w_1 = I_0(kr)$ and $w_2 = K_0(kr)$, where $k = \sqrt{T/D}$. In addition, there are two solutions which does not involve the Bessel-function. It can easily be verified that the constant, $w_3 = 1$, and the natural logarithm, $w_4 = \ln(r)$ are homogenous solutions to eq. (6.39). In the center of the CMUT ($r = 0$) we can only use the solutions which are finite at $r = 0$. This is true for the modified Bessel-function of first kind, I_0 and the constant 1. The modified Bessel function of second kind, K_0, and the natural logarithm, $\ln(r)$, diverges as r becomes 0.

A particular solution, ($P \neq 0$), is given by $w_p = \frac{-Pr^2}{4T}$. This can easily be verified by inserting w_p into eq. (6.39).

The DC-deflection profile, w_{DC}, is found along a radial line of the circular CMUT. The line is divided into a fixed number of elements, and we assume a constant mass, stiffness and external load on each element. There are four continuity conditions which must be fulfilled between each element; continuous deflection, w, continuous gradient of deflection $\frac{dw}{dr}$, continuous moment(torque), M_r, and continuous shear force, V_r, as illustrated in Fig. 6.6.
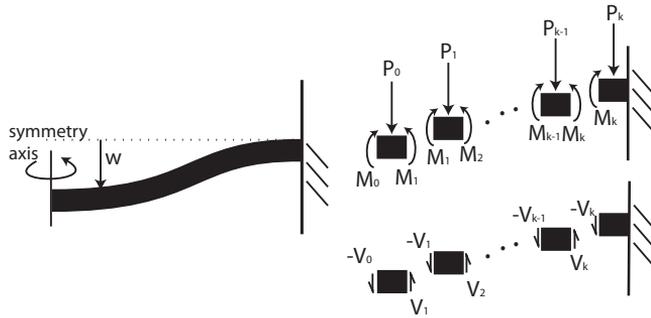

Figure 6.6: In the modeling of the CMUT, the circular area is a number of divided into concentric rings, as illustrated.

Dividing the circular membrane into concentric rings allows us to introduce variations in the external load and the geometry along the radius. It is for instance possible to include the top electrode in only parts of the mem-

brane area, or vary the thickness of the electrode or membrane as a function of the radius. The electrostatic forces are only induced in the area where the top- and bottom electrode overlap. A limitation is, however, that we assume a circular symmetric geometry. In order to model devices such as CMUT 1, which has four electrode fingers stretching from the center electrode to the perimeter of the membrane, we need to make some approximations. This is described in Paper VII.

The equations describing the bending moment, M_r, and shear force, V_r in cylindrical coordinates are as follows [151]:

$$M_r = -D\left[(1-\nu)\frac{\partial^2 w_{\mathrm{DC}}}{\partial r^2} + \nu\nabla^2 w_{\mathrm{DC}}\right] \quad , \tag{6.40}$$

$$V_r = -D\frac{\partial}{\partial r}(\nabla^2 w_{\mathrm{DC}}) \quad . \tag{6.41}$$

The bending stiffness for a single layer is given by:

$$D = \frac{Eh^3}{12(1-\nu^2)} \quad . \tag{6.42}$$

where ν is the Poisson's ratio, E is the Young's modulus and h is the membrane thickness. For a CMUT with a membrane consisting of several layers, the neutral axis of the stack must be found before the total stiffness can be calculated. With two layers, the distance, e_b, from the bottom surface to the neutral axis is given by:

$$e_b = \frac{(E_1\frac{h_1^2}{2} + E_2 h_2(h_1 + \frac{h_2}{2}))}{(E_1 h_1 + E_2 h_2)} \quad . \tag{6.43}$$

The total stiffness then becomes:

$$D = \frac{1}{(1-\nu^2)}\left(\frac{(E_1 h_1^3 + E_2 h_2^3)}{12} + h_1 E_1(e_b - \frac{h_1}{2})^2 + h_2 E_2(e_b - h_1 - \frac{h_2}{2})^2\right). \tag{6.44}$$

The total force P is calculated as the sum of the electrostatic forces induced by the applied DC-bias, described in eq. (6.8), and the ambient pressure, equal to the atmospheric pressure. The tensile forces in the membrane, denoted as T, is the sum of built-in stresses which are induced in the fabrication process and the total stretch force due the deflection of the membrane.

The deflection is found for a series of DC-voltages, and an example of the results which may be obtained is shown in Fig. 6.7. The cavity depth is 82 nm and with a silicon nitride membrane of 100 nm between the vacuum

gap and the top electrode, the effective gap, d_0, according to eq. (6.6) becomes 98.4 nm. The permittivity of silicon nitride is assumed to be 6.1. The maximum deflection before collapse, w_{collapse}, is 32.8 nm according to eq. (6.37). The collapse voltage of this structure is 57 V, and we see that the deflection at 55 V is about 29.5 nm, which is close to collapse.
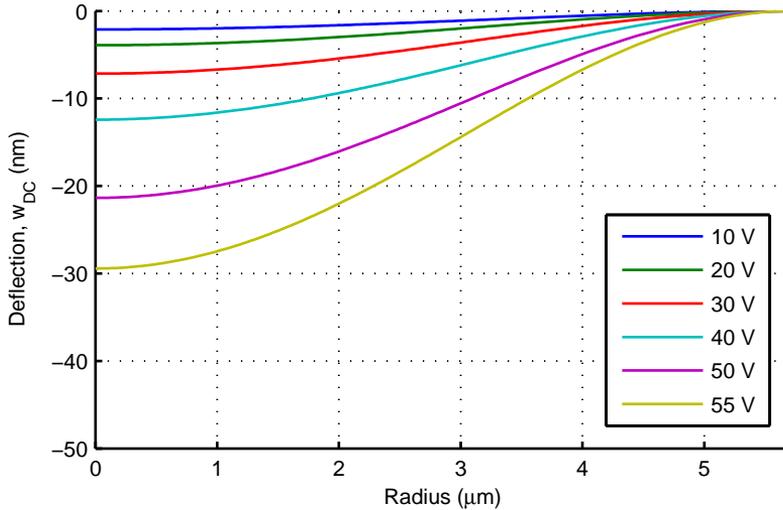
Figure 6.7: The DC-deflection of a CMUT at DC-bias from 1 V to 55 V. The cavity depth of the CMUT is 82 nm.

When the DC-deflection is known, the capacitance between the top and bottom electrode, C_{m}, may be derived as described in eq. (6.7), however, if the electrode area is only covering part of the area of the CMUT the capacitance becomes:

$$C_{\text{m}} = \int\limits_{\text{electrode}} \frac{\varepsilon_0}{d_0 - w_0} dx dy \quad . \tag{6.45}$$

Fast transversal changes in the distance between capacitor plates and the build up of charges on the edges of the plates are disregarded.

CMUT vibration modes

In addition to the DC-bias, a time varying AC-voltage is also applied to the CMUT in transmission. This will lead to harmonic vibrations of the membranes. A number of different vibration modes may be excited in the

circular CMUT membrane at the same time, and the total motion is a sum of contributions from different eigenmodes. Each of the eigenmodes have a different resonance frequencies and resonance profiles, and the frequency of the AC-signal and the distribution of the excitation forces will determine which mode dominates the membrane motion. In the following section we will show how the effective mass, effective stiffness, deflection profile and resonance frequency of the various modes are found.

The eigenmodes are chosen to be the modes of a free circular CMUT membrane with fixed support, unaffected by external acoustic or electric pressures. In this situation the modes are orthogonal with the following scalar product:

$$\int_A m_a w_m w_n dA = \delta_{m,n} M_n \quad .$$ (6.46)

Here A is the membrane area, w_m and w_n are the normalized deflection profile of mode m and n respectively, and m_a is the mass per unit area of the membrane. This may vary over the membrane. $\delta_{m,n}$ is the Kronecker delta equal to 1 when $n = m$, otherwise zero. M_n becomes the effective mass of mode n, provided that a proper definition of the force acting on mode n is used.

When we calculate the mode profiles, we assume that all the vibration modes included in the model have deflection only in the vertical direction (z-direction). Modes with velocities in the transverse direction do not radiate into an adjacent fluid and are normally not excited. Thus, the only force on the CMUT from the surrounding medium is the normal stress T_{zz}. In Paper VII we model a situation where a soft lossy material has been added on top of the membrane. In that case we also account for transverse velocities, V_x and V_y and include shear stresses, T_{xz} and T_{yz}. That is, however, not included in the model presented in this section.

The total vibration profile of mode n is given by $W_n w_n(x,y)$, where $w_n(x,y)$ is the deflection profile of the mode, normalized to have a peak amplitude of 1, and W_n is the maximum deflection of the same mode. In order to solve the field equation for the harmonic vibration modes, w_n, we need to take the frequency into account. The equation given in eq. (6.39) is hence expanded with a frequency dependant term and becomes:

$$D\nabla^4 w - T\nabla^2 w - \omega^2 M_n w = 0 \quad ,$$ (6.47)

where w in this case represents the deflection $W_n w_n$. The equations representing the bending moment, M_r, and shear forces V_r remain the same as given in eqs. (6.40) and (6.41). Since we are looking for resonant solutions,

there is no external load working on the structure, hence, there are no particular solution. The parameters D, T, M_n and, w are circular symmetric. The equations are solved in a similar manner as for the static case, but in this case both regular and modified Bessel functions of order 0 to p are used.

A range of frequencies are searched through in the computation program to find the resonance frequencies and vibration profiles of the modes corresponding to the order of the Bessel functions used. In our work we have included $p = 0$ and $p = 1$. The vibration modes which are found are denoted by (p, a), where p gives the order of the involved Bessel function, and a gives the number of radial lobes in the vibration pattern. The vibration profiles with $p > 0$ may have two different angular dependencies which are orthogonal; namely $\sin(p\phi)$ and $\cos(p\phi)$, where ϕ is the angle between the radius and the x-axis. The normalized profiles of the first three modes, $(0,1)$, $(0,2)$ and $(0,3)$, can be seen in Fig. 6.8, and the normalized velocity profile for the same modes are shown in Fig. 6.9.
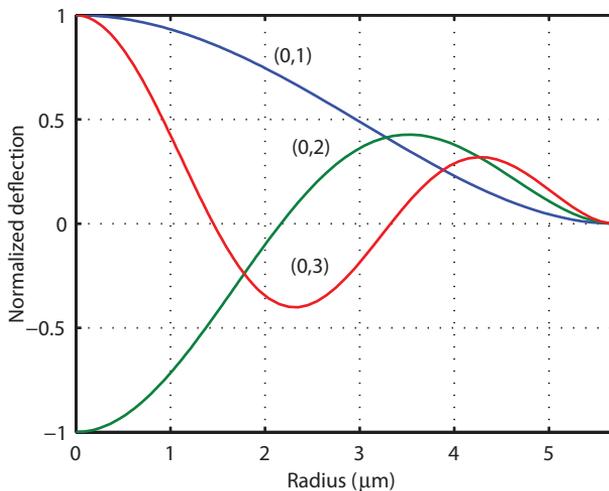
Figure 6.8: Deflection profile of three modes. The blue line is the $(0,1)$ mode, the green line is the $(0,2)$ mode and the red line is the $(0,3)$ mode. These modes does not have any angular variation, as is shown in Fig. 6.9.

Vibration modes with angular dependency are also found, and in Fig. 6.10 the two orthogonal velocity profiles of mode $(1,1)$ are shown. They vibrate in an antisymmetric fashion, and are hence not efficient when it comes to radiation of waves into the fluid. Thus they will harm the overall response from the array at their resonance frequency. For a collapsed mode
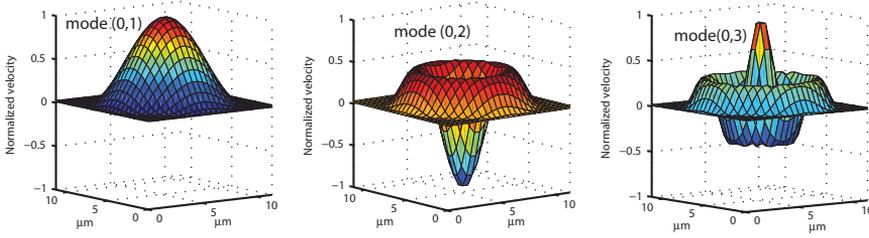
Figure 6.9: Velocity profile of the first three modes.

CMUT, it has been shown that the (1,1) mode becomes dominating at large steering angles, and affects the response of the array at approximately twice the center frequency [1].
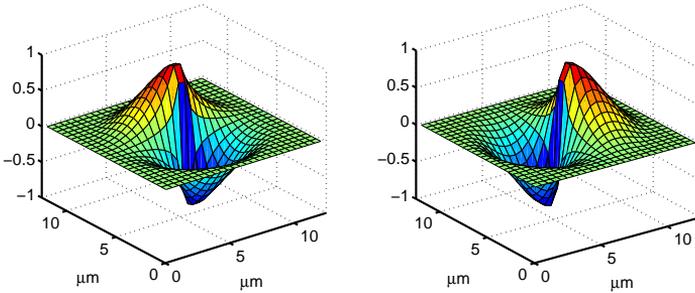
Figure 6.10: Two orthogonal velocity profile of mode (1,1). Both of them vibrate in an antisymmetric fashion.

Based on the calculated velocity profiles, w_n, the effective electrostatic forces induced by the small-signal voltage and the small-signal deflection, may be found. The forces are given for a parallel plate capacitor in eqs. (6.11) and (6.13), and we calculate the effective forces for each mode by introducing the vibration profile w_n into the expressions for K_v and K_w, and integrate over the area of the electrode:

$$K_n^{(v)} = \int\limits_{\text{electrode}} \frac{\varepsilon_0 V_0 w_n dA}{(\Sigma h_i/\varepsilon_r^{(i)} - w_{\text{DC}})^2} \quad , \tag{6.48}$$

$$K_{(n,m)}^{(w)} = \int\limits_{\text{electrode}} \frac{\varepsilon_0 V_0^2 w_n w_m dA}{(\Sigma h_i/\varepsilon_r^{(i)} - w_{\text{DC}})^3} \quad . \tag{6.49}$$

The DC-deflection is denoted w_{DC}. From eq. (6.49) we see that a small deflection in mode n will not only affect the forces on mode n, but it will also affect the electrostatic forces on mode m.

The effective mass of the membrane depends on the mode of vibration, and when the vibration profile is known, we may calculate the effective mass for each mode as:

$$M_{\mathrm{eff,n}} = \int_A M w_n^2 dA \quad , \tag{6.50}$$

where $M = \sum \rho_i h_i$, h_i and ρ_i are the thickness and density of the membrane and electrode layers. When the membrane has a top electrode which does not cover the entire membrane, the calculation of the effective mass is divided into an inner and an outer part, which are summed. The effective stiffness of the membrane is calculated based on the mass and resonance frequency in free space, ω_n, of each of the modes:

$$S_{\mathrm{eff,n}} = M_{\mathrm{eff,n}} \omega_n^2 \quad . \tag{6.51}$$

The resonance frequency, ω_n, effective mass, $M_{\mathrm{eff,n}}$, and coupling parameters, $K_n^{(v)}$ and $K_{n,m}^{(w)}$ for the CMUT model described in Paper VII is given in Table 6.1 and 6.2.

Table 6.1: Resonance frequency, effective mass, and coupling parameter, $K_n^{(v)}$ for selected modes for the CMUT used in Paper VII.

Mode no.	$\omega_n/2\pi$	$M_{\mathrm{eff,n}}$	$K_n^{(v)}$
n=(,)	(MHz)	$(10^{-12}\mathrm{g})$	$(\mu\mathrm{N/V})$
(0,1)	35.91	33.25	1.75
(0,2)	152.93	18.19	-0.67
(0,3)	355.22	12.26	-0.02
(1,1)	73.26	33.04	0

The reaction forces from the fluid were described as a complex sum in eq. (6.17) for a parallel plate capacitor. In order to account for the acoustic coupling between the various modes, we need an acoustic impedance matrix, denoted as $Z_{n,m}^{(\mathrm{me})}$. It contains the self and mutual acoustic impedances for each of the eigenmodes of the membrane, and is given by:

$$Z_{m,n}^{(\mathrm{me})} = \frac{1}{j\omega W_n} \int_{\mathrm{mem.}} t_{zz,n}^{(\mathrm{me})} w_m dA \quad , \tag{6.52}$$

Table 6.2: Coupling parameters, $K_{n,m}^{(w)}$ for selected modes for the CMUT used in Paper VII.

Mode no.	$K_{n,m}^{(w)}$	(kN/m)		
n=(,)	m = (0,1)	m = (0,2)	m = (0,3)	m=(1,1)
(0,1)	1.02	-0.45	0.06	0
(0,2)	-0.45	0.34	-0.20	0
(0,3)	0.06	-0.20	0.24	0
(1,1)	0	0	0	0.54

where $t_{zz,n}^{(\text{me})}$ is the normal tension on the membrane surface from the surrounding medium caused by the small-signal velocity, $j\omega W_n w_n$. The driving force on mode m from the fluid, equivalent to eq. (6.17), is $j\omega W_n Z_{m,n}^{(\text{me})}$. How the normal tension is calculated will be explained in the next section. From eq. (6.52) we see that the tension caused by one mode, influences the acoustic impedance that gives the reaction forces from the fluid to the other modes.

When balancing all the forces in a similar manner as in eq. (6.19) we find the deflection of each mode, W_m. This is a quadratic matrix equation of dimension equal to the number of included eigenmodes:

$$\left[\text{diag}(M_{\text{eff},n})(\omega^2 - \omega_n^2) - K_{n,m}^{(w)} + j\omega Z_{n,m}^{(\text{me})}\right] W_m = K_n^{(v)} v \quad . \tag{6.53}$$

It is also possible to expand this system of equations to include vibrations of the supporting structure. This is described in Paper VI. The acoustic impedance matrix may also include the effect of damping layers added on top of the CMUT membrane. Such layers will change the normal tension, $t_{zz,n}$, experienced by the membrane from the fluid, and hence, alter the coupling of acoustic modes and also the coupling between adjacent CMUTs.

The equations given in eqs. (6.19) and (6.53) are quite similar. The main difference is that eq. (6.53) takes several vibration modes into account, whereas in eq. (6.19) there is an assumption that the membrane deflection is parallel to the bottom substrate. If we were to use equivalent circuits to describe the multi-mode case, we would need several circuits which are coupled through the acoustic impedances given in $Z_{m,n}^{(\text{me})}$.

The current, i, into the capacitance C_{m}, as a function of the small-signal voltage v and the amplitudes W_n, is needed to complete the description of a biased, vibrating CMUT. Similarly to eq. (6.21), we can express the current

into CMUT as a function of the amplitudes of all the excited modes as:

$$
\begin{aligned}
i &= \frac{\partial}{\partial t}\left[(C_\mathrm{m} + \delta C_\mathrm{m})(V_0 + v)\right] \quad, \\
&= i\omega C_\mathrm{m} v + i\omega \sum_n W_n K_n^{(v)} \quad,
\end{aligned}
\tag{6.54}
$$

where δC_m is the changes in electrode capacitance caused by the membrane vibration. The contribution from the $\delta C_\mathrm{m} v$ is disregarded because it is very small compared to the other contributions. Note that the subscript m in C_m refers to the membrane and not the mode m. The total admittance of the CMUT can hence be found from $Y = i/v$.

6.3.2 Connecting the CMUTs with the environment

We assume that the CMUT array is immersed in fluid. In Paper II and VII, we include a damping layer between the membrane surface and the fluid, but in the general description given here, we assume that the membranes are in direct contact with the fluid.

As described in the introduction of this section the basis for this model is that the CMUTs are laid out in an infinite periodic array. This allows us to use Fourier transform methods to analyze the CMUT-fluid interface. However, in Paper III and VII we introduce what we denoted as double periodicity, which means that the distance between CMUTs in adjacent elements is larger than the distance between the CMUTs within the same element. This is illustrated in Fig. 5.5. In the general description of the interaction between the CMUTs and the fluid, we assume that the distance between all the CMUTs is the same throughout the array. How the added distance between elements is included in the model is described at the end of this section.

The vibration mode profiles described in the previous section (shown in Fig. 6.8), is the basis when we model the interaction between the CMUT and the surrounding medium, and the coupling between neighbor CMUTs. From eq. (6.52) it follows that we need to find the normal tension, $t_{zz,l}^{(\mathrm{me})}$, acting from the fluid on the membrane surface, when the membrane is vibrating in mode l. As mentioned in the previous section, the tension caused by one mode acts on all the other orthogonal modes as well, and the coupling between the modes is described through the impedance matrix, $Z_{m,n}^{(\mathrm{me})}$. However, the total pressure on one CMUT is not only dependent on the vibration of the various vibration modes of the same CMUT, but also on the vibration mode of the neighbor membranes.

We assume that the CMUT cells are laid out in an infinite periodic pattern, with periods (cell pitch) L_x and L_y which are aligned with the x- and y-axes. We will calculate the response from the array when it is transmitting waves to angles oblique to the z-direction. To achieve skew angle transmission, phase shifts of $-K_x L_x$ and $-K_y L_y$ between adjacent cells or elements are introduced. In the implementation of the infinite periodic array, we calculate the transfer functions for an array of M_a by N_a cells in the x- and y-directions, which is assumed to represent the period of the infinite array, as illustrated in Fig 6.11. M_a is usually chosen to be between 240 and 480, and if we chose to steer the beam perpendicular to the direction of the linear array elements, we may use $N_a = 1$. We calculate the k-space velocities and pressures for all discrete combinations of K_x and K_y, given by:

$$
\begin{aligned}
K_x &= \frac{m_a 2\pi}{M_a}, \text{ where } -M_a/2 \leq m_a < M_a/2 \quad, \\
K_y &= \frac{n_a 2\pi}{N_a}, \text{ where } -N_a/2 \leq n_a < N_a/2 \quad.
\end{aligned}
\tag{6.55}
$$

Because of the periodicity of the array, the velocity of the acoustic wave from the CMUT into the fluid at the membrane surface can be expressed as:

$$
v_z(x,y,0) = v_z^{(\mathrm{p})}(x,y,0)e^{-iK_x x - iK_y y} \quad,
\tag{6.56}
$$

where

$$
v_z^{(p)}(x,y,0) = v_z^{(p)}(x + mL_x, y + nL_y, 0) \quad.
\tag{6.57}
$$

m and n are independent arbitrary integers, and the superscript (p) is used to express that the velocity is periodic. The velocity profiles across the CMUT, $v_z^{(\mathrm{p})}(x,y,0)$ is taken to be the normalized profiles found previously. Fig 6.9 shows the velocity profiles of the first three modes, and Fig. 6.10 shows two antisymmetric velocity profiles. The velocity $v_z^{(\mathrm{p})}$ is periodic and can hence be written as a sum of Fourier components:

$$
v_z^{(\mathrm{p})}(x,y,0) = \sum_{m,n} V_{z0}^{(\mathrm{p})}(k_{mx}^{(\mathrm{p})}, k_{ny}^{(\mathrm{p})})e^{-ik_{mx}^{(\mathrm{p})}x - ik_{ny}^{(\mathrm{p})}y} \quad,
\tag{6.58}
$$

where

$$
\begin{aligned}
k_{mx}^{(\mathrm{p})} &= \frac{2\pi m}{L_x}, \text{ where } m = 0, 1, \cdots, \frac{M-1}{2}, -\frac{M}{2}, -\frac{M}{2}+1, \cdots, -2, -1 \quad, \\
k_{ny}^{(\mathrm{p})} &= \frac{2\pi n}{L_y}, \text{ where } n = 0, 1, \cdots, \frac{M-1}{2}, -\frac{M}{2}, -\frac{M}{2}+1, \cdots, -2, -1 \quad,
\end{aligned}
\tag{6.59}
$$
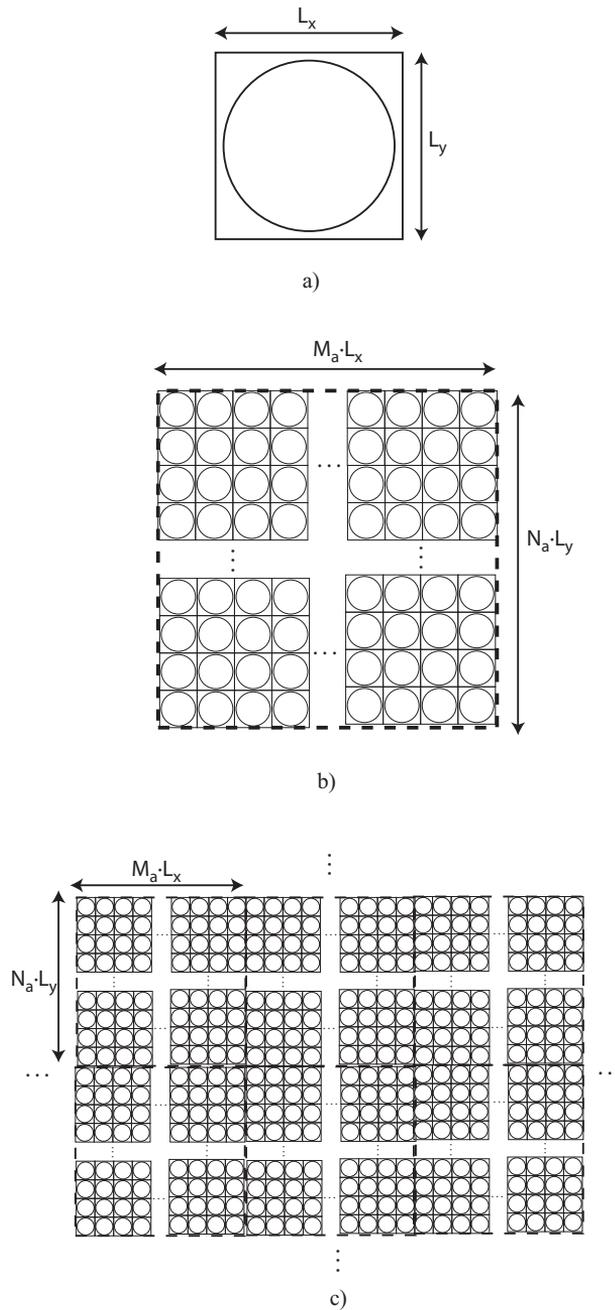
Figure 6.11: a) Illustration of a single CMUT with size $L_x \times L_y$. b) Illustration of the M_a by N_a cells which form the period of the infinite array. This is done to model phase-shifts between neighbor elements for off-axis beam steering. c) Illustration of the infinite array, which is periodic with the area shown in b) as the period.

The value of M and N have been chosen between 50 and 26 in this work. Large M and N will increase the accuracy, but also the computation time. This is actually an inverse Fourier transform, since we use the negative k-vector in the exponential. When we combine the equations from eqs. (6.56) to (6.59), the expressions for the actual k-vectors in x- and y-directions are given by:

$$
\begin{aligned}
k_{xm} &= k_{xm}^{(\mathrm{p})} + K_x = \frac{2\pi m}{L_x} + K_x \quad , \\
k_{yn} &= k_{yn}^{(\mathrm{p})} + K_y = \frac{2\pi n}{L_y} + K_y \quad .
\end{aligned}
\tag{6.60}
$$

To ease the calculations somewhat, we define a coordinate system where the x- and y-directions are combined in a x'-direction. The velocities and pressures we are seeking will not depend on the y'-direction. This can be done since the materials above the membrane are isotropic and uniform in the x- and y-directions. The k-vector along the membrane surface hence becomes:

$$
k_{x'} = \sqrt{k_{xm}^2 + k_{yn}^2} \quad .
\tag{6.61}
$$

The Fourier transform of the velocity in the z-direction will then be denoted $V_z'(k_{x'})$.

To find the pressure working on the membrane, we start with the wave equation for a viscous fluid and the stress tensor in the fluid, T_{ij} [152]:

$$
i\omega\rho\overrightarrow{V} = \nabla[-p + (\eta' + \eta)\nabla \cdot \overrightarrow{V}] + \eta\nabla^2\overrightarrow{V} \quad ,
\tag{6.62}
$$

$$
T_{ij} = \left[-p + \eta'\frac{\partial V_k}{\partial x_k}\right]\delta_{ij} + \eta\left(\frac{\partial V_i}{\partial x_j} + \frac{\partial V_j}{\partial x_i}\right) \quad ,
\tag{6.63}
$$

$$
p = \frac{\gamma_f}{i\omega}\nabla \cdot \overrightarrow{V} \quad .
\tag{6.64}
$$

The pressure in the fluid is denoted as p, and gives the isotropic pressure without influence of the viscosity. An alternative definition of the pressure, $\hat{p}$, which takes viscosity into account, used in Paper VII, where $\hat{p} = -(T_{xx} + T_{yy} + T_{zz})/3$. Note that it is only the contribution from the longitudinal wave which should be included. The constants η, η' and γ_f are the shear viscosity, dynamic viscosity and stiffness of the fluid, respectively. The stiffness, γ_f is given by ρc^2, where ρ is the density and c is the longitudinal velocity of sound in the fluid.

An excitation from a velocity in the z-direction in the fluid at $z = 0$ will lead to a longitudinal and a shear wave with velocities at $z = 0$ equal to V_{l0}

and V_{s0} excited in the fluid. Both have $k_{y'} = 0$ and they have the same k'_x. The waves may be expressed by:

$$V'_{x'} = \left[V_{l0}\frac{k_{x'}}{k_{l0}}e^{-k_{lz}z} + V_{s0}\frac{k_{sz}}{k_{s0}}e^{-k_{sz}z} \right] e^{-k_{x'}x'} \quad , \tag{6.65}$$

$$V'_z = \left[V_{l0}\frac{k_{lz}}{k_{l0}}e^{-k_{lz}z} - V_{s0}\frac{k_{x'}}{k_{s0}}e^{-k_{sz}z} \right] e^{-k_{x'}x'} \quad . \tag{6.66}$$

The equations given in eqs. (6.62) to (6.64) are all for real space. As we look at the interface between a fluid and a solid material, and examine each Fourier component, we may introduce the k-space velocities, eqs. (6.65) and (6.66), into eqs. (6.62) and (6.64), and derive the following expressions for k_{l0}, k_{lz}, k_{s0}, and k_{sz}:

$$
\begin{aligned}
k_{l0} &= \sqrt{\frac{\omega^2\rho}{\gamma_f + i\omega(\eta' + 2\eta)}} \quad , \\
k_{lz} &= \sqrt{k_{l0}^2 - k_{x'}^2} \quad , \\
k_{s0} &= \sqrt{\frac{-i\omega\rho}{\eta}} \quad , \\
k_{sz} &= \sqrt{k_{s0}^2 - k_{x'}^2} \quad .
\end{aligned}
\tag{6.67}
$$

To find an expression for the normal stress and fluid pressure at the surface ($z = 0$) we put eqs. (6.65) and (6.66) into eqs. (6.64) and (6.63), and obtain the following expression for P' and T'_{zz} at $z = 0$:

$$P'\big|_{z=0} = \frac{\gamma_f}{\omega}\left(V_{l0}\frac{k_{x'}^2 + k_{lz}^2}{k_{l0}} \right) \quad , \tag{6.68}$$

$$
\begin{aligned}
T'_{zz}\big|_{z=0} &= -\left[\left(\frac{\gamma_f}{\omega} + i\eta'\right)(k_{x'}^2 + k_{lz}^2) + i2\eta k_{lz}^2 \right]\frac{1}{k_{l0}}V_{l0} + i\eta\frac{2k_{x'}k_{sz}}{k_{l0}}V_{s0} \quad , \\
&= C_1 V_{l0} + C_2 V_{s0} \quad .
\end{aligned}
\tag{6.69}
$$

Both of these expressions should be multiplied with $e^{-ik_{x'}x}$. As long as the CMUT membrane is in direct contact with the fluid, we assume that the membrane is infinitely stiff in the x'-direction relative to the fluid, hence, the membrane velocity in the x'-direction $V'_{x'} = 0$ at $z = 0$. This allows us

to calculate the tension simply as:

$$T'_{zz}(k_{x'}) = \frac{C_1 k_{l0} k_{sz} - C_2 k_{x'} k_{s0}}{k_{lz} k_{sz} + k_{x'}^2} V'_z(k_{x'}) \quad , \tag{6.70}$$

$$P'(k_{x'}) = \frac{\gamma_f k_{l0}^2 k_{sz}}{\omega(k_{lz} k_{sz} + k_{x'}^2)} V'_z(k_{x'}) \quad , \tag{6.71}$$

where $V'_z(k_{x'})$ is the Fourier transform of the real space velocity profile given in eq. (6.56)[1]. T_{zz} is calculated for each of the vibration modes, and the real space tension, $t_{zz,n}^{(\mathrm{me})}$, can be found using inverse Fourier transform. Hence, the self and mutual acoustic impedance, $Z_{n,m}^{(\mathrm{me})}$, for the different eigenmodes of the membrane can be calculated according to eq. (6.52), as the sum of the normal tension across the membrane, weighted by the velocity profile. The impedance will vary along the array when the beam is steered off broadside, because of the $k_{x'}$-dependency of $t_{zz,n}^{(\mathrm{me})}$. When the impedance is found, the membrane deflection of each eigenmode can be calculated according to the system equation (6.53) given in Sec. 6.3.1. From eq. (6.54) we may also calculate the harmonic admittance $Y_c(K_x, K_y, \omega)$ as i/v.

To find a transfer function from the input voltage on the CMUT to total transmitted pressure from the array, we use only the first Fourier component of $P(k_{xm}, k_{yn}, \omega)$, which corresponds to the radiated pressure, if L_x and L_y are both less than half a wavelength in the fluid. This component is denoted $P_l(K_x, K_y, \omega)$ for mode l. To find the total pressure, we need to sum over all the vibrations modes, hence, the total radiated pressure is:

$$P_c(K_x, K_y, \omega) = \sum_n W_l P_l(K_x, K_y, \omega) \quad , \tag{6.72}$$

where W_l is the vibration amplitudes found in eq. (6.53). Note that P_c is the output pressure from a driving voltage of 1 V if v=1V is used to find W_l in eq. (6.53).

Transmitted power into the fluid

To calculate the transmitted power, we need to define the electrical source impedance, R_s which is coupled in series with each CMUT. We assume that there is a voltage source, V_0, driving the CMUT. The voltage across the CMUT is given by:

$$v = \frac{V_0}{R_s Y_c(K_x, K_y, \omega) + 1} \quad , \tag{6.73}$$

---

[1]There is an error in [1]: The right side of the equation for $P'(k_{x'})$ in eq. (23) should be divided by ω.

where $Y_c(K_x, K_y, \omega)$ is the harmonic admittance of the CMUT. Fig 6.12 shows a simple sketch of the driving voltage, source impedance and CMUT. The total available power from the voltage source, based on root mean
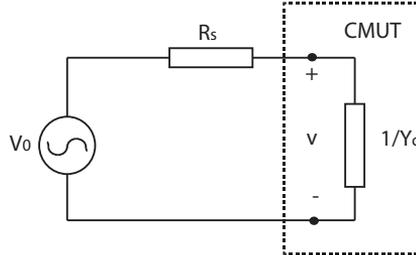

Figure 6.12: A simple circuit illustrating the CMUT with impedance $1/Y_c$ driven by a voltage V_0 and with a source impedance R_s.

square values is $\mathrm{Power}_{V_0} = V_0^2/(8R_s)$.

In order to express the transmitted pressure as a function of the driving voltage v we multiply with the pressure for a driving voltage of 1 V, P_c, and get:

$$P_{\mathrm{out}} = P_c v \quad , \tag{6.74}$$

where v includes the effect of the voltage division between the CMUT and the input resistor. The power transferred from the CMUT into the fluid medium outside is then given by:

$$\mathrm{Power}_{\mathrm{out}} = \frac{P_{\mathrm{out}}^2 A_b}{2Z_a} \quad , \tag{6.75}$$

where Z_a is the acoustic impedance of the fluid medium, and A_b is the effective aperture of the element. As the beam is steered to an off-axis direction the area becomes $A_b = A\cos\theta$, where θ is the steering angle and A is the total element area. To find an expression for the efficiency of the CMUT transducer, we calculated the relation between the transmitted power and the available power:

$$\frac{\mathrm{Power}_{\mathrm{out}}}{\mathrm{Power}_{V_0}} = \frac{4P_{\mathrm{out}}A_b R_s}{Z_a(R_s Y_c + 1)^2} \quad . \tag{6.76}$$

Fig. 6.13 shows an example of transmitted power in dB from an infinite CMUT array to plane waves radiated into water. In this array each element only consist of one infinite line of CMUTs.
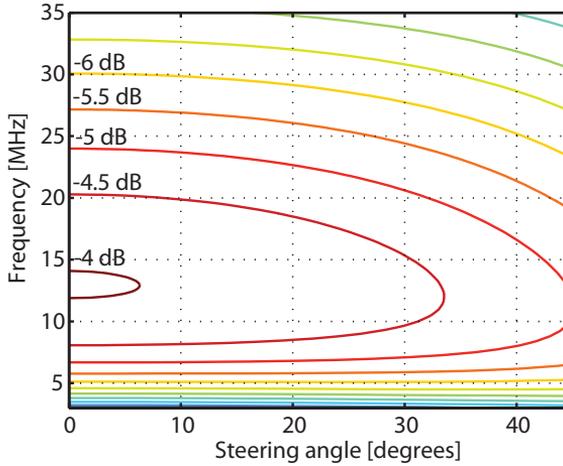
Figure 6.13: An example of transmitted power from an infinite array of single CMUTs into water. (The CMUTs are the same as the ones used in Paper VII.)

Combining several lines of CMUTs into elements

The method of harmonic transfer functions also opens for the modeling of an infinite array where several infinite lines of CMUTs are connected into elements. We choose to align the elements along the y-axis, hence, phase shifts between neighbor elements caused by off-axis steering will be given by $K_{x,\mathrm{el}}$. Fig. 6.14 illustrates how the infinite lines of CMUTs are combined into elements which are aligned along the y-axis.

If the ultrasound beam is steered off broadside, the driving voltage on each CMUT inside the same element should be the same, but there will be phase shifts between the voltages on adjacent elements. Since the phase shifts are between each element, and no longer between every CMUT, K_x given in eq. (6.55) will become:

$$K_{x,\mathrm{el}} = \frac{m_{\mathrm{el}}2\pi}{M_a/n_{\mathrm{cmut}}}, \text{ where } -M_a/(2n_{\mathrm{cmut}}) \leq m_{\mathrm{el}} < M_a/(2n_{\mathrm{cmut}}) \quad , \quad (6.77)$$

where n_{cmut} is the number of CMUT lines per element and m_{el} is an integer. The discrete excitation is given by:

$$v_{\mathrm{ex}}(x) = V_0 e^{-iK_{x,\mathrm{el}}x} \quad . \tag{6.78}$$

We find the discrete voltage spectrum, $V_{\mathrm{ex}}(K_{x,\mathrm{el}}, \omega)$ by inverse Fourier trans-
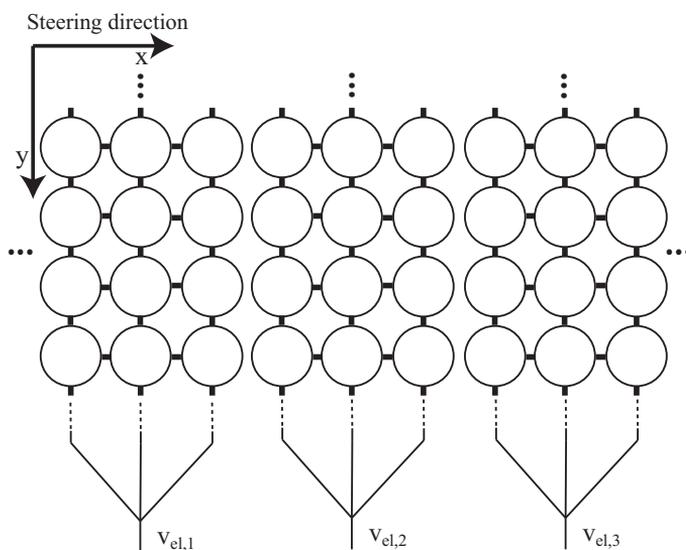
Figure 6.14: Illustration of the combination of infinite lines of CMUTs into elements. In the implementation of the model we have chosen to align the elements along the y-axis, and only steer the ultrasound beam in the x-direction.

forming the voltage distributions in the array:

$$V_{\text{ex}}(K_{x,\text{el}}, \omega) = \mathfrak{F}(v_{\text{ex}}(x)) \quad . \tag{6.79}$$

The currents are found by Fourier transforming the admittance, Y_c, multiplied with V_{ex}:

$$i_c(m,n) = \mathfrak{F}^{-1}\left\{Y_c(K_x, K_y, \omega)V_{\text{ex}}(K_{x,\text{el}}, \omega)\right\} \quad . \tag{6.80}$$

The harmonic admittance of the element is found by summing the current in each CMUT in the element, and dividing by the voltage, v_{el}, on this element:

$$Y_{\text{el}} = \sum_{\text{elem}} \left[\frac{i_c(m,n)}{v_{\text{el}}}\right] \quad . \tag{6.81}$$

The harmonic transfer function from voltage to pressure for the elements is found as:

$$P_{\text{el}}(K_x, K_y, \omega) = P_c(K_x, K_y, \omega)V_{\text{ex}}(K_x, K_y, \omega)/|v_{\text{el}}| \quad . \tag{6.82}$$

When the harmonic pressure and admittance is found, the efficiency of the array can be calculated as in eq. (6.76). An example is shown in Fig. 6.15, where we see that there are high Q resonances in the frequency range below the center frequency of the transducer.
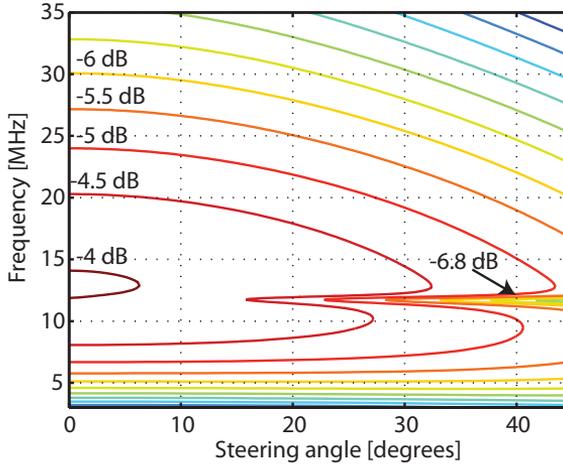

Figure 6.15: An example of transmitted power from an infinite array where two and two infinite lines of CMUTs are combined into elements.

A possible way of reducing these unwanted effects is to introduce a lossy layer on top of the CMUT, or by introducing low electrical source impedance, R_s. This is described in Paper VII.

Introducing double periodicities

Instead of connecting CMUTs into elements in k-space, as described above, it is possible to combine them in real space. This also makes it possible to include extra distance between elements, as illustrated in Fig. 5.5. When the acoustic impedance matrix is calculated, the period defined as L_x does not only include a single CMUT, but the width of a whole element, as shown in Fig. 6.16. The result is that the deflection, W_n, must be calculated for each mode and each CMUT within the element, thus it is a somewhat more time consuming approach. If many CMUTs are included in each element,
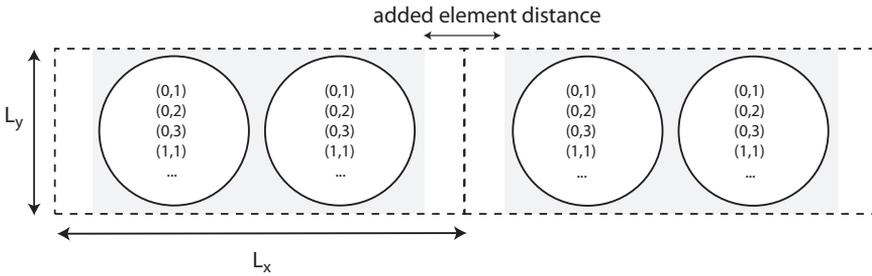
Figure 6.16: Illustration of two adjacent elements, each with two CMUTs in the x-direction and added distance between the elements.

and many modes are included for each CMUT, the processing time increases substantially. However, arrays with two or three CMUTs per element, and an element distance equivalent to the width of one CMUT, the analysis of the frequency range of interest and steering angles from $0°$ to $45°$ only takes a few minutes. If no extra distance is added between adjacent elements, this method produces exactly the same results as the Fourier based method described above.

Chapter 7

Summary of included work

I **Backing Requirements for CMUT Arrays on Silicon**

Sigrid Berg and Arne Rønnekleiv

Proc. IEEE Ultrasonics Symposium, 1952-1955,(2005)

This paper describes the modeling of well backed CMUT arrays with a center frequency around 3.5 MHz. The motion of the silicon substrate caused by the membrane excitation is included in the CMUT model. Three different crystal direction of silicon are compared, and we investigate the importance of limiting the thickness of the silicon substrate in order for the backing material to damp the generated surface acoustic waves, and hence limit the coupling of such waves into the fluid. This work is followed up in Paper VI.

II **Reducing Fluid Coupled Crosstalk Between Membranes in CMUT Arrays by Introducing a Lossy Top Layer**

Sigrid Berg and Arne Rønnekleiv

Proc. IEEE Ultrasonics Symposium, 594-597,(2006)

This paper described the investigation of how local resonances in the CMUT-fluid interface affect the CMUT array response, and how the introduction of a thin layer of a lossy material may damp the effects of such resonances significantly. Through simulations we also show that it is feasible to add an additional stiff coating for protection, without reducing the positive effects of the damping layer. The issues brought up in this work are further investigated and discussed in Paper VII.

III Reduction of Crosstalk in CMUT Arrays by Introducing Double Periodicities

Sigrid Berg and Arne Rønnekleiv

Proc. IEEE Ultrasonics Symposium, 2155-2158,(2007)

This paper describes CMUT array models with 3, 6 and 8 lines of CMUT cells in each element. We compare the CMUT-fluid crosstalk from arrays with single and double periodicities, and show that introducing an added distance between array elements reduces the high-Q resonances generated in the CMUT-fluid interface at the frequencies closest to the center frequency of the array. However, the dip in the response is increased at lower frequencies, and for arrays with double periodicity, the response is affected by the CMUT-fluid resonances even at broadside transmission. Single vs. double periodicities is further discussed in Paper VII.

IV Co-optimization of CMUT and Receive Amplifiers to Suppress Effects of Neighbor Coupling Between CMUT Elements

Sigrid Berg, Trond Ytterdal, and Arne Rønnekleiv

Proc. IEEE Ultrasonics Symposium, 2103-2106,(2008)

The paper argues that co-optimization of CMUTs and the receive amplifiers is an efficient way of reducing the effect of the dispersive guided modes which are caused by resonances in the CMUT-fluid interface. Transimpedance Amplifiers (TIAs) and Charge Sampling Amplifiers (CSAs) are proposed because the input impedance level easily can be adjusted. Simulations show that a low impedance path between the CMUT and the receive amplifiers results in suppression of the crosstalk effects, and that even though there is an impedance mismatch between the CMUT and the electronics, the noise figure is at an acceptable level. The use of a low impedance path is further discussed in Paper VII.

V Measurements of CMUT Neighbour Coupling Resonances in Fluids of Different Viscosities

Sigrid Berg and Arne Rønnekleiv

Proc. IEEE Ultrasonics Symposium, 435-438,(2010)

This paper compare measurements and simulations of the input admittance of two different CMUT arrays in air, kerosene and rapeseed oil, when neighbor elements are excited with 180° phase difference. The comparison shows that the model is well suited to describe the CMUT-fluid interaction. The model is further used to simulate the response from CMUT arrays radiating at 0°, 30° and 45° off broadside i water, kerosene and rapeseed oil, and low and high impedance paths between the CMUT and the transmit electronics are compared. Parts of the measurements of this work are also presented in Paper VII.

VI Acoustic Backing in 3-D Integration of CMUT With Front End Electronics

Sigrid Berg and Arne Rønnekleiv

IEEE Transactions on Ultrasonics, Ferroelectrics and Frequency Control, vol. 59, no 7, pp. 1537-1549, July 2012

This paper describes the modeling of 30 MHz CMUT arrays mounted on top of three additional silicon layers (for integrated circuits). The stack is modeled with an epoxy-tungsten composite acoustic backing, and three different bonding techniques are compared. We show that the total silicon thickness should be lower than 100 μm and that fusion bonding is the most suitable bonding method in order to avoid negative effects on the transmit pattern from surface acoustic waves generated in the silicon substrate.

VII Neighbor Coupling Resonances in CMUT Arrays Immersed in Fluids

Sigrid Berg and Arne Rønnekleiv

Submitted to IEEE Transactions on Ultrasonics, Ferroelectrics and Frequency Control, 21. March 2012.

In this paper we present a validation of the method of modeling the CMUT-fluid interaction. This is done by comparing measurements and simulations of a CMUT array where adjacent elements are excited with 180° phase difference. Further, the model is used to describe how dispersive guided modes generated in the CMUT-fluid interface may affect the response from CMUT arrays with single and double periodicity. Two different methods of reducing the negative impact

from these unwanted modes are discussed, namely the introduction of a thin layer of PDMS, and using a low impedance path between the CMUT and the transmit and receive electronics. The measurements presented in this paper were also presented in Paper V. Compared to Paper II, the model in this paper also includes the membrane motion in the y-direction.

Chapter 8

Conclusions

Capacitive Micromachined Ultrasonic Transducers (CMUTs) have been referred to as a promising technology for many years, and some have predicted that they will take over for traditional piezoelectric transducers in medical ultrasound imaging. Despite of many year's research both in academic institutions and in industry, there has still not been a proper commercial breakthrough. It seems that long term reliability and membrane charging are challenges that are not yet resolved. In addition, the issues concerning unwanted acoustic effects should be properly understood and dealt with.

This work shows that undesired acoustic effects, both caused by waves traveling in the silicon substrate and caused by local resonances in the CMUT-fluid interface should be taken into account when designing a CMUT transducer for immersion applications.

An important advantage for CMUTs is believed to be the relative ease of transducer-electronics integration. However, when several silicon wafers are included in a 3-D stack with bonding material between each silicon layer, the total thickness of the silicon substrates and the acoustic properties of the bonding materials must be considered in order to avoid coupling to surface acoustic waves (SAWs) in the silicon wafer, which further may couple into the fluid. Leakage of acoustic energy into the fluid may harm the transducer response at certain steering angles if the SAWs do not penetrate deep enough to be damped by the acoustic backing material. The penetration depth is frequency dependent. Through simulations, we have shown that it is feasible to make a 30 MHz CMUT array with three integrated circuit wafers beneath. However, each of the substrates should be thinner than 25 μm, adding to a total silicon thickness below 100 μm. In addition, state of the art fusion bonding techniques should be used for the 3-D integration. If anisotropic conductive adhesive (ACA) or solid liquid interdiffusion (SLID) bonding is

used, the silicon layers must be even thinner. The thickness requirements scale inversely with frequency, thus a 3 MHz CMUT transducer meets less strict requirements for the manufacturing process and must have a total silicon thickness of less than 1 mm.

A concern which has been put forward by several research groups is the effect of the cross coupling between CMUT membranes through the fluid. We have shown that local resonances in the CMUT-fluid interface may affect the array performance both for high and low frequency transducers. Depending on the array configuration, such crosstalk effects may be limited to off-axis steering. However, for arrays where the distance between elements is larger than between CMUTs within the element, such resonances may become radiating even at broadside transmission, and lead to high-Q dips in the frequency response. This indicates that it is advantageous to design CMUT arrays with equal spacing between the CMUTs. Many research groups characterize their CMUT arrays in high viscosity fluids such as vegetable oil, and measurements are often limited to transmission in the forward direction. We have shown that the dispersive guided modes are more pronounced in low viscosity fluids, such as water and kerosene, than in vegetable oil, and that the impact of the resonances increases with steering angle. This indicates that it is important to characterize the CMUT performance in a fluid with roughly the same viscosity as the fluid it is intended to operate in, and to include off-axis beam steering.

Through simulations we have shown that it is possible to damp the dispersive guided modes by introducing a soft damping material with high shear losses. A 2 μm thick layer of the PDMS material RTV615 damps most of the unwanted effects in a CMUT array with a center frequency of 15 MHz. The insertion loss increases with about 0.5 dB. Another way of reducing the impact of the CMUT-fluid interaction it to provide a low impedance path between the CMUT and the transmit and receive electronics. A smooth response is possible to achieve for arrays with single periodicity, whereas the high-Q dips still remains in the response from arrays with double periodicity. The overall efficiency of the transducer is poorer if a low impedance path is used, however, we believe that low power amplifiers based on field effect transistors may manage to detect the signal without adding too much noise, and hence, provide a signal path of good quality.

Bibliography

[1] A. Rønnekleiv, "CMUT array modelling through free acoustic CMUT modes and analysis of the fluid CMUT interface through fourier transform methods," *IEEE Transactions on Ultrasonics, Ferroelectrics and Frequency control*, vol. 52, no. 12, pp. 2173–2184, 2005.

[2] "Smart microsystems for diagnostic imaging in medicine, project number 159559," Project description of project financed by the Research Council of Norway (www.forskningsradet.no), 2004.

[3] S. C. Saha, "RF MEMS switches and switch circuits : Modeling of RF MEMS switches and development of RF MEMS capacitive switches and MEMS tunable filters," Ph.D. dissertation, Norwegian University of Science and Technology, Department of Electronics and Telecommunications, 2008.

[4] L. R. Cenkeramaddi, "Nanoscale analog front-end amplifiers for medical ultrasound imaging," Ph.D. dissertation, Norwegian University of Science and Technology, Department of Electronics and Telecommunications, 2011.

[5] H. Martinussen, "Heterodyne interferometry for dynamic and static characterization of micro and nanostructures," Ph.D. dissertation, Norwegian University of Science and Technology, Department of Electronics and Telecommunications, 2009.

[6] M. Sherar, B. Starkoski, W. Taylor, and F. Foster, "A 100 MHz B-scan ultrasound backscatter microscope," *Ultrasonic Imaging*, vol. 11, no. 2, pp. 95–105, 1989.

[7] N. Hozumi, R. Yamashita, C.-K. Lee, M. Nagao, K. Kobayashi, Y. Saijo, M. Tanaka, N. Tanaka, and S. Ohtsuki, "Time-frequency analysis for pulse driven ultrasonic microscopy for biological tissue characterization," *Ultrasonics*, vol. 42, no. 1-9, pp. 717–722, 2004.

[8] L. Zhang, X. Xu, C. Hu, L. Sun, J. T. Yen, J. M. Cannata, and K. K. Shung, "A high frequency, high frame rate duplex ultrasound linear array imaging system for small animal imaging," *IEEE Transactions of Ultrasonics, Ferroelectrics and Frequency control*, vol. 57, no. 7, pp. 1548–1557, 2010.

[9] M. I. Haller and B. T. Khuri-Yakub, "A surface micromachined electrostatic ultrasonic air transducer," *IEEE Transactions on Ultrasonics, Ferroelectrics and Frequency Control*, vol. 43, no. 1, pp. 1–6, 1996.

[10] I. Ladabaum, B. Khuri-Yakub, D. Spoliansky, and M. I. Haller, "Micromachined ultrasonic transducers (MUTs)," in *Ultrasonics Symposium (IUS), 1995 IEEE*, 1995, pp. 501–504.

[11] R. Waksman and P. W. Serrauys, *Handbook of vulnerable plaque.* Taylor and Francis, London, 2004.

[12] P. Libby, "Atherosclerosis: The new view," *Scientific Americanl*, Oct. 2002.

[13] "National heart lung and blood institute, disease and conditions index," US department on health and human services, Feb. 2009, http://www.nhlbi.nih.gov/health/dci/Diseases/Cad/CAD_WhatIs.html.

[14] Online: [Accessed January 10, 2012], URL: http://eu.volcanocorp.com/products/.

[15] Online: [Accessed January 12, 2012], URL: http://www.bostonscientific.com.

[16] Online: [Accessed January 10, 2012], URL: http://www.terumo.co.jp/English/products/index.html.

[17] Online: [Accessed January 12, 2012], URL: http://www.infraredx.com/.

[18] S. Z. Pinter and J. C. Lacefield, "Detectability of small blood vessels using high-frequency power doppler ultrasound," in *Ultrasonics Symposium (IUS), 2007 IEEE*, 2007, pp. 1085–1088.

[19] H. Verheul, E. Voest, and R. Schlingemann, "Are tumours angiogenesis-dependent?" *The Journal of Pathology*, vol. 202, no. 1, pp. 5–13, 2004.

[20] J. Folkman, "What is the evidence that tumors are angiogenesis dependent?" *Journal of National Cancer Institute*, vol. 82, no. 1, pp. 4–6, 1990.

[21] J.-J. Chen, Y.-H. Lin, C.-S. Chiang, J.-H. Hong, and C.-K. Yeh, "Characterization of tumor vasculature derived from angiogenesis and vasculogenesis by high frequency three dimensional doppler ultrasound," in *Ultrasonics Symposium (IUS), 2010 IEEE*, 2010, pp. 2319–2322.

[22] M. Jugold, M. Palmowski, J. Huppert, E. Woenne, M. Mueller, W. Semmler, and F. Kiessling, "Volumetric high-frequency doppler ultrasound enables the assessment of early antiangiogenic therapy effects on tumor xenografts in nude mice," *European Radiology*, vol. 18, pp. 753–758, 2008.

[23] K. K. Shung, J. Cannata, Q. Zhou, and J. Lee, "High frequency ultrasound: a new frontier for ultrasound," in *31st Annual International Conference of the IEEE EMBS*, 2009, pp. 1953–1955.

[24] G. R. Lockwood, D. Turnbull, D. A. Christopher, and F. S. Foster, "Beyond 30 MHz - applications of high frequency ultrasound imaging," *IEEE Engineering in Medicine and Biology*, no. November/December, pp. 60–71, 1996.

[25] Online: [Accessed January 15, 2012], URL: http://www.quantel-medical.com.

[26] C. J. Pavlin, M. D. Sherar, and F. Foster, "Subsurface ultrasound microscopic imaging of the intact eye," *Ophtalamology*, vol. 97, pp. 244–250, 1990.

[27] C. J. Pavlin, K. Harasiewicz, M. D. Sherar, and F. Foster, "Clinical use of ultrasound biomicroscopy," *Ophtalamology*, vol. 98, pp. 287–295, 1991.

[28] N. Arden and M. C. Nevitt, "Osteoarthritis: Epidemiology," *Best Practice & Research Clinical Rheumatology*, vol. 20, no. 1, pp. 3–25, 2006.

[29] T. Virén, S. Saarakkala, E. Kaleva, H. Nieminen, J. Jurvelin, and J. Töyräs, "Minimally invasive ultrasound method for intra-articular diagnostics of cartilage degeneration," *Ultrasound in Medicine & Biology*, vol. 35, no. 9, pp. 1546–1554, 2009.

[30] Y.-P. Huang and Y.-P. Zheng, "Intravascular ultrasound (IVUS): A potential arthroscopic tool for quantitative assessment of articular cartilage," *The Open Biomedical Engineering Journal*, vol. 3, pp. 13–20, 2009.

[31] Online: [Accessed January 14, 2012], URL: http://www.visualsonics. com.

[32] Online: [Accessed January 20, 2012], URL: http://en.wikipedia.org/ wiki/Sonar.

[33] T. L. Szabo, *Diagnostic Ultrasound Imaging: Inside Out.* Elsevier Academic Press, 2004.

[34] K. K. Shung, "Diagnostic ultrasound: Past, present, and future," *Journal of Medical and Biological Engineering*, vol. 31, no. 6, pp. 371–374, 2011.

[35] B. Odum, "Ultrasound analog electronics primer," *Analog Dialogue*, vol. 33, no. 5, pp. 1–3, 1999.

[36] Online: [Accessed January 10, 2012], URL: http://vscanultrasound. gehealthcare.com/.

[37] B. Angelsen, *Ultrasound Imaging - waves, signals and signal processing Vol I.* Emantec, 2000, www.ultrasoundbook.com.

[38] T. Gururaja, W. Schulze, L. Cross, R. Newnham, B. Auld, and Y. Wang, "Piezoelectric composite materials for ultrasonic transducer applications. part I: Resonant modes of vibration of PZT rod-polymer composites," *Sonics and Ultrasonics, IEEE Transactions on*, vol. 32, no. 4, pp. 481 – 498, 1985.

[39] D. Certon, O. Casula, F. Patat, and D. Royer, "Theoretical and experimental investigations of lateral modes in 1-3 piezocomposites," *Ultrasonics, Ferroelectrics and Frequency Control, IEEE Transactions on*, vol. 44, no. 3, pp. 643 –651, 1997.

[40] T. Gururaja, W. Schulze, L. Cross, and R. Newnham, "Piezoelectric composite materials for ultrasonic transducer applications. part II: Evaluation of ultrasonic medical applications," *Sonics and Ultrasonics, IEEE Transactions on*, vol. 32, no. 4, pp. 499 – 513, 1985.

[41] A. Nguyen-Dinh, L. Ratsimandresy, P. Mauchamp, R. Dufait, A. Flesch, and M. Lethiecq, "High frequency piezo-composite transducer array designed for ultrasound scanning applications," in *Ultrasonics Symposium (IUS), 1996 IEEE*, vol. 2, 1996, pp. 943 –947 vol.2.

[42] O. Oralkan, S. Hansen, B. Bayram, G. Yaralioglu, A. Ergun, and B. Khuri-Yakub, "High-frequency CMUT arrays for high-resolution medical imaging," in *Ultrasonics Symposium (IUS), 2004 IEEE*, vol. 1, 2004, pp. 399 – 402 Vol.1.

[43] J. Cannata, J. Williams, Q. Zhou, T. Ritter, and K. Shung, "Development of a 35-MHz piezo-composite ultrasound array for medical imaging," *Ultrasonics, Ferroelectrics and Frequency Control, IEEE Transactions on*, vol. 53, no. 1, pp. 224 –236, 2006.

[44] S. Michau, P. Mauchamp, and R. Dufait, "Piezocomposite 30MHz linear array for medical imaging: design challenges and performances evaluation of a 128 elements array," in *Ultrasonics Symposium (IUS), 2004 IEEE*, vol. 2, 2004, pp. 898 – 901 Vol.2.

[45] S. Carey, C. Gregory, M. Brewin, M. Birch, S. Ng, and J. Hatfield, "PVdF array characterisation for high frequency ultrasonic imaging," in *Ultrasonics Symposium (IUS), 2004 IEEE*, vol. 3, 2004, pp. 1930 – 1933 Vol.3.

[46] E. C. Wente, "A condenser transmitter as a uniformly sensitive instrument for the absolute measurement of sound intensity," *Phys. Rev.*, vol. 10, pp. 39–63, 1917.

[47] J. H. Cantrell, J. S. Heyman, W. T. Yost, M. A. Torbett, and M. A. Breazeale, "Broadband electrostatic acoustic transducer for ultrasonic measurements in liquids," *Review of Scientific Instruments*, vol. 50, no. 1, pp. 31 –33, 1979.

[48] D. Schindel and D. Hutchins, "Applications of micromachined capacitance transducers in air-coupled ultrasonics and nondestructive evaluation," *Ultrasonics, Ferroelectrics and Frequency Control, IEEE Transactions on*, vol. 42, no. 1, pp. 51 –58, 1995.

[49] H. Carr and C. Wykes, "Diagnostic measurements in capacitive transducers," *Ultrasonics*, vol. 31, no. 1, pp. 13–20, 1993.

[50] D. Schindel and D. Hutchins, "Capacitance devices for the controlled generation of ultrasonic fields in liquids," in *Ultrasonics Symposium (IUS), 1991 IEEE*, 1991, pp. 301 –304 vol.1.

[51] D. Schindel, L. Zou, D. Hutchins, and M. Sayer, "Capacitance devices for the generation of airborne ultrasonic fields," in *Ultrasonics Symposium (IUS), 1992 IEEE*, 1992, pp. 843 –846 vol.2.

[52] K. Suzuki, K. Higuchi, and H. Tanigawa, "A silicon electrostatic ultrasonic transducer," *Ultrasonics, Ferroelectrics and Frequency Control, IEEE Transactions on*, vol. 36, no. 6, pp. 620 –627, 1989.

[53] D. Schindel, D. Hutchins, L. Zou, and M. Sayer, "The design and characterization of micromachined air-coupled capacitance transducers," *Ultrasonics, Ferroelectrics and Frequency Control, IEEE Transactions on*, vol. 42, no. 1, pp. 42 –50, 1995.

[54] A. Ergun, B. Temelkuran, E. Ozbay, and A. Atalar, "A new detection method for capacitive micromachined ultrasonic transducers," in *Ultrasonics Symposium (IUS), 2008 IEEE*, vol. 2, 1998, pp. 1007 –1010 vol.2.

[55] A. Bozkurt, F. Degertekin, A. Atalar, and B. Khuri-Yakub, "Analytic modeling of loss and cross-coupling in capcitive micromachined ultrasonic transducers," in *Ultrasonics Symposium (IUS), 1998 IEEE*, 1998, pp. 1025–1028.

[56] S. Hansen, N. Irani, F. L. Degertekin, and B. T. Khuri-Yakub, "Defect imaging by micromachined ultrasonic air transducers," in *Ultrasonics Symposium (IUS), 1998 IEEE*, 1998, pp. 1003–1007.

[57] I. Ladabaum, X. Jin, H. Soh, F. Pierre, A. Atalar, and B. Khuri-Yakub, "Microfabricated ultrasonic transducers: towards robust models and immersion devices," in *Ultrasonics Symposium (IUS), 1996 IEEE*, vol. 1, 1996, pp. 335 –338 vol.1.

[58] H. T. Soh, I. Ladabaum, A. Atalar, C. F. Quate, and B. T. Khuri-Yakub, "Silicon micromachined ultrasonic immersion transducers," *Appl. Phys. Lett*, vol. 69, pp. 3674–3676, 1996.

[59] X. Jin, F. Degertekin, S. Calmes, X. Zhang, I. Ladabaum, and B. Khuri-Yakub, "Micromachined capacitive transducer arrays for medical ultrasound imaging," in *Ultrasonics Symposium (IUS), 1998 IEEE*, vol. 2, 1998, pp. 1877 –1880 vol.2.

[60] S. Machida, S. Migitaka, H. Tanaka, K. Hashiba, H. Enomoto, Y. Tadaki, and T. Kobayashi, "Analysis of the charging problem in capacitive micro-machined ultrasonic transducers," in *Ultrasonics Symposium (IUS), 2008 IEEE*, 2008, pp. 383 –385.

[61] S. Machida, T. Kobayashi, M. Degawa, T. Takezaki, H. Tanaka, S. Migitaka, K. Hashiba, H. Enomoto, T. Nagata, Y. Yoshimura, K. Asafusa, K. Ishida, S. Sano, and M. Izumi, "Capacitive micromachined ultrasonic transducer with driving voltage over 100 V and vibration durability over 10^{11} cycles," in *Solid-State Sensors, Actuators and Microsystems Conference, 2009. TRANSDUCERS 2009. International*, 2009, pp. 2218 –2221.

[62] B. Bayram, E. Hæggström, G. G. Yaralioglu, and B. T. Khuri-Yakub, "A new regime for operating capacitive micromachined ultrasonic transducers," *IEEE Transactions on Ultrasonics, Ferroelectrics and Frequency Control*, vol. 50, no. 9, pp. 1184–1190, 2003.

[63] Y. Huang, E. Hæggstrøm, B. Bayram, X. Zhuang, A. Ergun, C.-H. Cheng, and B. Khuri-Yakub, "Comparison of conventional and collapsed region operation of capacitive micromachined ultrasonic transducers," *Ultrasonics, Ferroelectrics and Frequency Control, IEEE Transactions on*, vol. 53, no. 10, pp. 1918 –1933, 2006.

[64] D. Yeh, O. Oralkan, I. Wygant, M. O'Donnell, and B. Khuri-Yakub, "3-D ultrasound imaging using a forward-looking CMUT ring array for intravascular/intracardiac applications," *Ultrasonics, Ferroelectrics and Frequency Control, IEEE Transactions on*, vol. 53, no. 6, pp. 1202 –1211, 2006.

[65] F. Degertekin, R. Guldiken, and M. Karaman, "Annular-ring CMUT arrays for forward-looking IVUS: transducer characterization and imaging," *Ultrasonics, Ferroelectrics and Frequency Control, IEEE Transactions on*, vol. 53, no. 2, pp. 474 –482, 2006.

[66] U. Demirci, O. Oralkan, J. Johnson, A. Ergun, M. Karaman, and B. Khuri-Yakub, "Capacitive micromachined ultrasonic transducer arrays for medical imaging: experimental results," in *Ultrasonics Symposium (IUS), 2001 IEEE*, vol. 2, 2001, pp. 957 –960 vol.2.

[67] I. O. Wygant, X. Zhuang, D. T. Yeh, O. Oralkan, A. S. Ergun, M. Karaman, and B. T. Khuri-Yakub, "Integration of 2D CMUT array with front-end electronics for volumetric ultrasound imaging,"

IEEE Transactions of Ultrasonics, Ferroelectrics and Frequency control, vol. 55, no. 2, pp. 327–342, 2008.

[68] P. Cristman, O. Oralkan, X. Zhuang, T.-J. Ma, S. Vaithilingam, T. Carver, I. Wygant, and B. Khuri-Yakub, "A 2D CMUT hydrophone array: Characterization results," in *Ultrasonics Symposium (IUS), 2009 IEEE International*, 2009, pp. 992 –995.

[69] A. Logan, L. Wong, and J. Yeow, "2-D CMUT wafer bonded imaging arrays with a row-column addressing scheme," in *Ultrasonics Symposium (IUS), 2009 IEEE International*, 2009, pp. 984 –987.

[70] Y. Huang, E. O. Hæggström, X. Zhuang, A. S. Ergun, and B. T. Khuri-Yakub, "Optimized membrane configuration improves CMUT performance," in *Ultrasonics Symposium (IUS), 2004 IEEE*, 2004, pp. 505–508.

[71] S. Wong, M. Kupnik, X. Zhuang, D. song Lin, K. Butts-Pauly, and B. Khuri-yakub, "Evaluation of wafer bonded CMUTs with rectangular membranes featuring high fill factor," *Ultrasonics, Ferroelectrics and Frequency Control, IEEE Transactions on*, vol. 55, no. 9, pp. 2053 –2065, 2008.

[72] O. Oralkan, B. Bayram, G. Yaralioglu, A. Ergun, M. Kupnik, D. Yeh, I. Wygant, and B. Khuri-Yakub, "Experimental characterization of collapse-mode CMUT operation," *Ultrasonics, Ferroelectrics and Frequency Control, IEEE Transactions on*, vol. 53, no. 8, pp. 1513 –1523, 2006.

[73] R. Guldiken, M. Balantekin, J. Zahorian, and F. Degertekin, "Characterization of dual-electrode CMUTs: demonstration of improved receive performance and pulse echo operation with dynamic membrane shaping," *Ultrasonics, Ferroelectrics and Frequency Control, IEEE Transactions on*, vol. 55, no. 10, pp. 2336 –2344, 2008.

[74] B. Bayram, O. Oralkan, A. Ergun, E. Hæggstrøm, G. Yaralioglu, and B. Khuri-Yakub, "Capacitive micromachined ultrasonic transducer design for high power transmission," *Ultrasonics, Ferroelectrics and Frequency Control, IEEE Transactions on*, vol. 52, no. 2, pp. 326 –339, 2005.

[75] I. Ladabaum, X. Jin, H. T. Soh, A. Atalar, and B. T. Khuri-Yakub, "Surface micromachined capacitive ultrasonic transducer,"

IEEE Transactions on Ultrasonics, Ferroelectrics and Frequency Control, vol. 45, no. 3, pp. 678–690, 1998.

[76] G. Caliano, R. Carotenuto, E. Cianci, V. Foglietti, A. Caronti, A. Iula, and M. Pappalardo, "Design, fabrication and characterization for a capacitive micromachined ultrasonic probe for medical imaging," *IEEE Transactions of Ultrasonics, Ferroelectrics and Frequency control*, vol. 52, no. 12, pp. 2259–2269, 2005.

[77] D. M. Mills, "Medial imaging with capacitive micromachined ultrasonic transducer (CMUT) arrays," in *Ultrasonics Symposium (IUS), 2004 IEEE*, 2004, pp. 384–390.

[78] M. Legros, C. Meynier, R. Dufait, and F. Tranquart, "Piezocomposite and CMUT array asessment through in vitro imaging performance," in *Ultrasonics Symposium (IUS), 2008 IEEE*, 2008, pp. 1142–1145.

[79] S. Zhou, P. Reynolds, and J. A. Hossack, "Improving the performance of capacitive micromachined ultrasound transducers using modified membrane and support structures," in *Ultrasonics Symposium (IUS), 2005 IEEE*, 2005, pp. 1925–1928.

[80] R. Guldiken, J. McLean, and F. Degertekin, "CMUTs with dual electrode structure for improved transmit and receive performance," *Ultrasonics, Ferroelectrics and Frequency Control, IEEE Transactions on*, vol. 53, no. 2, pp. 483 –491, 2006.

[81] C. Goldsmith, J. Ehmke, A. Malczewski, B. Pillans, S. Eshelman, Z. Yao, J. Brank, and M. Eberly, "Lifetime characterization of capacitive RF MEMS switches," in *Microwave Symposium Digest, 2001 IEEE MTT-S International*, 2001, pp. 227 –230 vol.1.

[82] H. Martinussen, A. Aksnes, and H. Engan, "Investigation of charge diffusion in CMUTs using optical interferometry," in *Ultrasonics Symposium (IUS), 2008 IEEE*, 2008, pp. 1218 –1221.

[83] Y. Huang, X. Zhuang, E. O. Hæggstrøm, A. S. Ergun, C.-H. Cheng, and B. T. Khuri-Yakub, "Capacitive micromachined ultrasonic transducers (CMUTs) with isolation posts," *Ultrasonics*, vol. 48, no. 1, pp. 74–81, 2008.

[84] Y. Huang, E. Hæggström, B. Bayram, X. Zhuang, A. Ergun, C. Cheng, and B. Khuri-Yakub, "Collapsed regime operation of capacitive micromachined ultrasonic transducers based on wafer-bonding

technique," in *Ultrasonics Symposium (IUS), 2003 IEEE*, 2003, pp. 1161–1164.

[85] Y. Huang, E. O. Hæggström, X. Zhuang, A. S. Ergun, and B. T. Khuri-Yakub, "A solution to the charging problem in capacitive micromachined ultrasonic transducers," *IEEE Transactions of Ultrasonics, Ferroelectrics and Frequency control*, vol. 52, no. 4, pp. 578–580, 2005.

[86] M. Kupnik, A. Ergun, Y. Huang, and B. Khuri-Yakub, "Extended insulation layer structure for CMUTs," in *Ultrasonics Symposium, 2007. IEEE*, 2007, pp. 511 –514.

[87] J. Knight and F. Degertekin, "Fabrication and characterization of cMUTs for forward looking intravascular ultrasound imaging," in *Ultrasonics Symposium (IUS), 2003 IEEE*, 2003, pp. 577 – 580.

[88] A. Buhrdorf, A. Lohfink, S. Junge, P. Eccardt, and W. Benecke, "Fabrication and characterization of a new capacitive micromachined ultrasonic transducer (cMUT) using polysilicon as membrane and sacrificial layer material," in *Ultrasonics Symposium (IUS), 2003 IEEE*, 2003, pp. 1951 – 1954.

[89] A. S. Ergun, G. G. Yaralioglu, and B. T. Khuri-Yakub, "Capacitive micromachined ultrasonic transducers: Theory and technology," *Journal of Aerospace Engineering*, pp. 76–84, 2003.

[90] Y. Huang, A. Ergun, E. Hæggstrøm, M. Badi, and B. Khuri-Yakub, "Fabricating capacitive micromachined ultrasonic transducers with wafer-bonding technology," *Microelectromechanical Systems, Journal of*, vol. 12, no. 2, pp. 128 – 137, 2003.

[91] G. Caliano, A. Caronti, A. Savoia, C. Longo, M. Pappalardo, E. Cianci, and V. Foglietti, "Capacitive micromachined ultrasonic transducer (cMUT) made by a novel "reverse fabrication process"," in *Ultrasonics Symposium (IUS), 2005 IEEE*, 2005, pp. 479 – 482.

[92] A. Stoffel, A. Kovács, W. Kronast, and B. Müller, "LPCVD against PECVD for micromechanical applications," *Journal of Micromechanics and Microengineering*, vol. 6, no. 1, p. 1, 1996.

[93] I. Ladabaum, P. Wagner, C. Zanelli, J. Mould, P. Reynolds, and G. Wojcik, "Silicon substrate ringing in microfabricated ultrasonic

transducers," in *Ultrasonics Symposium (IUS), 2000 IEEE*, 2000, pp. 943–946.

[94] A. Caronti, A. Coppa, A. Savoia, C. Longo, P. Gatta, B. Mauti, A. Corbo, B. Calabrese, G. Bollino, A. Paz, G. Caliano, and M. Pappalardo, "Curvilinear capacitive micromachined ultrasonic transducer (CMUT) array fabricated using a reverse process," in *Ultrasonics Symposium (IUS), 2008 IEEE*, 2008, pp. 2092 –2095.

[95] X. Zhuang, I. O. Wygant, D.-S. Lin, M. Kupnik, Ömer Oralkan, and B. T. Khuri-Yakub, "Wafer bonded 2-D CMUT arrays incorporating through-wafer trench-isolated interconnects with a supporting frame," *IEEE Transactions of Ultrasonics, Ferroelectrics and Frequency control*, vol. 56, no. 1, pp. 182–192, 2009.

[96] K. K. Park, H. Lee, M. Kupnik, and B. Khuri-Yakub, "Fabrication of capacitive micromachined ultrasonic transducers via local oxidation and direct wafer bonding," *Microelectromechanical Systems, Journal of*, vol. 20, no. 1, pp. 95 –103, 2011.

[97] K. Midtbø, A. Rønnekleiv, and D. T. Wang, "Fabrication and characterization of CMUTs realized by wafer bonding," in *Ultrasonics Symposium (IUS), 2006 IEEE*, 2006, pp. 934–937.

[98] A. Logan and J. Yeow, "1-D CMUT arrays fabricated using a novel wafer bonding process," in *Ultrasonics Symposium (IUS), 2008 IEEE*, 2008, pp. 1226 –1229.

[99] ——, "Fabricating capacitive micromachined ultrasonic transducers with a novel silicon-nitride-based wafer bonding process," *Ultrasonics, Ferroelectrics and Frequency Control, IEEE Transactions on*, vol. 56, no. 5, pp. 1074 –1084, 2009.

[100] P.-C. Eccardt, K. Niederer, T. Scheiter, and C. Hierold, "Surface micromachined ultrasound transducers in CMOS technology," in *Ultrasonics Symposium (IUS), 1996 IEEE*, 1996, pp. 959–962.

[101] R. A. Noble, R. R. Davies, M. M. Day, L. Koker, D. O. King, A. R. D. Jones, J. S. McIntosh, D. A. Hutchins, T. J. Robertson, and P. Saul, "A cost-effective and manufacturable route to the fabrication of high-density 2D micromachined ultrasonic transducer arrays and (CMOS) signal conditioning electronics on the same silicon substrate," in *Ultrasonics Symposium (IUS), 2001 IEEE*, 2001, pp. 941–945.

[102] R. A. Noble, R. R. Davies, D. O. King, M. M. Day, A. R. D. Jones, J. S. McIntosh, D. A. Hutchins, and P. Saul, "Low-temperature micromachined CMUTs with fully-integrated analogue front-end electronics," in *Ultrasonics Symposium (IUS), 2002 IEEE*, 2002, pp. 1045–1050.

[103] C. Daft, S. Calmes, D. da Graca, K. Patel, P. Wagner, and I. Ladabaum, "Microfabrication ultrasonic transducers monolithically integrated with high voltage electronics," in *Ultrasonics Symposium (IUS), 2004 IEEE*, 2004, pp. 493–496.

[104] C. Daft, P. Wagner, B. Bymaster, S. Panda, K. Patel, and I. Ladabaum, "cMUTs and electonics for 2D and 3D imaging: Monolithic integration, in-handle chip sets and system implications," in *Ultrasonics Symposium (IUS), 2005 IEEE*, 2005, pp. 463–474.

[105] M. Hochmann, J. Zahorian, S. Satir, G. Furun, T. Xu, M. Karaman, P. Hasler, and F. L. Degertekin, "CMUT-on-CMOS for forward-looking IVUS: Improved fabrication and real-time imaging," in *Ultrasonics Symposium (IUS), 2010 IEEE*, 2010.

[106] J. Zahorian, M. Hochman, T. Xu, S. Satir, G. Gurun, M. Karaman, and F. Degertekin, "Monolithic CMUT-on-CMOS integration for intravascular ultrasound applications," *Ultrasonics, Ferroelectrics and Frequency Control, IEEE Transactions on*, vol. 58, no. 12, pp. 2659 –2667, 2011.

[107] C. H. Cheng, E. M. Chow, X. Jin, S. Ergun, and B. Khuri-Yakub, "An efficient electrical addressing method using through-wafer vias for two-dimensional ultrasonic arrays," in *Ultrasonics Symposium (IUS), 2000 IEEE*, 2000, pp. 1179–1182.

[108] I. O. Wygant, X. Zhuang, D. T. Yeh, O. Oralkan, A. S. Ergun, M. Karaman, and B. T. Khuri-Yakub, "Integration of 2D CMUT array with front-end electronics for volumetric ultrasound imaging," *IEEE Transactions of Ultrasonics, Ferroelectrics and Frequency control*, vol. 55, no. 2, pp. 327–342, 2008.

[109] X. Zhuang, D.-S. Lin, A. Ergun, O. Oralkan, and B. Khuri-Yakub, "P2P-6 trench-isolated CMUT arrays with a supporting frame," in *Ultrasonics Symposium (IUS), 2006 IEEE*, 2006, pp. 1955 –1958.

[110] J. Due-Hansen, K. Midtbø, E. Poppe, A. Summanwar, G. Jensen, L. Breivik, and D. Wang, "CMUT arrays with polysilicon bottom

electrodes and nanometer precision cavity gaps," in *Proceedings of Micro Mechanics Europe, Tønsberg, Norway, June 19-22*, 2011.

[111] J. Due-Hansen, K. Midtbø, E. Poppe, A. Summanwar, G. Jensen, L. Breivik, D. Wang, and K. Schjølberg-Henriksen, "Fabrication processes for CMUT arrays with polysilicon electrodes, nanometer precision cavity gaps, and through-silicon vias," *Accepted for publication in J. Micromech. Microeng*, 2012.

[112] S. Berg, K. Chapagain, J. Due-Hansen, K. A. Ingebrigtsen, G. U. Jensen, K. Midtbø, E. U. Poppe, A. Rønnekleiv, and D. T. Wang, "Wafer bond CMUT array with conductive VIAs," Patent, September, 2010, WO/2010/109205.

[113] B. Bayram, M. Kubnik, G. G. Yaralioglu, O. Oralkan, A. S. Ergun, D.-S. Lin, S. H. Wong, and B. T. Khuri-Yakub, "Finite element modeling and experimental characterization of crosstalk in 1-D CMUT arrays," *IEEE Transactions of Ultrasonics, Ferroelectrics and Frequency Control*, vol. 54, no. 2, pp. 418–428, 2007.

[114] M. Wilm, A. Reinhardt, V. Laude, R. Armati, W. Daniau, and S. Ballandras, "Three-dimensional modelling of micromachined-ultrasonic-transducer arrays operating in water," *Ultrasonics*, vol. 43, no. 6, pp. 457–465, 2005.

[115] I. Ladabaum and P. A. Wagner, "Microfabricated ultrasonic transducer with suppressed substrate modes," Patent, March, 2005, united States Patent, Patent no: US 6862254B2.

[116] Khuri-Yakub, A. S. Ergum, and G. Yaralioglu, "Capacitive membrane ultrasonic transducers with reduced bulk wave generation and method," Patent, January, 2008, united States Patent, Patent no: US 7,321,181 B2.

[117] L. Rayleigh, "On waves propagated along the plane surface of an elastic solid," *London Math. Soc,*, vol. 17, pp. 4–11, 1885.

[118] I. A. Viktorov, *Rayleigh and Lamb Waves, Physical theory and applications.*   Plenum Press, New York, 1967.

[119] H. Meier, T. Baier, and G. Riha, "Miniaturization and advanced functionalities of SAW devices," *Microwave Theory and Techniques, IEEE Transactions on*, vol. 49, no. 4, pp. 743 –748, 2001.

[120] A. Zaki, H.-C. Ou, M. Zaghloul, and H. Elsimary, "Implementation of MEMS-SAW device on RF circuits for wireless applications," in *Circuits and Systems, 2007. MWSCAS 2007. 50th Midwest Symposium on*, 2007, pp. 614 –617.

[121] H. Lamb, "On waves in an elastic plate," *Proceedings of the Royal Society of London. Series A*, vol. 93, no. 648, pp. 114–128, 1917.

[122] X. Jin, Ömer Oralkan, L. Degertekin, and B. T. Khuri-Yakub, "Characterization of one-dimensional capacitive micromachined ultrasonic immersion transducer arrays," *IEEE Transactions of Ultrasonics, Ferroelectrics and Frequency control*, vol. 48, no. 3, pp. 750–760, 2001.

[123] C. E. Baumgartner, R. S. Lewandowski, D. M. Mills, L. S. Smith, and D. G. Wildes, "Backing material for micromachined ultrasonic transducer devices," Patent, December, 2004, US6831394.

[124] M. Grewe, T. Gururaja, T. Shrout, and R. Newnham, "Acoustic properties of particle/polymer composites for ultrasonic transducer backing applications," *Ultrasonics, Ferroelectrics and Frequency Control, IEEE Transactions on*, vol. 37, no. 6, pp. 506 –514, 1990.

[125] A. J. Devaney and H. Levine, "Effective elastic parameters of random composites," *Appl. Physics Lett.*, vol. 37, no. 4, pp. 377–379, 1980.

[126] K. Chapagain and A. Rønnekleiv, "Minimizing the bottom reflections in ultrasonic CMUT transducer backing using low profil structuring," in *Ultrasonics Symposium (IUS), 2009 IEEE*, 2009.

[127] B. Bayram, M. Kupnik, G. G. Yaralioglu, Ömer Oralkan, D. Lin, X. Zhuang, A. S. Ergun, A. F. Sarioglu, S. H. Wong, and B. T. Khuri-Yakub, "Characterization of cross-coupling in capacitive micromachined ultrasonic transducers," in *Ultrasonics Symposium (IUS), 2005 IEEE*, 2005, pp. 601–604.

[128] P.-C. Eccardt, A. Lohfink, and H.-G. von Garssen, "Analysis of crosstalk between fluid coupled CMUT membranes," in *Ultrasonics Symposium (IUS), 2005 IEEE*, 2005, pp. 593–596.

[129] A. Caronti, A. Savoia, G. Caliano, and M. Pappalardo, "Acoustic coupling in capacitive micromachined ultrasonic transducers: Modeling and experiments," *IEEE Transactions of Ultrasonics, Ferroelectrics and Frequency control*, vol. 52, no. 12, pp. 2220–2234, 2005.

[130] A. Caronti, C. Longo, A. Savoia, P. Gatta, G. Caliano, and M. Pappalardo, "Analysis of acoustic interaction effects and crosstalk in CMUT linear arrays for medical imaging," in *Ultrasonics Symposium (IUS), 2006 IEEE*, 2006, pp. 582–585.

[131] E. Campbell, L. A. J. Davis, G. Hayward, and D. Hutchins, "Cross-coupling in sealed CMUT arrays for immersion applications," in *Ultrasonics Symposium (IUS), 2007 IEEE*, 2007, pp. 2135–2138.

[132] A. Caronti, R. Carotenuto, G. Caliano, and M. Pappalardo, "A finite element study of cross coupling in 1-d capacitive micromachined ultrasonic transducer arrays," in *Ultrasonics Symposium (IUS), 2002 IEEE*, 2002, pp. 1059–1062.

[133] B. Bayram, G. G. Yaralioglu, M. Kupnik, and B. T. Khuri-Yakub, "Acoustic crosstalk reduction method for CMUT arrays," in *Ultrasonics Symposium (IUS), 2006 IEEE*, 2006, pp. 590–593.

[134] S. Zhou and J. Hossack, "Reducing inter-element acoustic crosstalk in capacitive micromachined ultrasound transducers," *IEEE Transactions on ultrasonics, ferroelectrics and frequency control*, vol. 54, no. 6, pp. 1217–1228, 2007.

[135] S. Zhou, G. L. Wojcik, and J. Hossack, "An approach for reducing adjacent element crosstalk in ultrasound arrays," *IEEE Transactions of Ultrasonics, Ferroelectrics and Frequency Control*, vol. 50, no. 12, pp. 1752–1761, 2003.

[136] P.-C. Eccardt, K. Niederer, T. Scheiter, and C. Hierold, "Surface micromachined ultrasound transducers in CMOS technology," in *Ultrasonics Symposium (IUS), 1996 IEEE*, vol. 2, 1996, pp. 959 –962 vol.2.

[137] G. G. Yaralioglu, A. S. Ergun, B. Bayram, E. Hæggstrøm, and B. T. Khuri-Yakub, "Calculation and measurement of electromechanical coupling coefficient of capacitive micromachined ultrasonic transducers," *IEEE Transactions on Ultrasonics, Ferroelectrics and Frequency Control*, vol. 50, no. 4, pp. 449–456, 2003.

[138] A. Lohfink and P.-C. Eccardt, "Linear and nonlinear equivalent circuit modeling of CMUTs," *Ultrasonics, Ferroelectrics and Frequency Control, IEEE Transactions on*, vol. 52, no. 12, pp. 2163 –2172, 2005.

[139] A. Aksnes, E. Leirset, H. Martinussen, and H. Engan, "Modeling and optical characterization of vibrating micro- and nanostructures," in

Society of Photo-Optical Instrumentation Engineers (SPIE) Conference Series, ser. Society of Photo-Optical Instrumentation Engineers (SPIE) Conference Series, vol. 7063, 2008.

[140] E. Leirset, A. Rønnekleiv, and A. Aksnes, "Radiation pattern deterioration for phase steered capacitive micromachined ultrasonic transducer arrays due to cross coupling," in *Ultrasonics Symposium (IUS), 2011 IEEE*, 2011.

[141] W. P. Mason, *Electromechanical Transducers and wave filters*. New York: Van Nostrand, 1942.

[142] L. E. Kinsler, A. R. Frey, A. Coppers, and J. V. Sanders, *Fundamentals of Acoustics*. John Wiley & Sons, Fourth edition, 2000.

[143] J. W. Nilsson and S. A. Riedel, *Electric circuits*, 5th ed. Addison-Wesley Publishing Company, 1996.

[144] A. Caronti, R. Carotenuto, and M. Pappalardo, "Electromechanical coupling factor of capacitive micromachined ultrasonic transducers," *The Journal of the Acoustical Society of America*, vol. 113, no. 1, pp. 279–288, 2003.

[145] S. Berg and A. Rønnekleiv, "Backing requirements for CMUT arrays on silicon," in *Ultrasonics Symposium (IUS), 2005 IEEE*, 2005, pp. 1952–1955.

[146] ——, "Reducing fluid coupled crosstalk between membranes in CMUT arrays by introducing a lossy top layer," in *Ultrasonics Symposium (IUS), 2006 IEEE*, 2006, pp. 594–597.

[147] ——, "Reduction of crosstalk in CMUT arrays by introducing double periodicities," in *Ultrasonics Symposium (IUS), 2007 IEEE*, 2007, pp. 2155–2158.

[148] S. Berg, T. Ytterdal, and A. Ronnekleiv, "Co-optimization of CMUT and receive amplifiers to suppress effects of neighbor coupling between CMUT elements," in *Ultrasonics Symposium (IUS), 2008 IEEE*, 2008, pp. 2103 –2106.

[149] S. Berg and A. Ronnekleiv, "Challenges with acoustic backing of CMUT arrays on silicon with integrated electronics," in *Ultrasonics Symposium (IUS), 2009 IEEE International*, 2009, pp. 980 –983.

[150] ——, "Measurements of CMUT neighbour coupling resonances in fluids of different viscosities," in *Ultrasonics Symposium (IUS), 2010 IEEE*, 2010, pp. 435 –438.

[151] P. Karasudhi, *Foundations of Solid Mechanics*. Kluwer Academic publishers: Dordrecht, Boston, London, 1991.

[152] L. A. Segel and G. H. Handelman, *Mathematics Applied to Continuum Mechanics*. New York: Dover, 1987.

Paper I

Backing requirements for CMUT arrays on silicon

Sigrid Berg and Arne Rønnekleiv

Proc. IEEE Ultrasonics Symposium, 1952-1955,(2005)

Paper II

Reducing fluid coupled crosstalk between membranes in CMUT arrays by introducing a lossy top layer

Sigrid Berg and Arne Rønnekleiv.

Is not included due to copyright

Paper III

Reduction of Crosstalk in CMUT Arrays by Introducing Double Periodicities

Sigrid Berg and Arne Rønnekleiv.

Is not included due to copyright

Paper IV

Co-optimization of CMUT and receive amplifiers to suppress effects of neighbor coupling between CMUT elements

Sigrid Berg, Trond Ytterdal, and Arne Rønnekleiv.

Is not included due to copyright

Paper V

Measurements of CMUT neighbour coupling resonances in fluids of different viscosities

Sigrid Berg and Arne Rønnekleiv

Is not included due to copyright

Paper VI

Acoustic Backing in 3-D integration of CMUT with Front-End Electronics

Sigrid Berg and Arne Rønnekleiv

Paper VII

Neighbor Coupling Resonances in CMUT Arrays Immersed in Fluids

Sigrid Berg and Arne Rønnekleiv

Neighbor Coupling Resonances in CMUT Arrays Immersed in Fluids

Sigrid Berg, *Student Member, IEEE,* and Arne Rønnekleiv, *Member, IEEE,*

Abstract—In medical imaging it is in most cases necessary to steer the beam electronically to form an ultrasound image. This is done by adding delays leading to phase shifts between neighbor elements. When using CMUT arrays for this kind of imaging, neighbor coupling between elements through the fluid might give unwanted local resonances within the frequency range of interest. Such resonances may degrade the image quality.

A CMUT model describing the vibration of the CMUTs and the coupling of waves to the fluid medium is used in this work. To verify the model's ability to describe the CMUT-fluid interaction, we compare measurements and simulations of input conductance of a linear array of CMUT elements, where neighbor elements are excited 180 degrees out of phase.

Through simulations we show that local resonances in the CMUT-fluid interface may be damped at the interface if the fluid has a high viscosity, whereas radiation into fluids of low viscosity may be severely affected by such resonances. The model is further developed to show how a thin layer of a lossy soft material might damp the resonances, and simulations show that by introducing a thin layer of the PDMS material RTV615, acceptable results may be obtained without adding more than 0.5 - 1 dB in transmit losses.

Another crosstalk reduction method which is investigated, is using a low impedance path between the CMUTs and the electronics. We show that if the array has a single periodicity throughout the array, a reduced source/load impedance in the transmit or receive electronics will reduce the effect of the local resonances on the transmitted wave or received signal. However, if the periodicity is broken by introducing larger distances between elements than between CMUTs within the elements, the low impedance path will not have the desired effect.

I. Introduction

CAPACITIVE micromachined ultrasonic transducers (CMUTs) have been subject to extensive investigation since the mid 1990s [1]–[3]. In fabrication, photolithographic techniques developed for integrated circuit manufacturing are used, which may enable high volume production at low cost. It also facilitates the manufacturing of small elements and electrical addressing of elements using through wafer via interconnects [4].

Neighbor coupling between CMUT elements through the fluid is known to give resonances at the CMUT-fluid interface at some frequencies, especially for off axis steering angles. Degradation in axial resolution and bright patterns in the near field has been observed in imaging experiments [5]. The most important contribution to crosstalk is often referred to as dispersive guided modes which are due to the geometric nature of the transducer and its interaction with

S. Berg and A. Rønnekleiv are with the Norwegian University of Science and Technology, Department of Electronics and Telecommunications, Trondheim, Norway. (e-mail: sigrid.berg@iet.ntnu.no)

the fluid. The membrane vibration is a combination of many vibration modes with different resonance frequencies, and the excitation frequency determines which mode is dominating. Beam steering to an off axis direction involves phase shifts between adjacent elements, where each element usually consist of more than one CMUT. Both asymmetric modes within each CMUT and interactions between membrane vibrations within an element or in adjacent elements can cause local resonances in the CMUT-fluid interface. The fluid acts as a coupling medium between the membranes, and the result may be a distortion of the overall array response. This is described through modeling and experiments in [6]. The crosstalk due to such local resonances is most evident in the frequency range below the center frequency, but still within the band of operation and hence something that needs to be taken into consideration when designing CMUT arrays [7]–[9]. Losses in the CMUT, in the fluid or in the interface layer between the CMUTs and the fluid may damp the resonances mechanically.

Other contributions to crosstalk can be interface waves, often referred to as Stonely-Scholte waves, and surface acoustic waves (SAW) exited in the silicon wafer. The interface wave may be generated at the interface between a solid and a liquid medium. This wave is evanescent in both media, and is mostly localized in the fluid. This is theoretically shown in [9], [10] and shown experimentally in [11]. The generation of the SAW depends on acoustic properties of the silicon wafer and any other layers of integrated circuits or acoustic backing which is included underneath the chip carrying the CMUTs. This effect is discussed in [12], and will not be further discussed in this work, and we disregard the surface acoustic waves in the simulations by assuming that the CMUTs are mounted on a perfectly rigid backing.

Several methods for crosstalk reduction have been presented over the last years. An acoustic band gap resulting from an additional vacuum gap between the CMUT cells was investigated by Bayram et al. [13]. According to finite element calculations the crosstalk was reduced by 10 dB in the conventional operation mode without loss of acoustic pressure of the transmitter element. Modified transmit waveforms has been proposed by Zhou et al, [14], [15], reducing crosstalk by 25 dB for small AC excitation conditions. This approach requires a programmable waveform transmitter as a part of the ultrasound scanner system. The effect of the resonances on the received response can be reduced by using low impedance amplifiers, as was shown in [16]. Another approach to electrically damp the resonances is by introducing resistors between each CMUT cell, which was proposed by Rønnekleiv [17]. This was very efficient in simulations, but might be a challenge to fabricate.

The simulations also showed that increasing the viscosity of the fluid outside the array by a factor of 1000 from that of water at 3.5 MHz damped the unwanted resonances mechanically.

Adding a protective sealant layer on top of the CMUT membranes has been done by several groups [18]–[23]. For medical applications it is important that the transducer surface is electrically isolated from the human tissue and that it is physically protected against bodily fluids or chemicals that might harm the structures. A possible benefit when coating the CMUTs would be if the chosen coating material also damps the crosstalk that is generated in the CMUT-fluid interface. Both polydimethylsiloxane (PDMS) and Parylene coatings have been proposed for this purpose. PDMS is softer and has a higher attenuation coefficient and a lower shear wave velocity, making it more suitable for damping crosstalk. Both materials add mass and stiffness to the membrane, and care must be taken when designing the CMUTs so that they meet frequency and collapse voltage requirements after coating.

In this work we will use a CMUT model which is thoroughly presented in [17], and also used in [7], [16], [24], [25]. In order to verify the CMUT model that has been used in the simulation of acoustic coupling through the fluid, we will compare simulations and measurements of the conductance of a CMUT array radiating into three different media when adjacent elements are excited 180 degrees out of phase.

Through simulations we investigate how the described resonances in the CMUT-fluid interface affect the response of infinite arrays where several CMUTs are electrically coupled to form elements. The arrays may steer the ultrasonic beam up to 45 degrees off broadside. We include both arrays where the distance between CMUT cells is the same throughout the array, and arrays where the distance between CMUTs in adjacent elements is larger than between CMUTs within the element. We denote the configurations as single and double periodicity arrays respectively. An illustration is shown in Fig. 1.

We include simulations that show that fluids with high viscosity, such as rapeseed oil, damp the resonances more efficiently than low viscosity fluids, such as water and kerosene. Further, the CMUT model is modified to include a thin layer of a solid lossy material on top of the CMUT array in order to mechanically damp the described resonances. This is done by using a matrix method for acoustic waves in multilayered structures [26].

An alternative approach to reduce the effect of the resonances, which is investigated in this work, is to provide a low impedance path for the electric signal from the CMUT to the transmit or receive electronics. We show how the impedance mismatch may be used to limit the effect of acoustic resonances on the crosstalk in arrays with single periodicity. In arrays with added distance between elements, the resonances will distort the transmission even with low impedance electronics, because the fairly narrow-band resonances may couple directly to radiated waves. This is further elaborated in Section V.
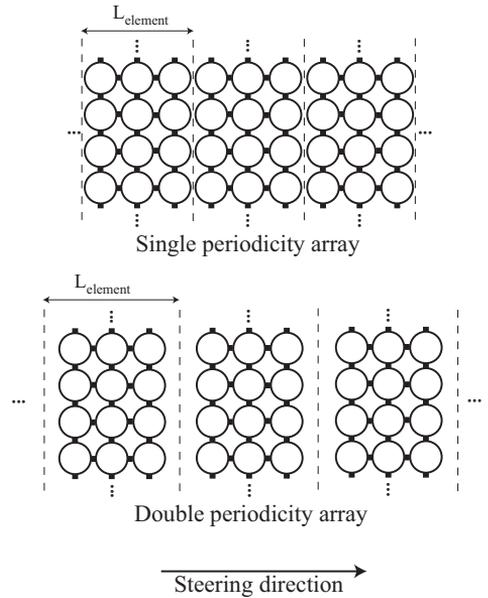

Fig. 1. Arrays where the distance between elements is the same as between CMUTs within the elements are denoted as single periodicity arrays, whereas arrays with a larger distance between CMUTs in adjacent elements than between CMUTs within the element is denoted as double periodicity arrays. In the illustration each element consist of three infinite rows of CMUTs. In the simulation we have used two, three and five rows of CMUTs per element. The dashed vertical lines emphasize the width of each element. In our simulations we have chosen a steering direction perpendicular to the rows, as shown by the arrow.

II. MODEL VALIDATION

A. CMUT fabrication

The CMUTs used in this work have been fabricated at the SINTEF MiNaLab in Oslo, Norway. The fabrication process of CMUTs equivalent to those used here, is described by Midtbø et al [27]. However the CMUTs in this work have thicker and a slightly different pattern of the top electrodes. The CMUT membranes consist of a 100 nm LPCVD silicon nitride layer which is wafer bonded to a silicon substrate with pre-etched cavities, and an aluminium top electrode of 500 nm which covers the center of the membrane. The top electrode has four arms, each of width 2 μm to connect to adjacent CMUTs, as shown in Fig. 2. The bottom wafer is doped to work as the bottom electrode of the capacitor. The top electrode of the CMUT cell has a radius of 3.5 μm.

The CMUT membrane radius is 5.7 μm and the CMUT cell pitch is 12.5 μm. Lines of 104 CMUT cells are connected by the top electrodes, and two and two lines are connected to the same bonding pad, resulting in an element size of 25 μm $\times$ 1300 μm. There are 36 elements on one array.

The cavities were designed to be 120 nm deep, but thermally induced strains in the membrane and the aluminium partly covering the membrane may bend it downwards, hence reducing the effective gap of the device [28]. Midtbø et al. [27] showed that a 300 nm thick aluminium electrode led to
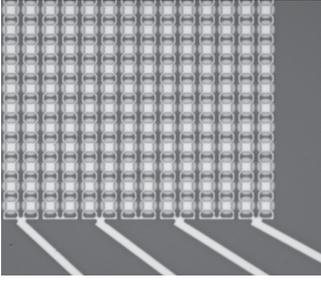
Fig. 2. Optical image of the front side of the CMUT used in the measurements. Each element consists of 2 × 104 CMUT cells.

an effective gap of 100 nm. The simulations performed in this work show that the cavity depth must be as small as 82 nm, in order to match the simulated collapse voltage and resonance frequencies in air to the measurements.

B. General model

Simulations are based on a model developed in [17], which describes the motion of a circular CMUT membrane as a combination of movement in free acoustic modes of an acoustically isolated CMUT, and the coupling of these modes to the fluid outside the CMUTs and the electronics. The coupling between the modes is also included. The method is used to analyze infinitely large arrays of CMUTs, where groups of CMUTs can be connected to form elements. We assume that the CMUTs are laid out in a two-dimensional periodic pattern, where the x- and y-axis are along the surface of the array and the positive z-axis points upwards into the fluid.

For a lossless and acoustically isolated CMUT with clamped support, the various fundamental acoustic modes are orthogonal. The mode profile of mode n is given by $W_n w_n(x, y)$, consisting of a normalized mode profile, $w_n(x, y)$ and the small signal deflection amplitude of the membrane W_n. Waves in the fluid may however couple to several of the acoustic modes at the same time. By exciting the CMUTs with a voltage v, the deflection W_m for each of the excited modes are found through solving for W_m in eq. (10) from [17]:

$$\left[diag \left(M_n(\omega_n^2 - \omega^2) \right) - K_{n,m}^{(w)} + i\omega Z_{n,m}^{(me)} \right] W_m = K_n^{(v)} v, \tag{1}$$

where ω is the driving frequency and ω_n is the resonance frequency of mode n. M_n is the effective mass of the membrane for eigenmode number n, $K_{n,m}^{(w)} W_m$ is the effective electrostatic force on mode n due to the deflection of mode m, also known as the spring softening effect, and $K_n^{(v)} v$ gives the electrostatic force on mode n due to the voltage v. The effective stiffness of the membrane for eigenmode n is given by $M_n \omega_n^2$. $Z_{n,m}^{(me)}$ is the self and mutual acoustic impedance of the fluid outside, as seen by the different eigenmodes of the membranes. Several CMUTs are connected to form elements, and the elements are excited with phase shifts to give beam steering. Then the matrix describing the acoustic impedance also contains the coupling between modes in different CMUTs, both within the element and outside the element. In this case,

$Z_{n,m}^{(me)}$ is not necessarily symmetric ($Z_{n,m}^{(me)} \neq Z_{m,n}^{(me)}$). The pressure field from mode n in the first CMUT of the element, might be experienced differently by the second CMUT, than the field from mode n in the second CMUT is experienced by the first, due to the phase shifts of the excitation between elements [29]. For more details on the various components of (1), we refer to [17].

In these calculations we deal with transmitting arrays since they are found mathematically simpler than receiving arrays, however the result also apply to receiving arrays since the circuits of which the model is based, are reciprocal.

C. Simulations

To verify that the CMUT model describes the CMUT-fluid interaction in an accurate way, we have simulated and measured the response from CMUT arrays with 180 degrees phase shift between adjacent elements. Similar measurements have been performed by Thränhardt et al [30], [31], where they use surface resonances in a CMUT array to characterize different fluids. Some aspects of the physical structures are subject to approximations in the model in order to facilitate the simulations. In order to account for losses in the CMUT, the membrane materials are modeled with a material Q-value of 100 in the simulations. This makes the response in the simulations and the measurements quite similar when it comes to Q-value.

An obvious difference between the fabricated CMUT arrays and the modeled CMUT array is the size. The arrays in the simulations are infinite in both in-plane directions, whereas the arrays used in the measurements are of finite size. The element width is however the same for the two cases.

As shown in Fig. 2, the top electrodes of the CMUTs are not circular symmetric. In order to account for the stiffness added by the aluminium lines from the center to the outer edge of the top electrode, we calculate the weight and the added stiffness due to the metal lines at a number of radial points, and distribute the effect of the added weight and stiffness to all points along the perimeter at this radius. The effect of the lines decreases towards the edge of the CMUT, due to increased circumference. This approximation results in a membrane that is modeled as a circular-symmetric object.

The Young's modulus of the silicon nitride and aluminium used in the simulation are adjusted to get a membrane stiffness and mass that makes the simulations match with the measured resonance frequency in air at different DC biases. The same material parameters are then used in the modeling of CMUTs radiating into kerosene and rapeseed oil. All the material properties are given in Table I. The mechanical support of the membrane is not perfectly stiff, and only present on one side of the membrane. Hence the membrane will move, even at the nominal border. In the simulations we have thus assumed an increase in the radius by a factor of $0.71\times$*(total membrane thickness)*, resulting in a total radius of 6.12 μm. The other geometric parameters, such as membrane thickness, electrode radius, width of electrode fingers and CMUT cell pitch, have been kept as in the design. We believe that the etching process and possibly an incomplete fusion bonding process may have

resulted in membranes that are slightly larger than the design parameter of 5.7 μm radius. This is not included in the modeling.

There are many combinations of membrane material stiffnesses and mass that may result in a CMUT model which match the measurements. The most important issue in the comparison performed here, is however to find a reasonable effective membrane stiffness, effective mass, and mode profile for each of the eigenmodes. This is achieved with the material properties listed in Table I, which may be somewhat wrong.

TABLE I
MATERIAL PROPERTIES OF MEMBRANE MATERIALS USED IN THE
SIMULATIONS

	Si_3N_4	Aluminium
Thickness (nm)	100	500
Radius (μm)	6.12	3.5
Y (GPa)	153	42.7
Poisson ratio	0.263	0.355
Density, (kg/m^3)	2916	2610
Built in stresses (MPa)	950	0
Cavity depth	82 nm	
Top electrode finger width	2 μm	
Cell pitch	12.5 μm	
Collapse voltage	48.5 V	

D. Measurement and simulation results

The CMUT chip is mounted on a printed circuit board and connected to the circuit illustrated in Fig. 3 through wire bonding. In the measurements, we have excited every second element in phase and the intervening elements 180 degrees out of phase. This is illustrated in Fig. 4. The excitation is achieved by using a RF Transformer (ADT1-6T+) from Mini-circuits.
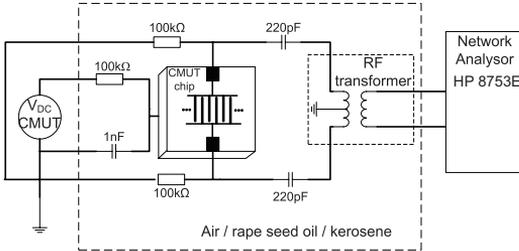

Fig. 3. Illustration of the measurement setup.
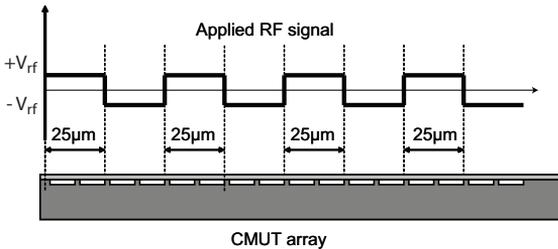
Fig. 4. Illustration of the how the voltages are applied to the array. All CMUTs have the same applied DC bias voltage.

Measurements are performed in air, rapeseed oil and kerosene (lamp oil). The viscosity of rapeseed oil has been measured using a StressTeck Rheometer (Reologica, Lund, Sweden). The viscosity of the kerosene was estimated based on comparing measurements of viscosity of distilled water and kerosene at 20°C in a capillary viscosimeter, assuming laminar flow and Newtonian liquids. Distilled water at 20 degrees is assumed to have a viscosity of 1 mPas. The properties of the fluids are listed in Table II. The CMUT array was cleaned with acetone between measurements in the different liquids. The collapse voltage of the CMUT is about 48.5 V, and measurements were performed at 10 V, 20 V, 30 V, and 40V DC bias. In kerosene and rapeseed oil an AC signal of -10 dBm was applied, while in air the applied AC signal was -30 dBm. The conductance was calculated based on measured S11 using a network analyzer from HP Agilent (HP8753E).

TABLE II
MECHANICAL PROPERTIES FOR FLUIDS

	Water[a]	Kerosene[b]	Rapeseed oil [b]
Density (kg/m^3)	1000	778	920
Sound velocity (m/s)	1500	1325	1460
Shear viscosity (mPas)	0.7	1.72	72

[a] 37 $^{\circ}$C   [b] 20 $^{\circ}$C

The comparison of input conductance from simulations and measurements are shown in Fig. 5. In the simulations the conductance increases and the resonance frequency decreases with higher DC bias as expected. However, in air the measured conductance at the highest DC bias voltage is lower than on the second highest. This may be due to variations in membrane stiffnesses, which lead to increased resonance frequency differences between individual CMUTs as the bias voltage is increased. This in turn leads to a broadened conductance peak with reduced amplitude. Also, some membranes may already have collapsed.

As expected, the top plots of Fig. 5 shows a good match in frequency at all DC voltages between the measured and simulated input conductance from the CMUT array in air. The Q-values are somewhat higher in the measurements than in the simulations. All model parameters are kept the same as in air, in the modeling of the CMUT's interaction with kerosene and rapeseed oil.

In the middle plot of Fig. 5 measurements and simulations in rapeseed oil are shown. There is good match in frequency and amplitude at all DC bias voltages. The measurements in kerosene in the bottom plot of Fig. 5, show good match in frequency, but slightly higher Q-values in simulations than measurements.

From the comparison of the measurements and simulations, we can conclude that the CMUT model is well suited for simulations of the CMUT-fluid interaction. The discrepancies that can be observed may be due to variation in the electrical and physical properties of the CMUTs within the array and uncertainties of material properties.

Results presented in [25] show measurements and simulations of yet another CMUT array with the same membrane diameter and element size as the array presented here, but with a different membrane composition, top electrode and bottom wafer thickness. Those results also indicates that the model is
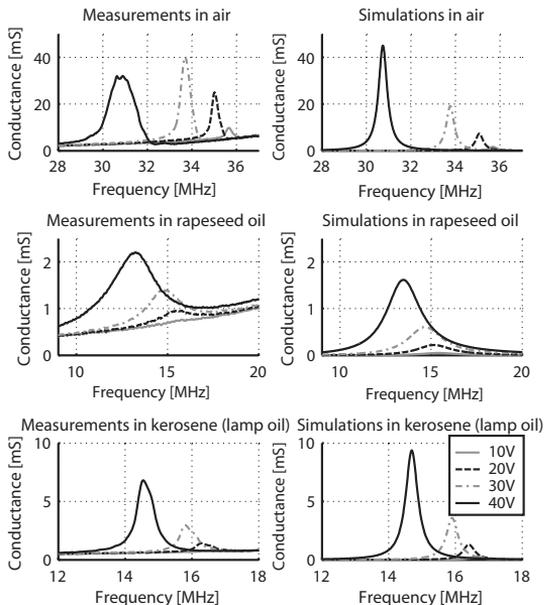
Fig. 5. Measurements and simulations of input conductance in air (top), rapeseed oil (middle) and kerosene (lamp oil) (bottom) of the CMUT array. The same DC voltages are used in measurements and simulations.

well suited to describe the CMUT-fluid interaction.

III. EXCITATION OF NEIGHBOR COUPLING RESONANCES

If the array is steered in a well defined direction with one connection to each CMUT, the resonances that might occur are connected to asymmetric modes in the CMUTs. Excitation of such resonant modes is shown for collapsed CMUTs in [17]. In conventional mode operation, the asymmetric modes have resonance frequencies which are much higher than the dominating symmetric mode, hence they will not be visible within the frequency range examined here.

Most CMUT arrays are, however, designed with several CMUTs electrically connected to form larger elements. If the structural period of the array is kept, but larger periodic elements are formed, the local resonances may also include modes where CMUTs within the same element move differently, even though the applied voltage is the same. Since the array is periodic, we can use Fourier series to describe the excitation. When each element consists of more than one CMUT, the excitation can be described as a combination of Fourier components with different k-vectors along the array surface. Each Fourier component is excited by voltages with stepwise phase shifts between CMUTs, regardless if they are within the same element or not. The number of Fourier components corresponds to the number of CMUTs per element, and each of the components may lead to resonant modes in the CMUT-fluid interface. As long as no grating lobes are excited, only one of these Fourier components couples to propagating waves in the fluid. The resonances in the interface have a negative impact on the performance by partly shorting the signal path

between the array and the electronics. This is further explained in Section V.

In arrays with double periodicity, the periodicity between CMUT cells is broken by increasing the distance between CMUTs in neighbor elements. In such configurations, each of the voltage series with stepwise phase shifts between CMUTs discussed above, will in principle excite field in the fluid, containing not only one, but a range of Fourier components with periodicities from about two times the CMUT width to about two times the element width. Hence all of the voltage series may excite both neighbor resonances and propagating waves. Thus the transfer functions from element voltage to output pressure and pressure from an incoming wave to short circuit current may also be distorted by the resonances. In addition one still has electrical shorting effects from the resonances. In this case the resonances may also occur for broadside radiation.

A. Simulation results

An infinite CMUT array, with CMUT cells equal to those used in the simulations and measurements presented in the previous section, is used in the following simulations. The DC bias is increased to 47 V, in order to enhance the electromechanical coupling between the CMUT and the fluid. The losses in the CMUT structure are assumed to be as in the previous section. We include array configurations with 2 to 5 rows of CMUTs per element, and both single and double periodicity arrays. To limit the complexity, elements are formed by connecting infinite rows of CMUTs electrically, and beams are steered perpendicular to the row direction of the array. This is illustrated in Fig. 1. We have calculated the transmitted power from the array as a function of frequency and steering angle.

Radiation into water at a temperature of 37 degrees from an array where each element consists of two rows of CMUTs is shown in Fig. 6. A source impedance of 1 MΩ is connected to each CMUT. This impedance is chosen to minimize the insertion loss and maximize the bandwidth. The CMUTs have a maximum transmission at about 13 MHz and a crosstalk resonance is apparent close to that frequency. The center frequency of the 3 dB bandwidth is almost 20 MHz and the bandwidth at broadside is about 150 %.

Many CMUT designers choose to make the distance between array elements larger than the distance between CMUT cells within the element. In Fig. 7a to 7d we have compared the response from arrays with single and double periodicity, and show that double periodicity arrays with more than two CMUTs per element may generate crosstalk resonances even at broadside transmission.

In arrays with a double periodicity, the CMUTs at the edge of the elements are adjacent to a non-vibrating area, so their physical surroundings are different from the CMUTs which are surrounded by other CMUTs. When an array is transmitting an ultrasonic wave straight forward, there are no phase shifts between neighbor CMUTs or elements. However, when an array with double periodicity and elements with three rows of CMUTs or more, is transmitting straight forward, the
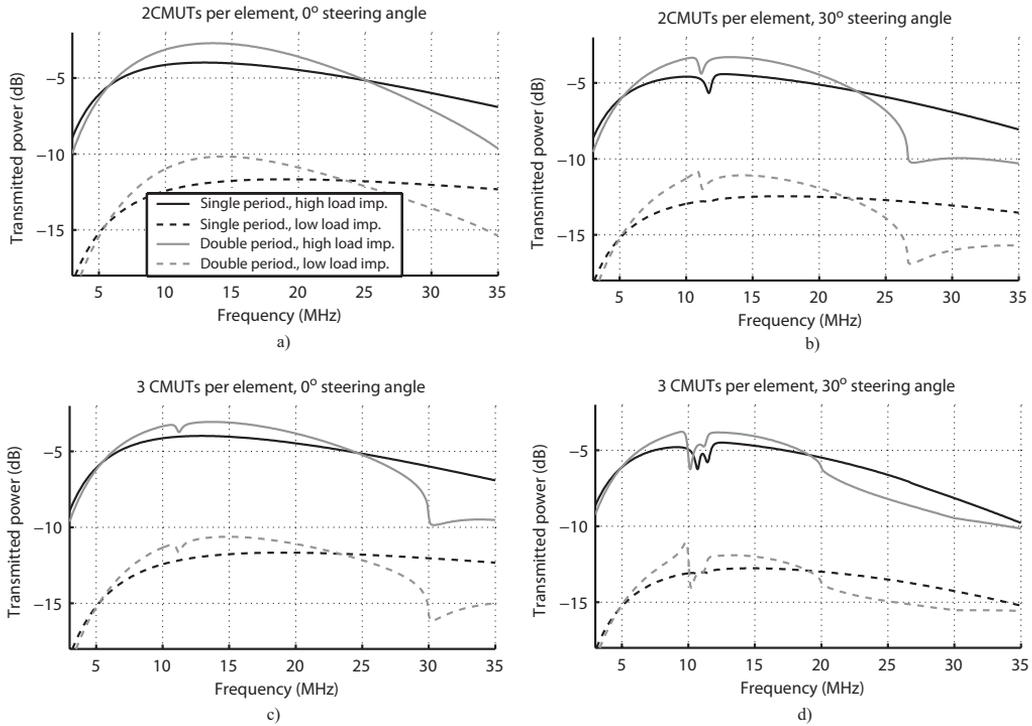
Fig. 7. Comparison of transmitted power from arrays with single and double periodicity at high and low amplifier impedance. Plot a) and b) represent arrays with 2 CMUTs per element, and plot c) and d) show the response from array with 3 CMUTs per element. The full lines represent transmission with good match to the source impedance (1 MΩ per CMUT), whereas the broken lines represent transmission with low source impedance (0.1 MΩ per CMUT).
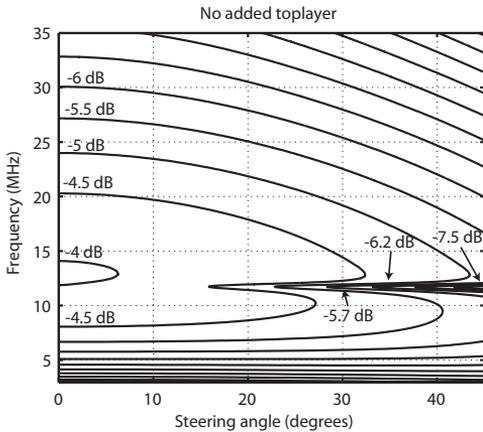

Fig. 6. The transmitted power as a function of steering angle and frequency, from an infinite CMUT array, where each element has two CMUTs across. The distance between contour lines is 0.5 dB.

CMUTs within the element will respond differently to the applied voltage due to the difference in physical surroundings. Resonant modes where the CMUTs are out of phase will hence

be excited, and a dip in the response curve will arise, as shown in grey lines in Fig. 7c. When there are only two rows of CMUTs per element, they will both be next to a non-vibrating area, and hence experience similar physical conditions. The result is that only one radiating mode is excited. Hence the response at 0 degrees transmission is smooth as a function of frequency, as is shown in Fig. 7a. When the beam is steered to an off axis direction, resonances occur in all the array configurations shown here. With 2 rows of CMUTs per element, there is a single dip in the response, whereas there are two dips in the response from the array with 3 rows of CMUTs per element. This illustrates that the more CMUTs there are per element, the number of resonances that may be excited between the CMUT cells increases.

It is also shown that the maximum power transmission at the center frequency is higher and that the bandwidth is reduced in arrays with double periodicity. With an added distance between the array elements, a larger volume of fluid needs to be moved by the CMUTs as they vibrate. This causes an increase in the mechanical Q of the membrane, and hence a reduction in the bandwidth. This should in turn reduce the electrical Q of the CMUT which leads to an improved match to the electrical transmit/receive circuits, which contributes positively to the transmitted power. The array with double

periodicity has an added distance between elements equivalent of one CMUT, in this case 12.5 μm. In cases with smaller element distance than shown here, the unwanted resonance dip around 12 MHz might become somewhat smaller compared to radiation from arrays with single periodicity, but the possible benefit seems to be limited.

The viscosity of the fluid into which the ultrasonic waves are transmitted, is an important parameter when the crosstalk is calculated. Table II show that the viscosity of rapeseed oil at a temperature of 20 degrees is 100 times higher than that of water at 37 degrees. As shown in Fig. 8, radiation into fluids like rapeseed oil will not result in much crosstalk, due to its high viscosity. Radiation in low viscosity fluids, such as water and kerosene, results in a severe dip in the response. This effect is also described through finite element simulations by Leirset et al. [32].

Fig. 9. The transmitted power from a transducer with 5 CMUTs per element and an added distance equivalent to 1 CMUT between each element is shown. The left plot shows the response in water, whereas the right plot shows the response in rapeseed oil. Since the resonances are sharp and deep in water, the response between 7 and 13 MHz has been enhanced and is shown in the corner of the left plot.


Fig. 8. The transmitted power as a function of frequency at 30 degrees steering angle, when CMUT arrays with single periodicity and two CMUTs per element are radiating ultrasonic waves into water, kerosene and rapeseed oil.

Several authors (e.g. [11], [33]) have presented pulse-echo responses from CMUT arrays radiating in vegetable oil. A dip in the response below the center frequency is often present, and sometimes commented as acoustic crosstalk. The shape of the response in fluids with lower viscosity or when steering the ultrasound beam in an off axis direction is most often not presented nor commented. In Fig. 9 we show the simulated response from an array with elements consisting of 5 rows of CMUTs in the width direction and with a distance between the elements equivalent to the width of one CMUT. The results from radiation into water and rapeseed oil at four different directions are compared. It is apparent that even without any beam steering, there is a dip in the response, both in water and oil, and that this unwanted effect is enhanced as the steering angle increases. In water, the size of the dip is up to 4.5 dB around 8.5 MHz at 30 degrees. The effect is less dominating in rape seed oil, but a response dip of 0.6 dB close to the center frequency as seen here, is not acceptable in most imaging situations. The bandwidth is reduced with increased steering angle. In this case the element pitch is 75 μm, which is larger than half the wave length at the center frequency. This may cause grating lobes in the response, which limits the transmitted power and the bandwidth, especially at large steering angles.

IV. MODELING CMUT ARRAYS WITH AN ADDED TOP LAYER

A. Model modifications

When an extra uniform solid layer is added at the surface of the membranes, the acoustic impedances $Z_{n,m}^{(me)}$ from equation (1) will change compared to the situation when the CMUT membranes were in direct contact with the adjacent fluid. $Z_{n,m}^{(me)}$ is given in eq. (9) in [17] as:

$$Z_{m,n}^{(me)} = \frac{1}{i\omega W_n} \int_{electr.} t_{zz,n}^{(me)} w_m dA \qquad (2)$$

where $t_{zz,n}^{(me)}$ is the normal tension on the surface of the array and the inverse spatial Fourier transform of T_{zz}^m. T_{zz}^m changes due to the added damping layer, and the new T_{zz}^m may be calculated using the vector formalism developed by E. Adler to describe transformation of stresses and velocities through multilayered structures of piezoelectric materials [26]. In [17] the approximation was made that the movement of the top surface of the membrane was purely in the z-direction. Dealing with a solid layer above the membrane, it is appropriate to include also the membrane velocities in x- and y-directions. It should however be emphasized that the shear stiffness of the damping material should be low such that the shear tensions on the membrane surface are small, and will not alter the position of the neutral axis in the membrane appreciably, as it bends.

Originally Adler's method requires an 8×8 transformation matrix to account for both piezoelectric effects and anisotropic properties of the materials. Since we can omit the piezoelectric effects, the transformation matrix is reduced to a 6×6 matrix.

In order to calculate the normal tension on the surface, we need to include all the tensions in the z-plane and the particle velocities in the k-space state vector, which becomes part of the matrix equation which we solve. The state vector becomes $\tau_t = [T_{xz} \ T_{yz} \ T_{zz} \ V_x \ V_y \ V_z]$ for the fluid-array interface, and $\tau_m = [T_{xz}^m \ T_{yz}^m \ T_{zz}^m \ V_x^m \ V_y^m \ V_z^m]$ for the surface of the CMUT membrane. The state vector τ_t is found through the following

transformation:

$$\tau_t = e^{(j\omega Ah)}\tau_m = \phi(h)\tau_m, \qquad (3)$$

where h is the thickness of the layer and the details of the A-matrix is defined in [26].

Since we include also the transverse velocities at the membrane surface, such velocities will also be present at the fluid interface, and we need the complete set of wave solutions in the fluid for a given k_x and k_y to match these velocities. This includes one longitudinal and two shear waves with velocity amplitudes of V_{l0}, V_{s10}, and V_{s20} at the interface $z = 0$. Using equation (17) - (19) from [17] these are found and presented in (5).

The k-vectors k_{s0} and k_{l0} are given in eq. (21) in [17] and the remaining k-vectors are given as:

$$
\begin{aligned}
k_{lz} &= \sqrt{k_{l0}^2 - k_x^2 - k_y^2}, \\
k_{sz} &= \sqrt{k_{s0}^2 - k_x^2 - k_y^2}, \\
k_{xy} &= \sqrt{k_x^2 + k_y^2}.
\end{aligned}
\qquad (6)
$$

When introducing (5) in the stress tensor T_{ij}, we find that the stresses at the fluid-array interface, T_{xz}, T_{yz} and T_{zz} can be expressed as:

$$T_{xz} = C_1 V_{l0} + C_2 V_{s10} + C_3 V_{s20}, \qquad (7)$$

$$T_{yz} = C_4 V_{l0} + C_5 V_{s10} + C_6 V_{s20}, \qquad (8)$$

$$T_{zz} = C_7 V_{l0} + 0 \cdot V_{s10} + C_9 V_{s20}, \qquad (9)$$

Using this description of stresses and velocities, (3) can be manipulated into the set of equations given in (10). This can easily can be solved in Matlab. V_{l0}, V_{s10}, and V_{s20} are the unknown longitudinal and shear wave velocities at the fluid-array interface, T_{xz}^m, T_{yz}^m, and T_{zz}^m are the shear and normal pressure on the membrane surface. Since T_{zz}^m is found through solving (10), we can easily calculate the acoustic impedance matrix $Z_{n,m}^{(me)}$ describing the acoustic coupling to the fluid, including effects of the added layers and losses at the fluid interface. The transmitted pressure from the surface into the fluid medium is given as $p = -(T_{xx} + T_{yy} + T_{zz})/3$, only including the contribution from the longitudinal wave. This results in the expression:

$$p = \left(\frac{\gamma_f}{\omega} + i(\eta' + \frac{2}{3}\eta) \right) k_{l0} V_{l0}. \qquad (11)$$

Together with available information about effective mass and stiffness of the membranes, this gives the basis to solve (1) to find the deflection amplitude for each of the exited modes when a damping layer is added on top of the CMUTs.

B. Damping materials

A group of materials that is commonly used as coatings for electronic circuits and MEMS devices, and which also has been tested as an encapsulating coating for CMUTs, is polydimethylsiloxane (PDMS) [20]–[22]. It is a viscoelastic material which is optically clear and can provide good transcutaneous contact without the use of ultrasonic gel [21]. Since

it is nontoxic, it is used both as a food additive and in medical applications.

RTV615 from GE Silicones is the PDMS material which we choose to use in the simulations of this work. At 12 MHz, the shear wave velocity and shear wave attenuation of RTV615 are found to be 130 m/s and 3900 Np/cm^{-1}, respectively [34]. The longitudinal velocity is reported to be 1080 m/s [22] and the density is 1020 kg/m^3 [34]. The attenuation of the polymer is frequency dependant and is included in the model through a complex k-vector for the shear wave, $k = \omega/v_s + i\alpha_s$, where v_s is the shear wave velocity, ω is the center frequency of the array, and α_s is the attenuation coefficient. The theory behind this description of the attenuation is given both in [34] and [35]. Based on material properties from the silicon rubber compound RTV615, we have investigated how a thin layer of such a soft material may damp the crosstalk, and how the insertion loss, bandwidth and center frequency of the transducer is affected.

The thickness of the coating layer is an important factor. In order to spin very thin layers of PDMS onto a surface, the uncured PDMS must be diluted in a solvent. Hexane has commonly been used for this purpose. Film thicknesses down to 70 nm can be achieved if the amount of solvent, the spin speed and spin time is optimal [36].

C. Simulation results

Simulations have been performed with thin layers of RTV615 (GE Silicones) on top of the CMUT membranes radiating into water. In Fig. 10 we show that a 2 μm layer of RTV615 damps the undesired resonance that is apparent at 12 MHz in Fig. 6. The insertion loss at broadside radiation has only increased by 0.5 dB.
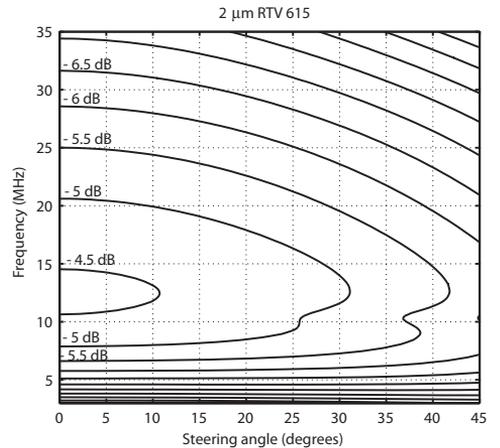

Fig. 10. The transmitted power as a function of steering angle and frequency for an infinite CMUT array, where each element has two CMUTs across. A 2 μm thick layer of RTV615 is included on top of the CMUT membrane. The distance between the contour lines is 0.5 dB.

Thicker layers of damping material, will reduce the unwanted resonance even further, but also introduce higher insertion loss. Fig. 11 shows the variation of the transmitted

$$V_x = \left[V_{l0} \frac{k_x}{k_{l0}} e^{(-ik_{lz}z)} - \left(V_{s10} \frac{k_y}{k_{xy}} + V_{s20} \frac{k_{sz}k_x}{k_{xy}k_{s0}} \right) e^{(-ik_{sz}z)} \right] e^{(-ik_x x - ik_y y)},$$

$$V_y = \left[V_{l0} \frac{k_y}{k_{l0}} e^{(-ik_{lz}z)} + \left(V_{s10} \frac{k_x}{k_{xy}} - V_{s20} \frac{k_{sz}k_y}{k_{xy}k_{s0}} \right) e^{(-ik_{sz}z)} \right] e^{(-ik_x x - ik_y y)}, \qquad (5)$$

$$V_z = \left[V_{l0} \frac{k_{lz}}{k_{l0}} e^{(-ik_{lz}z)} + V_{s20} \frac{k_{xy}}{k_{s0}} e^{(-ik_{sz}z)} \right] e^{(-ik_x x - ik_y y)}.$$

$$\begin{bmatrix} C_1 & C_2 & C_3 & -\phi_{11} & -\phi_{12} & -\phi_{13} \\ C_4 & C_5 & C_6 & -\phi_{21} & -\phi_{22} & -\phi_{23} \\ C_7 & 0 & C_9 & -\phi_{31} & -\phi_{32} & -\phi_{33} \\ \frac{k_{x'}}{k_{l0}} & -\frac{k_y}{k_{xy}} & -\frac{k_{sz}k_x}{k_{xy}k_{s0}} & -\phi_{41} & -\phi_{42} & -\phi_{43} \\ \frac{k_y}{k_{l0}} & \frac{k_x}{k_{xy}} & -\frac{k_{sz}k_y}{k_{xy}k_{s0}} & -\phi_{51} & -\phi_{52} & -\phi_{53} \\ \frac{k_{lz}}{k_{l0}} & 0 & \frac{k_{xy}}{k_{s0}} & -\phi_{61} & -\phi_{62} & -\phi_{63} \end{bmatrix} \begin{bmatrix} V_{l0} \\ V_{s10} \\ V_{s20} \\ T_{xz}^m \\ T_{yz}^m \\ T_{zz}^m \end{bmatrix} = \begin{bmatrix} \phi_{14} & \phi_{15} & \phi_{16} \\ \phi_{24} & \phi_{25} & \phi_{25} \\ \phi_{34} & \phi_{35} & \phi_{35} \\ \phi_{44} & \phi_{45} & \phi_{45} \\ \phi_{54} & \phi_{55} & \phi_{55} \\ \phi_{64} & \phi_{65} & \phi_{65} \end{bmatrix} \begin{bmatrix} V_x^m \\ V_y^m \\ V_z^m \end{bmatrix}. \qquad (10)$$

power as a function of frequency at 30 degrees steering angle for CMUT arrays with top layer thicknesses of RTV615 from 1 μm to 3 μm. This corresponds to 0.8 % to 2.4 % of the longitudinal wavelength in water at the center frequency of the array.
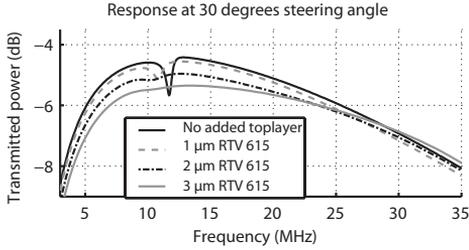

Fig. 11. The response from an undamped CMUT array is compared to the response from arrays with added damping layer with thicknesses from 1 μm to 3 μm RTV615.

Other PDMS materials and other material groups which might be used as coating materials, might have higher shear wave velocity and lower shear wave attenuation than RTV615. In Fig. 12 it is shown that the impact on crosstalk reduction is not very dependant on the shear wave velocity of the material. A higher shear wave velocity results in a slight decrease in center frequency and lower insertion loss. When reducing the shear wave attenuation of the damping material by 50% and 75 %, from the original 3900 Np/cm^{-1}, we see from Fig. 13, that the bandwidth decreases and the depth of the dip increases. This shows that a material with fairly high shear acoustic losses is needed.

V. SIGNAL PATH BETWEEN CMUT AND ELECTRONICS

As was mentioned in Section III, the unwanted resonances that are excited at certain frequencies, especially when the beam is steered to an off axis direction, may partly short the signal path between the array and the electronics. This is illustrated in Fig. 14, where Z_{rad} represents the desired
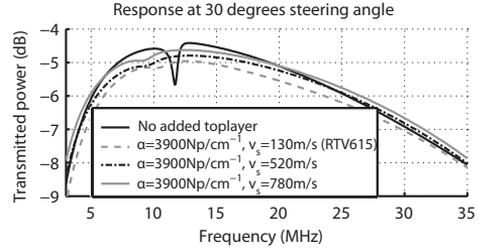

Fig. 12. The response from an undamped CMUT array is compared to the response from arrays with 2 μm damping layer with shear wave velocities from 130 m/s to 780 m/s. The attenuation is kept constant at 3900 Np/cm^{-1}.
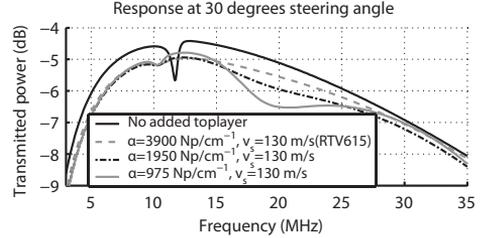

Fig. 13. The response from an undamped CMUT array is compared to the response from arrays with 2 μm damping layer with a shear loss of 3900 Np/cm^{-1} (equal to RTV615 at 12 MHz), 1950 Np/cm^{-1} and 975 Np/cm^{-1}. The shear wave velocity is kept constant at 130 m/s.

radiation from the array and Z_{res} represents the unwanted local resonances.

If the voltage source has a large internal impedance, Z_{source}, the radiating branch and the branch representing unwanted resonances will be strongly coupled, and Z_{res} might short circuit the signal path, and reduce the voltage across the radiating branch. This will affect the radiation from the array in a negative way. If the source impedance Z_{source} is very small or zero, the voltage across the resonator depends mainly on the voltage provided by the transmitter, V_{source}. Hence the resonances, Z_{res}, does not influence the voltage across the
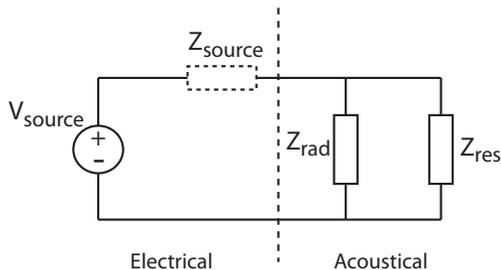
Fig. 14. A simple equivalent circuit illustrating the influence of the source impedance on the array response. If Z_{source} is small, it is the source that determines the voltage across the radiating branch, Z_{rad}, of the system. However, if Z_{source} is large, the unwanted resonance, Z_{res}, influences the radiation.

radiating part of the circuit, Z_{rad}. In the black dotted lines of Fig. 7a to 7d it is shown that the effect of the unwanted resonance are reduced if the source impedance is reduced by a factor 10 for arrays with single periodicity. However the maximum amplitude of the response is reduced by 7-8 dB.

If the array has a double periodicity, the local resonances will radiate, and even though the voltages on the CMUTs will be undisturbed if a sufficiently low source impedance is used in the transmission, there will be interference between the main broadband output signal and the narrowband signal radiating from the resonances. The same interference will be seen in the reception with a similarly low load impedance. Hence a smooth frequency response is not obtained. This is shown in the gray dotted lines in Fig. 7a to 7d.

VI. DISCUSSION

Comparison of measurements and simulations show that the CMUT model used here is suited to describe the interaction between a CMUT array and the fluid into which it is radiating. An excitation phase difference of 180 degrees between neighbor elements will not occur in a real imaging situation, the phase difference will in most cases be substantially smaller. However, verifying the model with these measurements allows us to use the CMUT model to simulate more realistic neighbor element phase shifts that occur in imaging. Such simulations show that resonances will impact the transmitted ultrasonic wave at frequencies close to the center frequency when the ultrasonic beam is steered off broadside. The Q-value of the resonances depends largely on the viscosity of the fluid in which the array is operating, and on whether the CMUT structure is of a single or double periodicity type, and to some extent on the inherent losses in the CMUT structure.

In immersion characterization of CMUTs, it is common to use vegetable oils as the transmission medium, and the characterization is often limited to transmission straight forward. Our simulations show that crosstalk is quite efficiently damped by the oil, and harmful effects that might affect the image quality when other imaging media are used, might not be detected by such a characterization scheme. We also show that effects that are barely visible at 0 degrees, might be severe at larger steering angles. In acoustic characterization of CMUT arrays,

it is therefore important to test the transducer in realistic fluid media, and to investigate the effect of beam steering, in order to be sure that the crosstalk effects do not harm the performance of the transducer.

Two different schemes of crosstalk reduction is suggested in this paper; adding a damping layer on top of the array and reducing the impedance of the electronics connected to the CMUT. If choosing one of the methods, or combining them is more efficient, depends on the requirements and limitations of the imaging system. When using already existing ultrasound imaging machines, the adjustment of transmit/receive electronics might not be an option. However, if the transducer is designed with custom made electronics which will be integrated in the front end of the transducer, impedance matching between the amplifiers and the CMUTs might be worth investigating.

The sensitivity of the transducer will however be reduced with a low impedance path between the CMUT and the electronics, and one might argue that the signal to noise ratio will be poor. In reception, an amplifier with a low load impedance must have a low noise figure in order to detect the current without adding too much noise to the signal. In transmit the electronics must provide sufficient power for the CMUTs to transmit despite of the low impedance. We believe that low power amplifiers based on field effect transistors will manage to detect the signal without adding too much noise, and hence provide a signal path of good quality [16], [37].

The simulations we present show that it is beneficial to have a single periodicity throughout the array. Such a configuration makes it possible to reduce the effect of local resonances by lowering the impedance of the electronics. Furthermore it allows manufacturing of arrays with the same distance between all cavities to be used in many different element configurations, by only changing the electrical connection between the CMUTs.

Adding a thin layer of PDMS on top of the membranes damp the crosstalk very well according to the presented simulations. Polymer and silicone manufacturers usually provide little information about acoustic losses and shear velocities in the data sheets describing their products. RTV615 from GE Silicones seems to have suitable properties for this kind of application, but there might also be a variety of other materials that can be used. Before choosing coating materials for CMUTs intended for medical application, care must be taken, that the material is non-toxic and approved by health authorities. The acoustic impedance of the damping material should also be considered, due to the possibility of echoes from the interface between the damping/coating layer and the fluid. RTV615 has an acoustic impedance of 1.1 MRayl, whereas Sylgard 160 has 1.5 MRayl, and is hence better matched with water [22].

Simulating the radiation through films that are thicker than about 3 % of the longitudinal wavelength can not be handled by the simulation program at this date. This is due to too high damping of some of the waves through the layers, which gives numerical instabilities. The matrix system needs to be modified to take this into account. Since a layer as thin as 2 μm reduces the unwanted acoustic effects, it has not been

done in this work.

In this work we have presented modeling of an infinite CMUT array. In practical use, all arrays will be of finite size, and undesired acoustic effects from the edges of the array might also contribute to the overall response. This has not been investigated here. However, we believe that a damping layer on top of the CMUT array which damps the crosstalk caused by local resonances in the CMUT-fluid interface, also will damp edge effects efficiently. Hence, basing crosstalk reduction only on load impedance adjustment might not be sufficient to avoid harmful acoustic effects from the edges of the array.

VII. CONCLUSION

Measurements of fabricated CMUT arrays where neighboring elements are excited 180 degrees out of phase are compared to simulations using an analytical CMUT model, and the results show good agreement between measurements and simulations for radiation into three different media; air, kerosene, and rapeseed oil. This implies that the CMUT model describes the interaction between the radiating CMUT elements and the fluid in an accurate way, and that the model is a good instrument to investigate the performance of CMUT arrays in a more realistic imaging situation.

Through simulations we find that the crosstalk due to local resonances in the CMUT-fluid interface may affect the image quality in a negative way. We have used the CMUT model to show two different methods of reducing such resonances or their effects. Adding a damping layer of a few micrometer thickness on top of the CMUT array reduces the resonances substantially, but also reduces the efficiency of the transducer somewhat. Silicone rubber materials such as PDMS, seems to have properties that match the requirements for the damping material. The other suggested solution is to use low impedance amplifiers. This will reduce the effect of the resonances. However, we show that if the transducer has larger distances between array elements than between CMUT cells within the elements, using low impedance amplifiers does not have the desired effect.

ACKNOWLEDGMENT

REFERENCES

[1] I. Ladabaum, B. Khuri-Yakub, D. Spoliansky, and M. I. Haller, "Micromachined ultrasonic transducers (MUTs)," in *Ultrasonics Symposium, 1995 IEEE*, 1995, pp. 501–504.

[2] I. Ladabaum, X. Jin, H. T. Soh, A. Atalar, and B. T. Khuri-Yakub, "Surface micromachined capacitive ultrasonic transducer," *IEEE Transactions on Ultrasonics, Ferroelectrics and Frequency Control*, vol. 45, no. 3, pp. 678–690, May 1998.

[3] M. I. Haller and B. T. Khuri-Yakub, "A surface micromachined electrostatic ultrasonic air transducer," *IEEE Transactions on Ultrasonics, Ferroelectrics and Frequency Control*, vol. 43, no. 1, January 1996.

[4] C. H. Cheng, E. M. Chow, X. Jin, S. Ergun, and B. Khuri-Yakub, "An efficient electrical addressing method using through-wafer vias for two-dimensional ultrasonic arrays," in *Ultrasonics Symposium, 2000 IEEE*, 2000, pp. 1179–1182.

[5] O. Oralkan, A. S. Ergun, J. A. Johnson, M. Karaman, U. Demirci, K. Kaviani, T. H. Lee, and B. T. Khuri-Yakub, "Capacitive micromachined ultrasonic transducers: Next-generation arrays for acoustic imaging?" *IEEE Transactions of Ultrasonics, Ferroelectrics and Frequency control*, vol. 49, no. 11, pp. 1596–1610, 2002.

[6] A. Caronti, A. Savoia, G. Caliano, and M. Pappalardo, "Acoustic coupling in capacitive micromachined ultrasonic transducers: Modeling and experiments," *IEEE Transactions of Ultrasonics, Ferroelectrics and Frequency control*, vol. 52, no. 12, pp. 2220–2234, 2005.

[7] S. Berg and A. Rønnekleiv, "Reducing fluid coupled crosstalk between membranes in CMUT arrays by introducing a lossy top layer," in *Ultrasonics Symposium, 2006 IEEE*, 2006, pp. 594–597.

[8] A. Caronti, C. Longo, A. Savoia, P. Gatta, G. Caliano, and M. Pappalardo, "Analysis of acoustic interaction effects and crosstalk in CMUT linear arrays for medical imaging," in *Ultrasonics Symposium, 2006 IEEE*, 2006, pp. 582–585.

[9] M. Wilm, A. Reinhardt, V. Laude, R. Armati, W. Daniau, and S. Ballandras, "Three-dimensional modelling of micromachined-ultrasonic-transducer arrays operating in water," *Ultrasonics*, vol. 43, no. 6, pp. 457–465, 2005.

[10] P.-C. Eccardt, A. Lohfink, and H.-G. von Garssen, "Analysis of crosstalk between fluid coupled CMUT membranes," in *Ultrasonics Symposium, 2005 IEEE*, 2005, pp. 593–596.

[11] X. Jin, Ömer Oralkan, L. Degertekin, and B. T. Khuri-Yakub, "Characterization of one-dimensional capacitive micromachined ultrasonic immersion transducer arrays," *IEEE Transactions of Ultrasonics, Ferroelectrics and Frequency control*, vol. 48, no. 3, pp. 750–760, 2001.

[12] S. Berg and A. Rønnekleiv, "Acoustic backing in 3D integration of CMUT with front end electronics," *Ultrasonics, Ferroelectrics and Frequency Control, IEEE Transactions on*, to be published in 2012.

[13] B. Bayram, G. G. Yaralioglu, M. Kupnik, and B. T. Khuri-Yakub, "Acoustic crosstalk reduction method for CMUT arrays," in *Ultrasonics Symposium, 2006 IEEE*, 2006, pp. 590–593.

[14] S. Zhou and J. Hossack, "Reducing inter-element acoustic crosstalk in capacitive micromachined ultrasound transducers," *IEEE Transactions on ultrasonics, ferroelectrics and frequency control*, vol. 54, no. 6, pp. 1217–1228, 2007.

[15] S. Zhou, G. L. Wojcik, and J. Hossack, "An approach for reducing adjacent element crosstalk in ultrasound arrays," *IEEE Transactions of Ultrasonics, Ferroelectrics and Frequency Control*, vol. 50, no. 12, pp. 1752–1761, 2003.

[16] S. Berg and A. Rønnekleiv, "Co-optimization of CMUT and receive amplifiers to suppress effects of neighbor coupling between CMUT elements," in *Ultrasonics Symposium, 2008 IEEE*, 2008, pp. 2103–2106.

[17] A. Rønnekleiv, "CMUT array modelling through free acoustic CMUT modes and analysis of the fluid CMUT interface through fourier transform methods," *IEEE Transactions on Ultrasonics, Ferroelectrics and Frequency control*, vol. 52, no. 12, pp. 2173–2184, 2005.

[18] B. Bayram, M. Kupnik, G. G. Yaralioglu, Ömer Oralkan, D. Lin, X. Zhuang, A. S. Ergun, A. F. Sarioglu, S. H. Wong, and B. T. Khuri-Yakub, "Characterization of cross-coupling in capacitive micromachined ultrasonic transducers," in *Ultrasonics Symposium, 2005 IEEE*, 2005, pp. 601–604.

[19] B. Bayram, M. Kubnik, G. G. Yaralioglu, O. Oralkan, A. S. Ergun, D.-S. Lin, S. H. Wong, and B. T. Khuri-Yakub, "Finite element modeling and experimental characterization of crosstalk in 1-D CMUT arrays," *IEEE Transactions of Ultrasonics, Ferroelectrics and Frequency Control*, vol. 54, no. 2, pp. 418–428, 2007.

[20] E. Campbell, L. A. J. Davis, G. Hayward, and D. Hutchins, "Cross-coupling in sealed CMUT arrays for immersion applications," in *Ultrasonics Symposium, 2007 IEEE*, 2007, pp. 2135–2138.

[21] X. Zhuang, A. Nikoozadeh, M. A. Beasley, G. G. Yaralioglu, B. T. Khuri-Yakub, and B. L. Pruitt, "Biocompatible coatings for CMUTs in a harsh aqueous environment," *Journal of Micromechanics and Microengineering*, vol. 17, pp. 994–1001, 2007.

[22] D.-S. Lin, X. Zhuang, S. H. Wong, M. Kupnik, and B. T. Khuri-Yakub, "Encapsulation of capacitive micromachined ultrasonic transducers using viscoelatic polymer," *Journal of Microelectromechanical Systems*, vol. 19, no. 6, pp. 1341–1351, 2010.

[23] E. Jeanne, C. Meynier, M. Roy, and D. Alquier, "Evaluation of parylene as protection layer for capacitive micromachined ultrasonic transducers," in *Meet. abstr. Electrochem. Soc*, no. 702, 2007, p. 1576.

[24] S. Berg and A. Rønnekleiv, "Reduction of crosstalk in CMUT arrays by introducing double periodicities," in *Ultrasonics Symposium, 2007 IEEE*, 2007, pp. 2155–2158.

[25] ——, "Measurements of CMUT neighbour coupling resonances in fluids of different viscosities," in *Ultrasonics Symposium (IUS), 2010 IEEE*, 2010, pp. 435–438.

[26] E. L. Adler, "Matrix methods applied to acoustic waves in multilayers," *IEEE Transactions on Ultrasonics, Ferroelectrics and Frequency control*, vol. 37, no. 6, pp. 485 – 490, 1990.

[27] K. Midtbø, A. Rønnekleiv, and D. T. Wang, "Fabrication and characterization of CMUTs realized by wafer bonding," in *Ultrasonics Symposium, 2006 IEEE*, 2006, pp. 934–937.

[28] Y. Huang, A. Ergun, E. Haeggstrom, M. Badi, and B. Khuri-Yakub, "Fabricating capacitive micromachined ultrasonic transducers with wafer-bonding technology," *Microelectromechanical Systems, Journal of*, vol. 12, no. 2, pp. 128–137, apr 2003.

[29] A. Rønnekleiv, "Fast and accurate CMUT modeling usiing equivalent circuits with lumped parameters," in *Ultrasonics Symposium, 2008 IEEE*, 2008, pp. 496–499.

[30] M. Thränhardt, P.-C. Eccardt, H. Mooshofer, and P. Hauptmann, "A resonant CMUT-based fluid sensor: Modeling and simulation," *Sensors and Actuators A: Physical*, vol. 156, no. 1, pp. 191–195, 2009.

[31] M. Thränhardt, P.-C. Eccardt, H. Mooshofer, P. Hauptmann, and L. Degertekin, "A resonant CMUT sensor for fluid applications," in *Sensors, 2009 IEEE*, oct. 2009, pp. 878 –883.

[32] E. Leirset, A. Rønnekleiv, and A. Aksnes, "Radiation pattern deterioration for phase steered capacitive micromachined ultrasonic transducer arrays due to cross coupling," in *Ultrasonics Symposium, 2011 IEEE*, 2011.

[33] X. Zhuang, I. O. Wygant, D.-S. Lin, M. Kupnik, Ömer Oralkan, and B. T. Khuri-Yakub, "Wafer-bonded 2D CMUT arrays incorporating through-wafer trench-isolated interconnects with a supporting frame," *IEEE Transactions of Ultrasonics, Ferroelectrics and Frequency control*, vol. 56, no. 1, pp. 182–192, 2009.

[34] E. L. Madsen, H. J. Sathoff, and J. A. Zabzavski, "Ultrasonic shear wave properties of soft tissues and tissuelike materials," *J. Acoust. Soc. Am.*, vol. 74, no. 5, pp. 1346–1355, 1983.

[35] L. E. Kinsler, A. R. Frey, A. Coppers, and J. V. Sanders, *Fundamentals of Acoustics*. John Wiley & Sons, Fourth edition, 2000.

[36] A. Thangawng, R. Ruoff, M. Swartz, and M. Glucksberg, "An ultra-thin PDMS membrane as a bio/micro-nano interface: fabrication and characterization," *Biomedical Microdevices*, vol. 9, pp. 587–595, 2007.

[37] C. Linga Reddy, T. Singh, and T. Ytterdal, "Inverter-based 1 V analog front-end amplifiers in 90 nm CMOS for medical ultrasound imaging," *Analog Integrated Circuits and Signal Processing*, vol. 67, pp. 73–83, 2011.

Sigrid Berg was born in Tromsø, Norway in 1978. She received her B.Sc. and M.Sc. degree from the Department of Engineering Cybernetics at the Norwegian University of Science and Technology, NTNU, Trondheim, Norway in 2002 and 2004, respectively. She is currently working on her Ph.D. degree in the Electronic Devices and Materials group at the Department of Electronics and Telecommunications at the same university. Her Ph.D. work mainly involves simulations and measurements of crosstalk in Capacitive Micromachined Ultrasonic Transducers (CMUTs).

Arne Rønnekleiv Arne Rønnekleiv (M'94) was born in Telemark, Norway, 14.02.1941. He earned his Siv.ing. Degree (1966) and Lic. techn. Degree (1970) at NTH. From 1971 he has been employed at NTH, later Norwegian University of Science and Technology, NTNU, Division of Electronics and telecommunications, from 1986 as professor. He is now professor emeritus. He has directed much of his scientific and technical work towards design and application of components based on surface acoustic waves (SAW), and in the later years CMUTs for medical applications. He is an IEEE member.